European Commission

JRC TECHNICAL REPORTS

JRC - Ispra
Atmosphere – Biosphere – Climate Integrated monitoring Station

2015 Report

J.P. Putaud, P. Bergamaschi, F. Cavalli, A. Dell'Acqua, K. Douglas, M. Duerr, I. Fumagalli, I. Goded, F. Grassi, C. Gruening, N.R. Jensen, F. Lagler, G. Manca, S. Martins Dos Santos, M. Matteucci, R. Passarella, V. Pedroni, O. Pokorska, D. Roux

2017

Joint Research Centre

EUR 28513 EN

Contact information
Name: Jean-Philippe Putaud
Address: European Commission, Joint Research Centre, Directorate for Energy, Transport and Climate, Air and Climate Unit, Via E. Fermi 2749, 21027 Ispra (VA), Italy
E-mail: jean.putaud@ec.europa.eu

JRC Science Hub
https://ec.europa.eu/jrc

JRC 104520

EUR 28513 EN

PDF	ISBN 978-92-79-66612-4	ISSN 1831-9424	doi:10.2760/409157
Print	ISBN 978-92-79-66613-1	ISSN 1018-5593	doi:10.2760/201458

Luxembourg: Publications Office of the European Union, 2017

How to cite this report: Putaud, J.P. et al., JRC-Ispra Atmosphere – Biosphere – Climate Integrated monitoring Station: 2015 report; EUR 28513 EN; doi:10.2760/409157.

TABLE OF CONTENTS

Executive Summary

A comprehensive set of essential atmospheric variables have been measured at the JRC-Ispra Atmosphere -Biosphere - Climate Integrated monitoring Station (ABC-IS) for several years to detect the impact of European policies and international conventions on air pollution and climate forcing. The variables we measure include greenhouse gas concentrations (CO_2, CH_4, N_2O, SF_6), radon (^{222}Rn) activity concentration, short-lived gaseous and particulate pollutants (CO, SO_2, NO, NO_2, O_3, $PM_{2.5}$ and its main ionic and carbonaceous constituents), atmospheric particle micro-physical characteristics (number concentration and size distribution) and optical properties (light scattering and absorption in-situ, light scattering and extinction vertical profiles remotely), eutrophying and acidifying species (SO_4^{2-}, NO_3^-, NH_4^+) wet deposition, and vegetation ⇆ atmosphere exchanges (CO_2, O_3, H_2O and heat), backed up by meteorological and pedological measurements. All the measurements performed at ABC-IS are made under international projects and programs like InGOS (Integrated non-CO2 Greenhouse gas Observation System), ACTRIS (the EU research Infra-Structure for the observation of Aerosols, Clouds and Trace gases), EMEP (co-operative Program for Monitoring and Evaluation of the long range transmission of air pollutants in Europe) and GAW (Global Atmosphere Watch), which implies the use of standard methods and scales, and the participation in quality assurance activities. The JRC has a leading role in ACTRIS and EMEP regarding the quality assurance for carbonaceous aerosol measurements. All the data obtained at ABC-IS are submitted to international open data bases (www.europe-fluxdata.eu, fluxnet.ornl.gov, www.ingos-infrastructure.eu, ebas.nilu.no) and can be freely downloaded from these web sites. The data we produce are used in European wide assessments, for model inputs and validation, and for calibrating satellite airborne sensors. The ABC-IS 2015 report presents the data produced during the past year in the context of the previous years of measurements.

Almost all the in-situ (3.5 to 36 m above ground level) measurement scheduled for 2015 were regularly performed across the year, except for short periods of preventive and corrective maintenance. The remote sensing of the aerosol vertical distribution was resumed only from October, when the LiDAR was re-installed by the manufacturer after a major laser failure in 2014.

Minimum values of CH_4, N_2O and SF_6 (measured under clear air conditions) are close to marine background, while CO_2 mixing ratios can be lower than the Mace Head baseline due to the continental biospheric CO_2 sink. Deviations from baseline concentrations provide key information about regional and larger scale European greenhouse gas sources.

The concentrations of all the short-lived pollutants monitored at the JRC-Ispra station (CO, SO_2, NO_2, O_3, atmospheric particulate matter) have increased in 2015 compared to 2014 by 5 to 30%. This can probably be at least partly explained by the weather conditions. In particular, 2014 was wetter than average while 2015 was exceptionally dry, with e.g. practically no rain in November and December. The greatest increase was observed for $PM_{2.5}$ concentration (17 μg/m³

annual mean in 2015), which is strongly influenced by precipitation. This was mainly due to increased concentrations in ammonium nitrate (NH_4NO_3) and carbonaceous aerosol (particulate organic matter and elemental carbon). The increased aerosol burden led to increased concentrations of acidifying and eutrophying species in rainwater, as well as to a doubling in the number of acidic rainwater samples. However, only the SO_4^{2-}deposition flux increased, and with respect to the last decade, 2015 did not break the general decreasing trend observed in most pollutant concentrations. A noticeable exception regards ozone (O_3), whose concentrations have been relatively high in 2015. The indicators for health and ecosystem safeguard have deteriorated since 2012 (2014 excluded) compared to the 2000's. It would be worth studying the geographical extent of this tendency across Europe to understand its origin.

The decreasing trend in particulate matter mass concentrations observed over the past 3 decades have been accompanied with a decrease in ultra-fine particle number between 2004 and 2010, but no longer since then (2015 annual average = 8040 cm^{-3}). It has also led to a decrease in visible light scattering by the atmospheric particles, but not much in light absorption. This means that the negative radiative forcing (climate cooling) of atmospheric particles is getting smaller and smaller in our area. Determining the climate effect of the aerosol remains a big challenge and further investment would be needed in this field.

The atmosphere vegetation exchange flux measurements show that the deciduous forest in Ispra is a strong net sink for O_3 (about 6 g/m² absorbed in 2015). The deciduous forest in Ispra and the pine tree forest of San Rossore are both net sinks for CO_2 as well (530 and 560 gC/m² absorbed in 2015, respectively). The different meteorological conditions prevailing in 2015 (dryer) compared to 2014 (wetter) allowed us to observe that the carbon sequestration by these two temperate and Mediterranean forests was 10% greater during the dryer compared to the wetter year.

1. Introduction

The mission of the Atmosphere-Biosphere-Climate Integrated monitoring Station (ABC-IS) is to measure changes in atmospheric variables to obtain data that are essential for the conception, development, implementation, and monitoring of the impact of European policies and International conventions on air pollution and climate change. Measurements include greenhouse gas concentrations, forest ⇆ atmosphere fluxes, and concentrations of pollutants in the gas phase, particulate matter and precipitations, as well as aerosol micro-physical and optical characteristics. The goal of ABC-IS is to establish real world interactions between air pollution, climate change and the biosphere, for highlighting possible trade-offs and synergies between air pollution and climate change policies. Possible interactions include the role of pollutants in climate forcing and CO_2 uptake by vegetation, the impact of climate change and air pollution on CO_2 uptake by vegetation, the effect of biogenic emission on air pollution and climate forcing, etc…

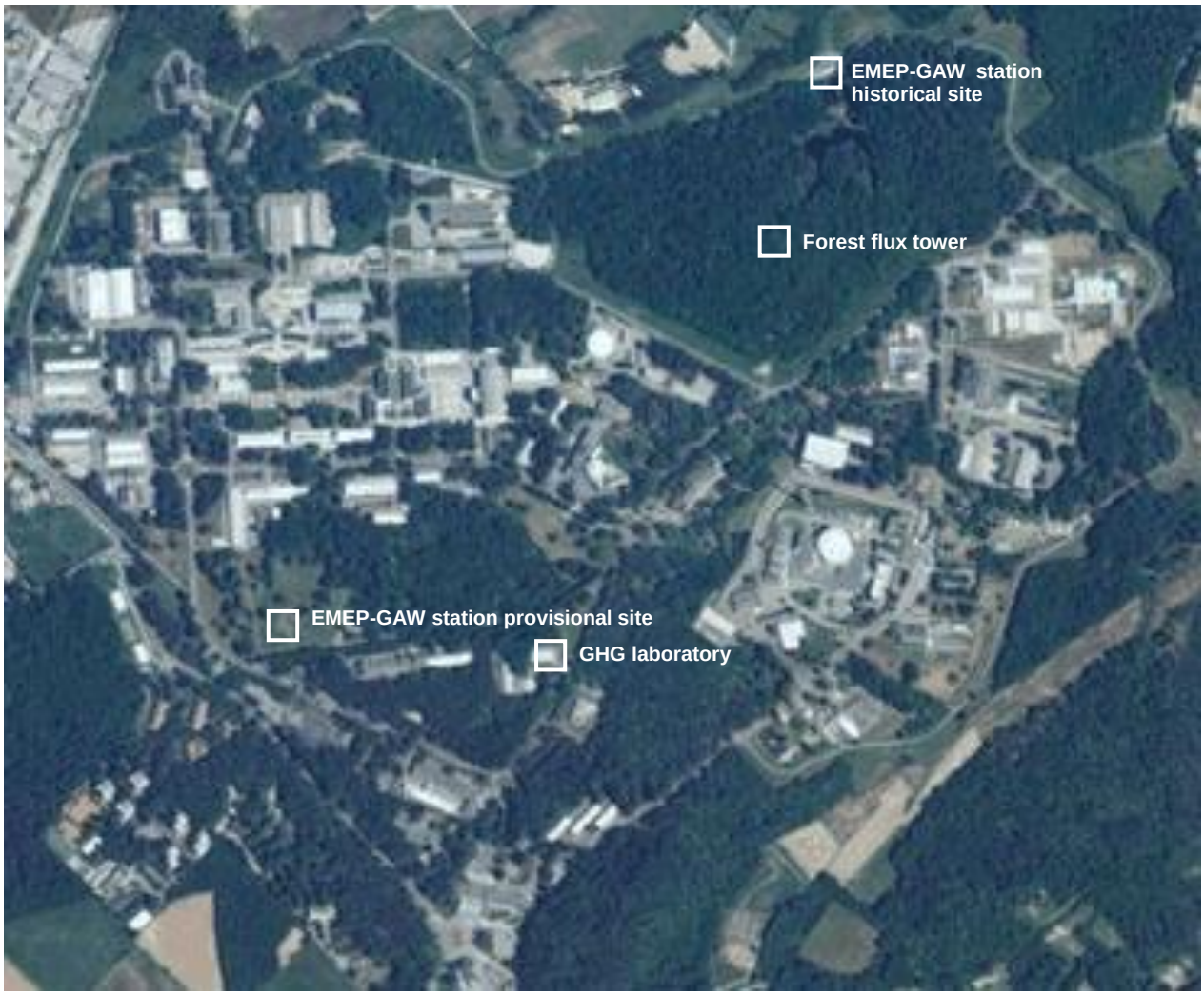

Fig. 1: The JRC-Ispra site and the location of the laboratory for greenhouse gas monitoring, the forest flux tower, the historical and the provisional EMEP-GAW station sites.

Measurements are performed in the framework of international monitoring programs like the new (from 2015) European Research Infrastructure Consortium project ICOS (Integrated Carbon Observation System), EMEP (Co-operative program for monitoring and evaluation of the long range transmission of air pollutants in Europe of the UN-ECE *Convention on Long-Range Transboundary Air Pollution* CLRTAP) and GAW (the Global Atmosphere Watch program of the World Meteorological Organization). The ABC-IS infrastructure is also used in competitive projects (e.g. ACTRIS, InGOS).

Through the participation of ABC-IS in international networks, inter-laboratory comparisons are conducted and standard methods are developed in the frame of the European Reference Laboratory for Air Pollution of the JRC-IES. Most measurements are performed at the JRC-Ispra site (*Fig. 1*), and some at the typical Mediterranean site of San Rossore site (*Fig. 51*).

2. Quality management system

ABC-IS is a research infrastructure of JRC's *Directorate for Energy, Transport and Climate*.

We achieved ISO 9001 re-certification in June 2013, which is also valid for the year 2015 (ISO 9001 is mainly about "project management"). In addition, external and internal ISO 9001 audits were also performed successfully in 2015.

In addition, JRC-Ispra also achieved in Nov. 2010 the ISO 14001 certificate (ISO 14001 is mainly about "environmental issues"), which is valid for several years. An audit also took place in 2015.

For information (the links below being accessible to JRC staff only), the "quality management system (QMS) for the ABC-IS regional station" includes server space at the following links:

\\ies.jrc.it\H02\H02QMS_year_2015_

\\ies.jrc.it\H02\LargeFacilities\ABC-IS\

\\ies.jrc.it\H02\Laboratories

\\Lake\lifecyclesheets\

where the following information can be found: list of instruments; information about calibrations; standards used and maintenance; standard operational procedures (SOP's); instrument lifecycle sheets and log-books; manuals for the instruments; *etc*. For additional specific details about QMS, for the year 2015 and the ABC-IS station, see e.g. the file 2015_Instruments'_calibration_&_standards_&_maintenance.xls, that can be found under \\ies.jrc.it\H02\LargeFacilities\ABC-IS\Quality_management.

More QMS information/details can also be found in the sections "Measurement techniques" in this report.

More general QMS information/documentations about how the AC Unit (H02/C5) was run in 2015, the management of all of the projects within the Unit and the running of the ABC-IS station can also be found at

\\ies.jrc.it\H02\H02QMS_year_2015_\1_UNIT\QMS_info\QMS_documents_H02

\\ies.jrc.it\H02\H02QMS_year_2016_\1_UNIT\QMS_info\QMS_documents_H02

and especially in the seven H02 Unit QMS documents listed here:

QMS_H02_SUMM_Scientific_Unit_Management_Manual_v11_0.pdf
QMS_H02_MANPROJ_PROJ_Laboratory_Management_v10_0.pdf
QMS_H02_MANPROJ_PROJ_Model_Management_v10_0.pdf
QMS_H02_MANPROJ_PROJ_Informatics_Management_v10_0.pdf
QMS_H02_MANPROJ_PROJ_Knowledge_Management_v10_0.pdf
QMS_H02_MANPROJ_PROJ_Review_Verification_Validation_Approval_v6_0.pdf
QMS_H02_MANPROJ_PROJ_Administration_Implementation_v5_0.pdf

The latest versions of these documents are available at:

\\ies.jrc.it\H02\H02QMS_year_2016_\1_UNIT\QMS_info\QMS_documents_H02

Fig. 2: the laboratory for greenhouse gas concentration monitoring (Bd 5).

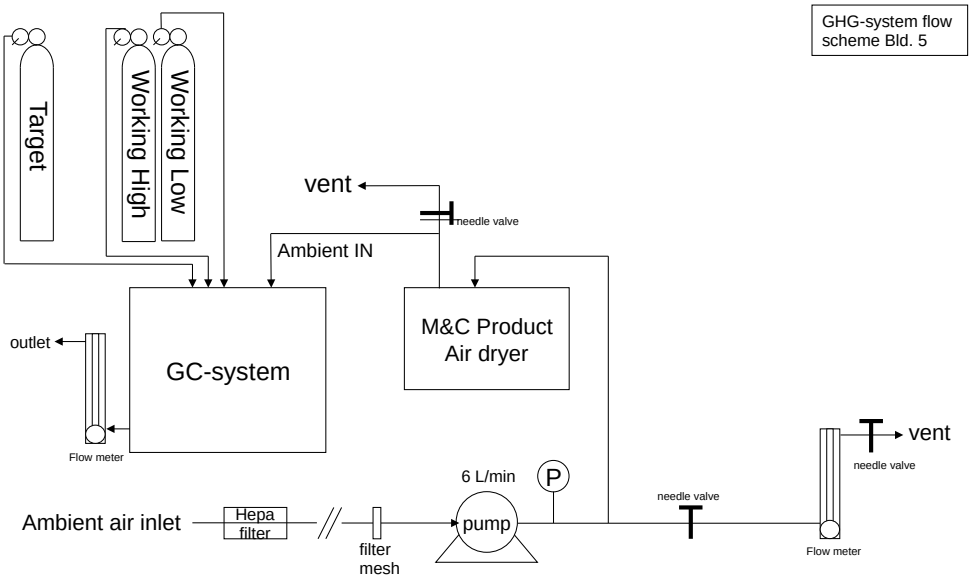

Fig. 3: Bd 5 GHG-system flow scheme

3. Greenhouse gas concentration monitoring at the JRC-Ispra site

3.1. Location

The greenhouse gas (GHG) monitoring station is located at Building 5 of the JRC site Ispra (45.807°N, 8.631°E, 223 m asl, Fig. 2). The station is currently the only low altitude measurement site for greenhouse gases near the Po Valley. The unique location of the station at the South-Eastern border of Lake Maggiore in a semi-rural area at the North-Western edge of the Po Valley allows sampling of highly polluted air masses from the Po Valley during meteorological conditions with southerly flow, contrasted by situations with northerly winds bringing relatively clean air to the site. A recent study analysed in detail the sensitivity of the atmospheric concentrations at the monitoring station (Bergamaschi and Brunner, 2015). The sensitivity usually shows a significant diurnal cycle, during night dominated by the area 40-60 km around the station, while daytime footprints are much larger, typically dominated by distances of more than 60 km. During summer daytime, the radius τ_{s50} (at which the cumulative surface sensitivity reaches 50% of the total sensitivity) is about 187 km on average. Furthermore, the diurnal cycle in local wind direction due to the regional mountain - lake/valley wind system leads to a significant diurnal cycle of the sensitivity (north-west vs. south-east), especially during summer time.

The main cities around the station are Varese, 20 km to the East, Novara, 40 km South, Gallarate - Busto Arsizio, about 20 km southeast and Milan, 60 km to the south-east.

3.2. Measurement program

The GHG monitoring station is in operation since October 2007 and is complementary to the JRC-Ispra EMEP-GAW station, which started in 1985 (*Putaud et al., 2014*), and to the flux measurement towers in the forests of JRC-Ispra and San Rossore. All activities together are referred to as ABC-IS (Atmosphere, Biosphere, Climate Integrated monitoring Station).

The GHG measurement program follows the recommendations of ICOS (www.ICOS-infrastructure.eu) for level 2 stations.

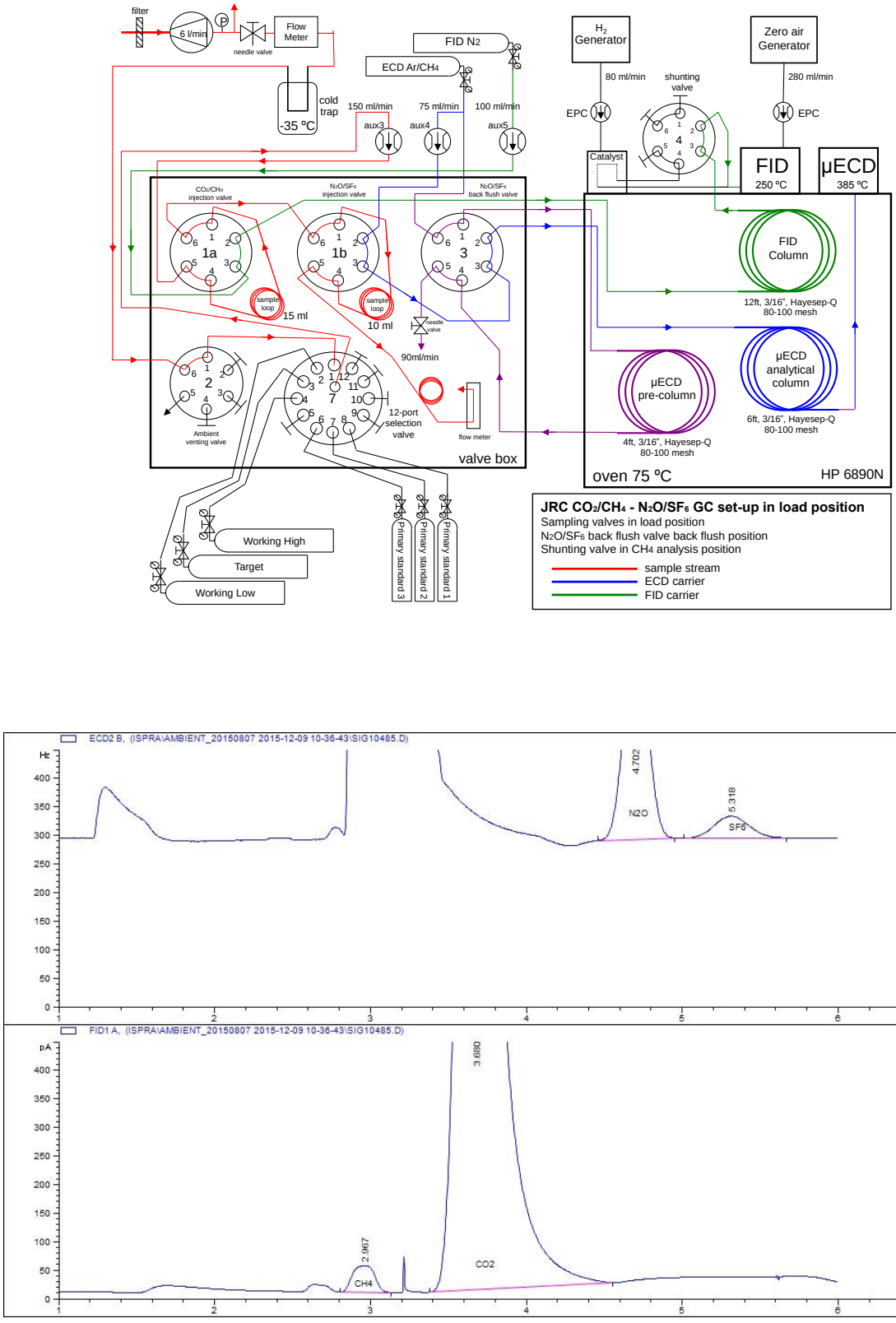

Fig. 4: The top panel shows a schematic of the GC-system set-up while typical chromatograms are shown in the lower panels.

3.3. Instrumentation

Here we summarize the most important aspects of the GHG and ^{222}Radon measurement system. Air is sampled from a 15 m high mast using a 50 m ½" Teflon tube at a flow rate of ~6 L /min using a KNF membrane pump (KNF N811KT.18).

3.3.1. Sampling

The sampled air is filtered from aerosols by a Pall Hepa filter (model PN12144) positioned 10 m downstream of the inlet and dried cryogenically by a commercial system from M&C TechGroup (model EC30 FD) down to a water vapour content of <0.015%v before being directed to the analyser. The remaining water vapour is equivalent to a maximum 'volumetric error' of <0.06 ppmv of CO_2 or <0.3 ppbv of CH_4 or <0.05 ppbv N_2O. A schematic overview of the sample flow set-up is shown in Fig. 3.

3.3.2. Analyses

3.3.2.1 Gas Chromatograph Agilent 6890N (S/N US10701038)

The continuous monitoring at 6 minute time resolution of CO_2, CH_4, N_2O, and SF_6 is performed by an Agilent 6890N gas chromatograph equipped with a Flame Ionization Detector (FID) and micro-Electron Capture Detector (μECD) with a set-up described by *Worthy el al.* (1998). The calibration strategy has been adopted from *Pépin et al.* (2001) and is based on a Working High (WH) and Working Low (WL) standard (namely bracketing standards), which are calibrated regularly using NOAA primary standards. The WH and WL are both measured 2 times per hour for calculating ambient mixing ratios, and a target (TG) sample is measured every 6 hours for quality control. Working standards and target cylinders are filled with synthetic air, while NOAA primary standards are filled with real air.

N_2O concentrations were also calculated using a second calibration strategy that is based on the one-point-reference method with a correction for non-linearity of μECD. The non-linear response of the μECD was estimated using NOAA primary standards and then it was applied to the entire time series. This second method improves the quality of the time series when the bracketing standards do not cover the range for N_2O ambient concentrations (i.e. range too large or range that does not include the ambient concentration). GHG measurements are reported as dry air mole fractions (mixing ratios) using the WMO NOAA2004 scale for CH_4, the WMOX2007 for CO_2, and the NOAA2006A scale for N_2O and SF_6. We apply a suite of five NOAA tanks ranging from 369-523 ppm for CO_2, 1782-2397 ppb for CH_4, 318-341 ppb for N_2O, and 6.1-14.3 ppt for SF_6 as primary standards. The GC control and peak integration runs on *ChemStation* commercial software. Further processing of the raw data is based on custom built software developed in C language and named GC_6890N_Pro. A schematic of the GC-system set-up and typical chromatograms are shown in Fig. 4, while Fig. 5 shows the graphical user interface of the GC_6890N_Pro software.

Fig. 5: Graphical User Interface of GC_6890N_Pro software, developed for the data processing of GC raw data

3.3.2.2 Cavity Ring-Down Spectrometer (Picarro G1301) (S/N CFDAS-42)

In addition to the low time resolution GC-system we have been operating a fast Picarro G1301 Cavity Ring-Down Spectrometer (Picarro CRDS) for measurement of CO_2 and CH_4 atmospheric concentration since February 2009. The instrument stopped running in July 2014 because of a major problem with the laser. The repair required a long time and the instrument was returned to Ispra at the beginning of 2015. However, the Picarro G1301 instrument was not operational during 2015 due to a lack of manpower.

3.3.2.3 Radon analyser ANSTO (custom built)

^{222}Radon activity concentrations in Bq m^{-3} have been semi-continuously monitored (30 minute time integration) applying an ANSTO dual-flow loop two-filter detector (Zahorowski et al., 2004) since October of 2008. The monitor is positioned close to the GHG-sampling mast and the air sample is taken from a separate inlet positioned at 3.5 m above the ground. A 500 L decay tank is placed in the inlet line to allow for the decay of Thoron (^{220}Rn with a half-life of 55.6 s) before reaching the ^{222}Radon monitor. The ANSTO ^{222}Radon monitor is calibrated once a month using a commercial passive ^{226}Radium source from Pylon Electronic Inc. (Canada) inside the calibration unit with an activity of 21.99 kBq, which corresponds to a ^{222}Radon delivery rate of 2.77 Bq min^{-1}. The lower limit of detection is 0.02 Bq m^{-3} for a 30% precision (relative counting error). The total measurement uncertainty is estimated to be <5% for ambient ^{222}Radon activities at Ispra. An inter-comparison between the ANSTO detector and an AlphaGUARD instrument was carried out from September 2014 till February 2015. The aim of this campaign was to derive a wind speed dependent correction to estimate the radon activity at 15m (inlet height used for the GHG measurements) from the measured radon concentrations at 3.5 m above ground level (Koffi et al., 2016).

3.4. Measurement uncertainties

The different types of uncertainties affecting the GC measurements have been estimated using the algorithms developed in the InGOS ("Integrated non-CO2 Greenhouse gas Observing System") project (http://www.ingos-infrastructure.eu/). These uncertainties are defined as follows and discussed in section 3.5:

- 'Working standard repeatability' is calculated as the 24-hours centred moving, 1σ standard deviation of the bracketing standards (or reference standard in case of the one-point-reference method).
- 'Laboratory internal scale consistency uncertainty' (LISC) is the median of the difference between measured and assigned values of the target gas. The median is calculated for different time periods where GC settings were constant (including the used working standards and target gas).
- 'Monthly reproducibility' represents the values of the smoothed target residuals. Smoothing is performed with a centred running median with a window length of 30 days.
- 'Scale transfer and non-linearity uncertainty' is based on the uncertainty of the assigned working standard concentration and it accounts for the uncertainty introduced by scale transfer from NOAA standards to the working standards.

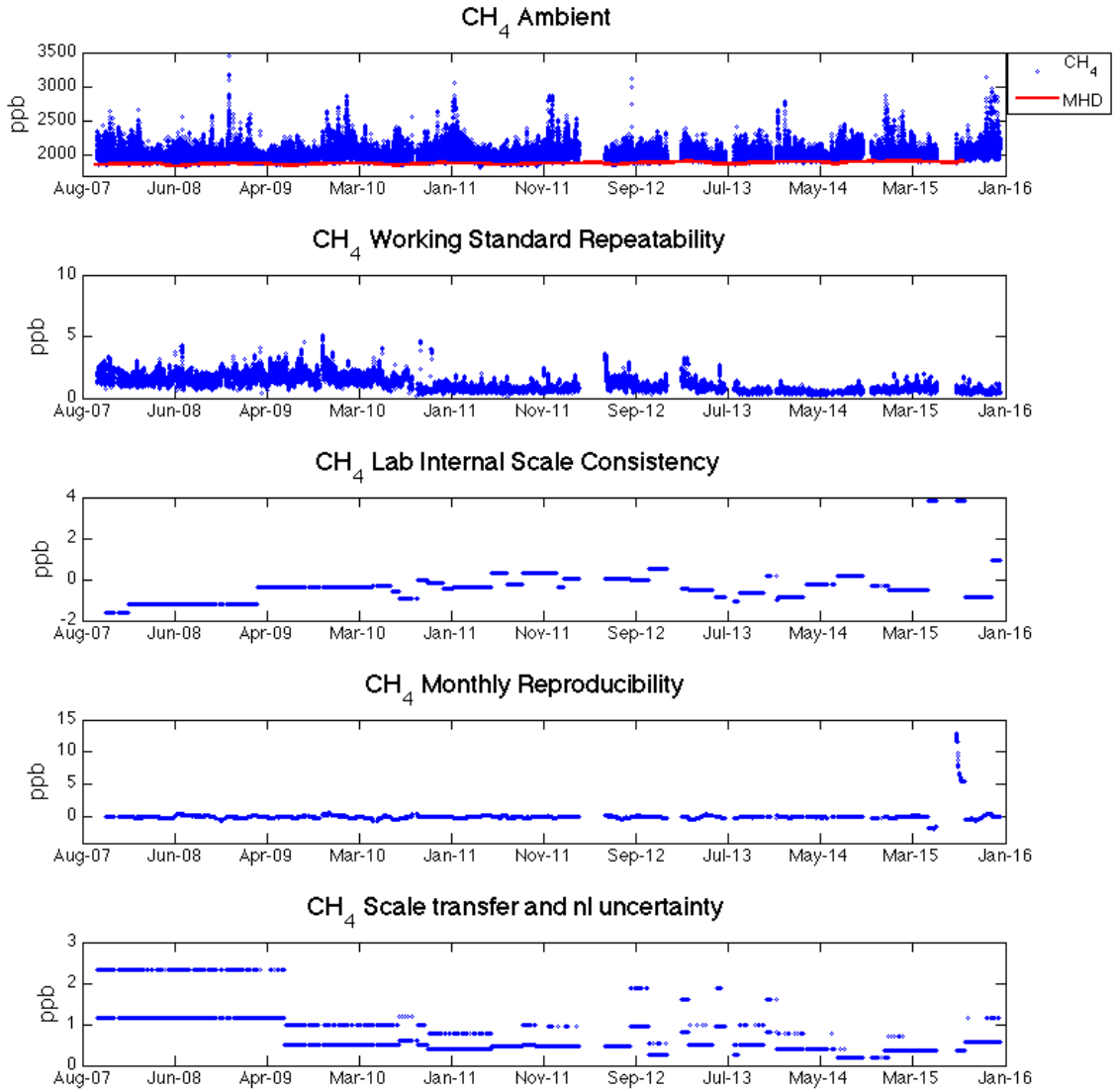

Fig. 6: Time series of continuous CH_4 ambient measurements at Ispra between October 2007 and December 2015 with associated uncertainties. CH_4 ambient concentrations are reported as hourly mean values of dry air mole fractions. Furthermore, monthly mean concentrations from the background station Mace Head (MHD) on the West coast of Ireland are also included (Mace Head data from Simon O'Doherty, University of Bristol).

3.5. Overview of measurement results

Fig. 6, 8, 9 and 10 give an overview of the GC greenhouse gas measurements since the start of the measurements in October 2007 until December 2015. These figures show also the uncertainties of the ambient concentrations; while the 'scale transfer and non-linearity' uncertainty has been calculated only for CH_4 and N_2O. For N_2O and SF_6 only data since 15/09/2010 are shown. Before this date there was a dilution problem of the sample loop connected to the column of the μECD detector. The flushing of the sample loop during ambient measurement was not sufficient to remove completely the carrier gas used in the previous analysis. The N_2O data shown in Fig. 6c are calculated using the one-point-reference method (see above).

The measurements at Ispra are plotted together with the monthly mean baseline data from the Mace Head (Ireland) station to illustrate the Atlantic background mixing ratios. Minimum values of CH_4, N_2O and SF_6 measured at the JRC-Ispra site are close to the Mace Head baseline, while CO_2 mixing ratios can be lower than the Mace Head baseline due to the continental biospheric CO_2 sink.

The gap in GC time series during summer 2015 was due to the GC maintenance in which the jet of the FID detector, the multi-position rotary valve and the nickel catalyser were replaced. After the maintenance, the precision of CO_2 measurements was initially worse than before (Fig. 6b) because of the continuous decrease in the efficiency of the new nickel catalyst used to convert the CO_2 into methane. This catalyser has been replaced in March 2016.

Fig. 7 shows hourly mean ^{222}Radon activities since October 2008.

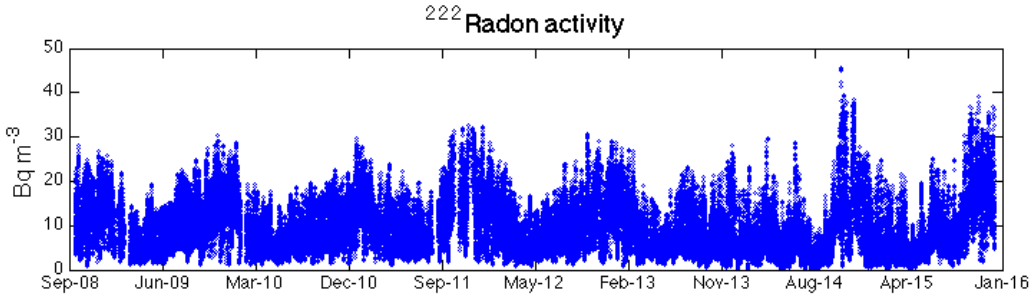

Fig. 7: Time series of hourly mean 222Radon activity from Oct. 2008 to Dec. 2015.

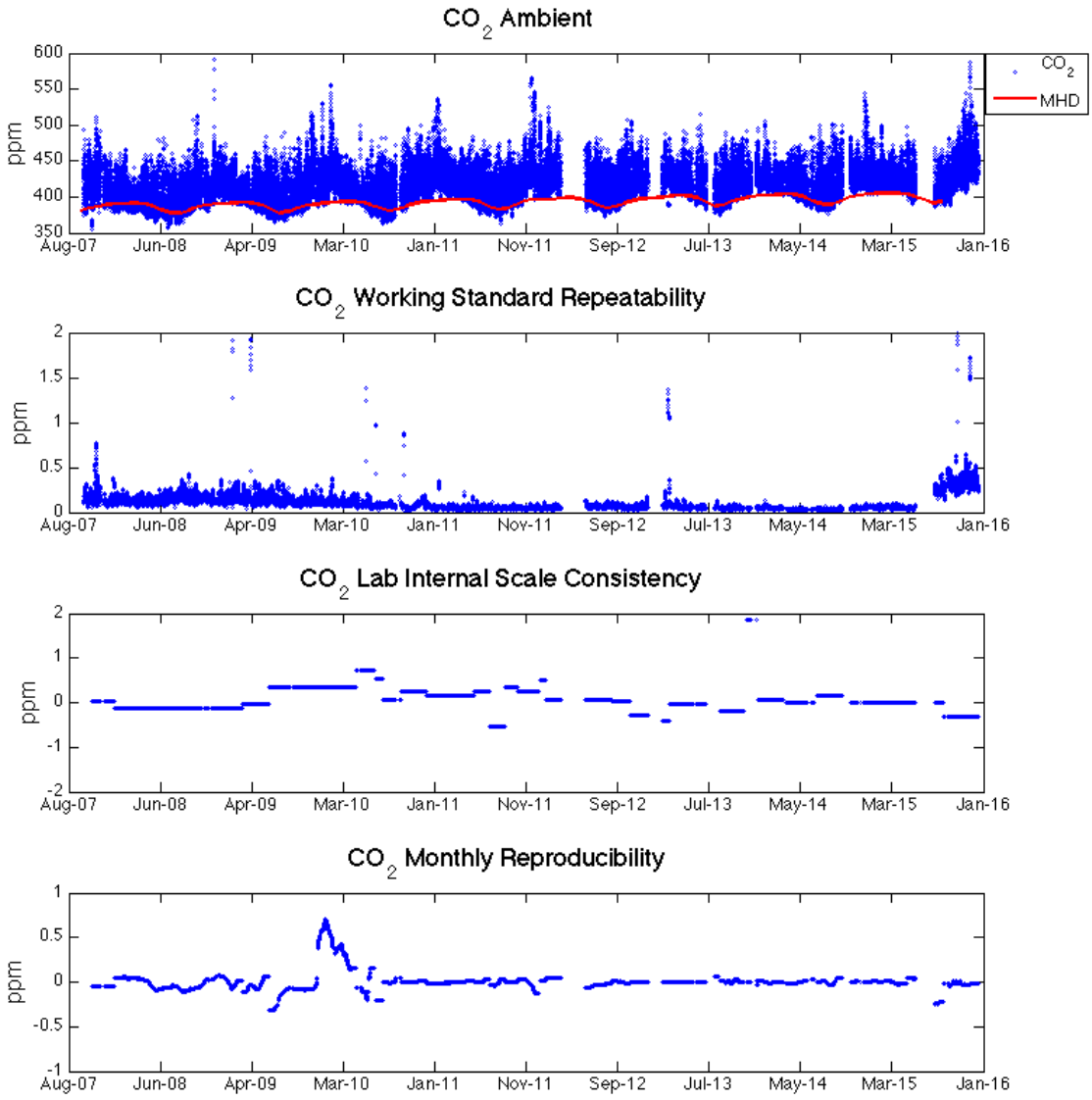

Fig. 8: Time series of continuous CO_2 ambient measurements at Ispra between October 2007 and December 2015 with associated uncertainties. CO_2 ambient concentrations are reported as hourly mean values of dry air mole fractions. Furthermore, flask measurements from the background station Mace Head (MHD) on the West coast of Ireland are also included (Dlugokencky et al., 2016).

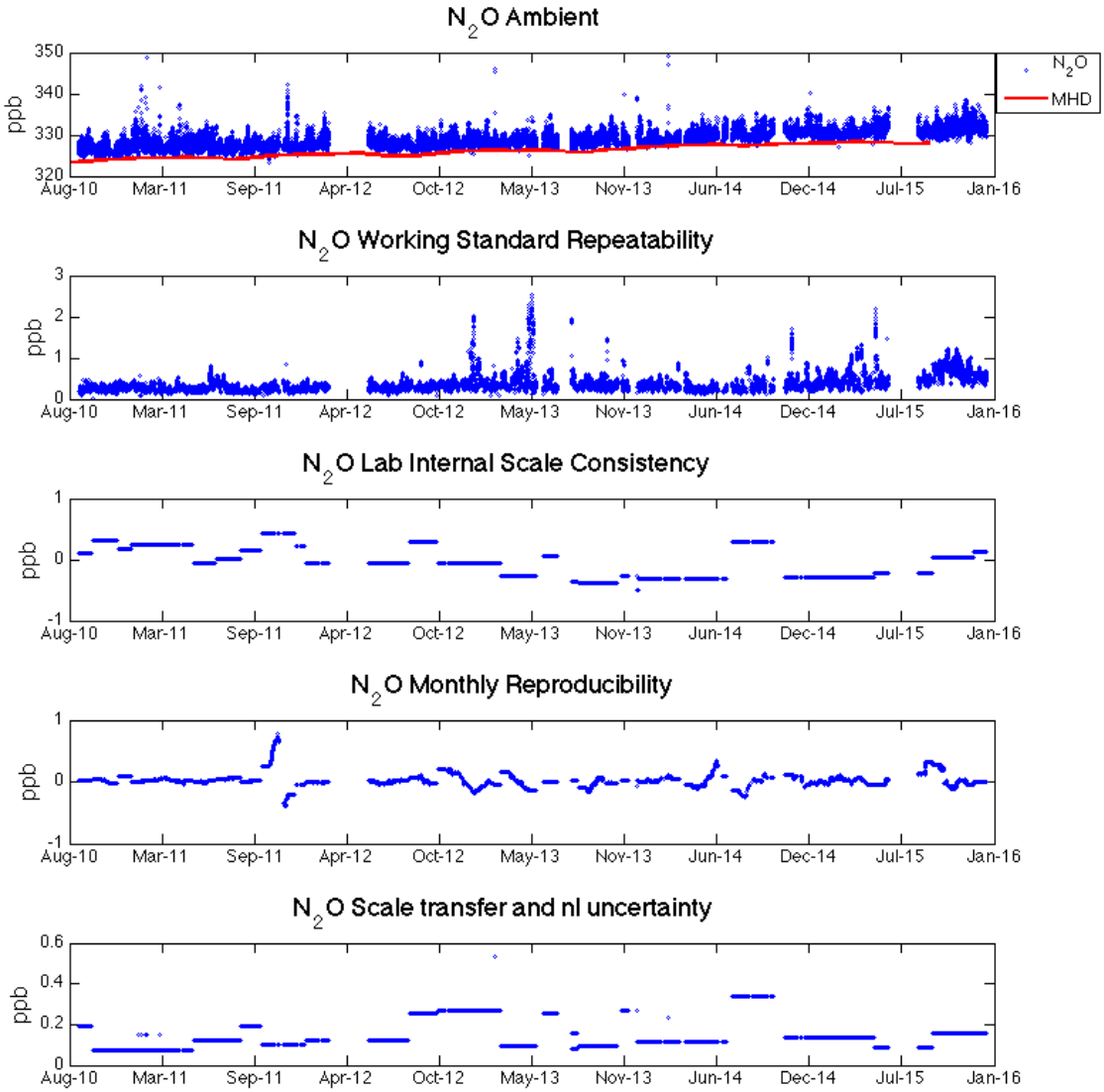

Fig. 9: Time series of continuous N_2O ambient measurements at Ispra between September 2010 and December 2015 with associated uncertainties. N_2O ambient concentrations are reported as hourly mean values of dry air mole fractions. Furthermore, monthly mean concentrations from the background station Mace Head (MHD) on the West coast of Ireland are also included (Mace Head data from Simon O'Doherty, University of Bristol).

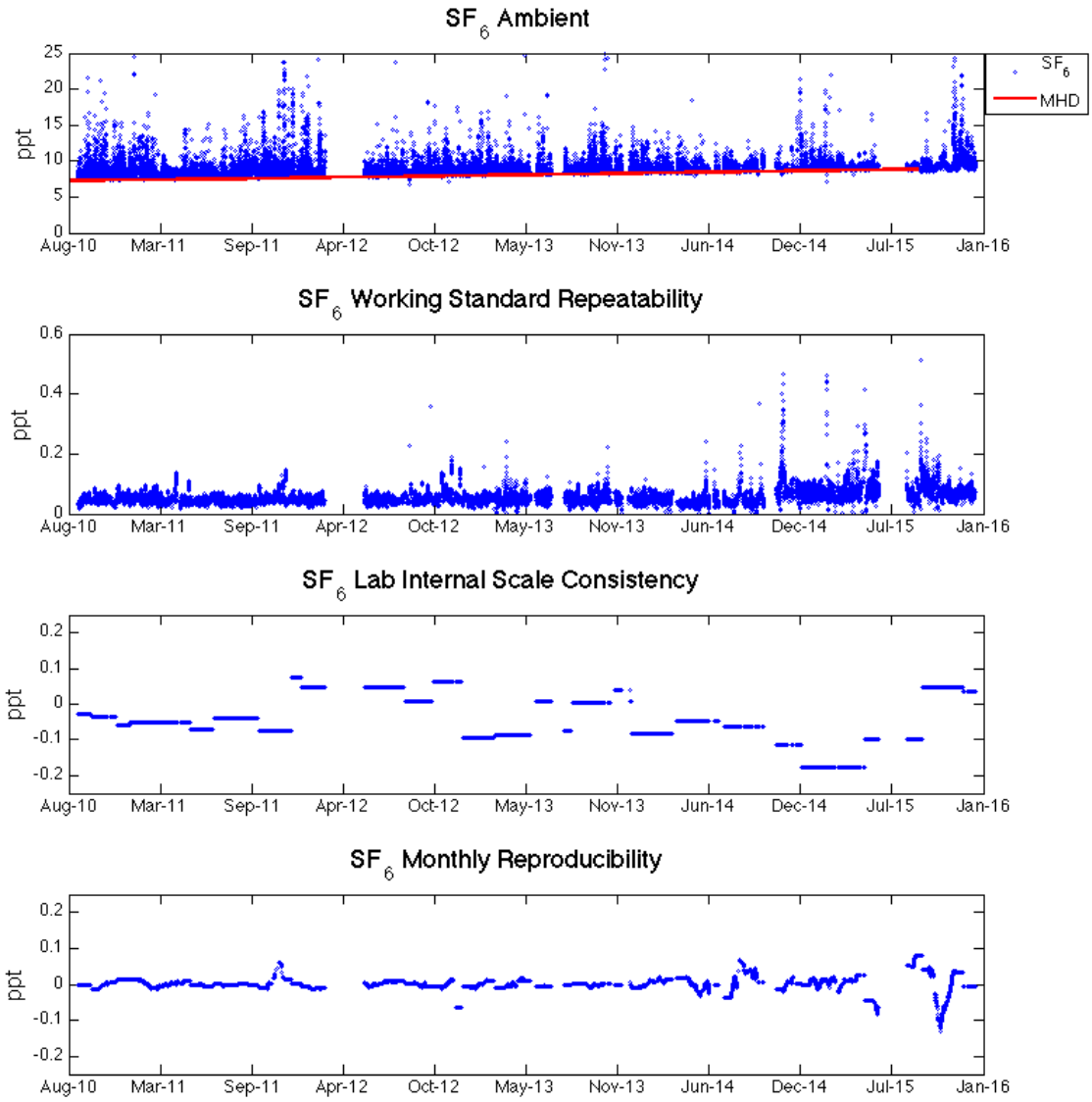

Fig. 10: Time series of continuous SF_6 ambient measurements at Ispra between September 2010 and December 2015 with associated uncertainties. SF_6 ambient concentrations are reported as hourly mean values of dry air mole fractions. Furthermore*, monthly mean concentrations from the background station Mace Head (MHD) on the West coast of Ireland are also included (Mace Head data from Simon O'Doherty, University of Bristol).*

Page left intentionally blank

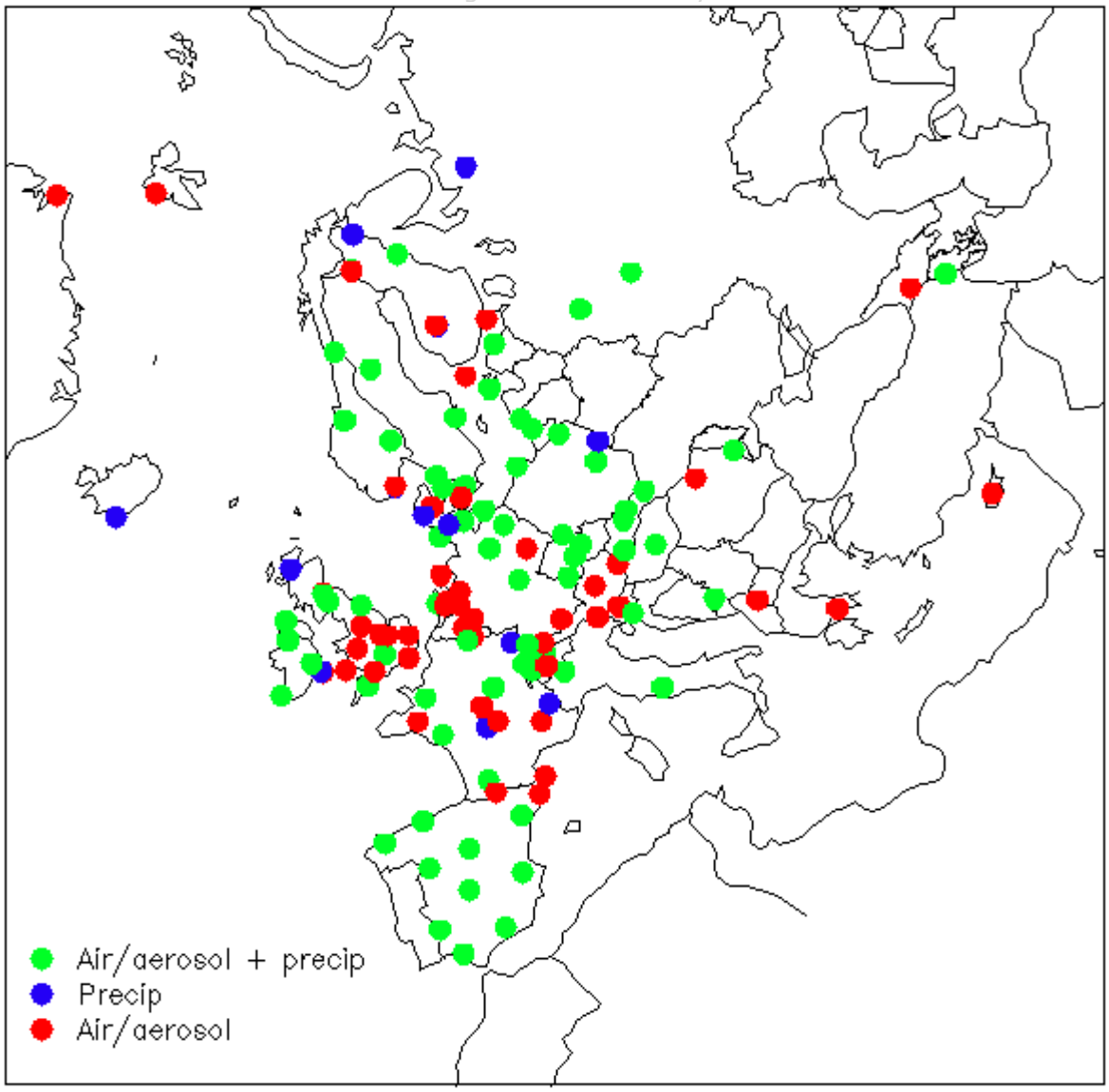

Fig. 11: most recent available map of the EMEP stations across Europe (2014).

4. Short-lived atmospheric species at the JRC-Ispra site

4.1. Introduction

4.1.1. Location

Air pollution has been monitored since 1985 at the EMEP and regional GAW station for atmospheric research (45°48.881'N, 8°38.165'E, 209 m a.s.l.) located by the Northern fence of the JRC-Ispra site (see Fig. 1), situated in a semi-rural area at the NW edge of the Po valley in Italy. From the end of March 2013, the measurement of short-lived atmospheric species (Table 2) has been performed at the provisional site (45°48.438'N, 8°37.582'E, 217 m a.s.l.), due to the reconstruction of the laboratory at the historical site (*Fig. 1*). The main cities around are Varese (20 km east), Novara (40 km south), Gallarate - Busto Arsizio (about 20 km south-east) and the Milan conurbation (60 km to the south-east). Busy roads and highways link these urban centres. Emissions of pollutants reported for the four industrial large point sources (CO_2 emissions > 1500 tons d^{-1}) located between 5 and 45 km NE to SE from Ispra also include 2 and 3 tons of CO per day, plus 3 and 5 tons of NOx (as NO_2) per day for the 2 closest ones (**PRTR emissions**, 2010).

4.1.2. Underpinning programs

4.1.2.1. The EMEP program (*http://www.emep.int/*)

Currently, about 50 countries and the European Community have ratified the **CLRTAP**. Lists of participating institutions and monitoring stations (Fig. 11) can be found at: ***http://www.nilu.no/projects/ccc/network/index.html***

The set-up and running of the JRC-Ispra EMEP station resulted from a proposal of the Directorate General for Environment of the European Commission in Brussels, in agreement with the Joint Research Centre, following the Council Resolution **N° 81/462/EEC**, article 9, to support the implementation of the EMEP programme.

The JRC-Ispra station operates on a regular basis in the extended EMEP measurement program since November 1985. Data are transmitted yearly to the EMEP Chemical Coordinating Centre (CCC) for data control and statistical evaluation, and available from the EBAS data bank (Emep dataBASe, ***http://ebas.nilu.no/***).

4.1.2.2. The GAW program (*http://www.wmo.int/web/arep/gaw/gaw_home.html*)

WMO's Global Atmosphere Watch (GAW) system was established in 1989 with the scope of providing information on the physico-chemical composition of the atmosphere. These data provide a basis to improve our understanding of both atmospheric changes and atmosphere-biosphere interactions. GAW is one of WMO's most important contributions to atmosphere-biosphere the study of environmental issues, with about 80 member countries participating in GAW's measurement program. Since December 1999, the JRC-Ispra station is also part of the GAW coordinated network of regional stations. Aerosol data submitted to EMEP and GAW are available from the World Data Centre for Aerosol (**WDCA**).

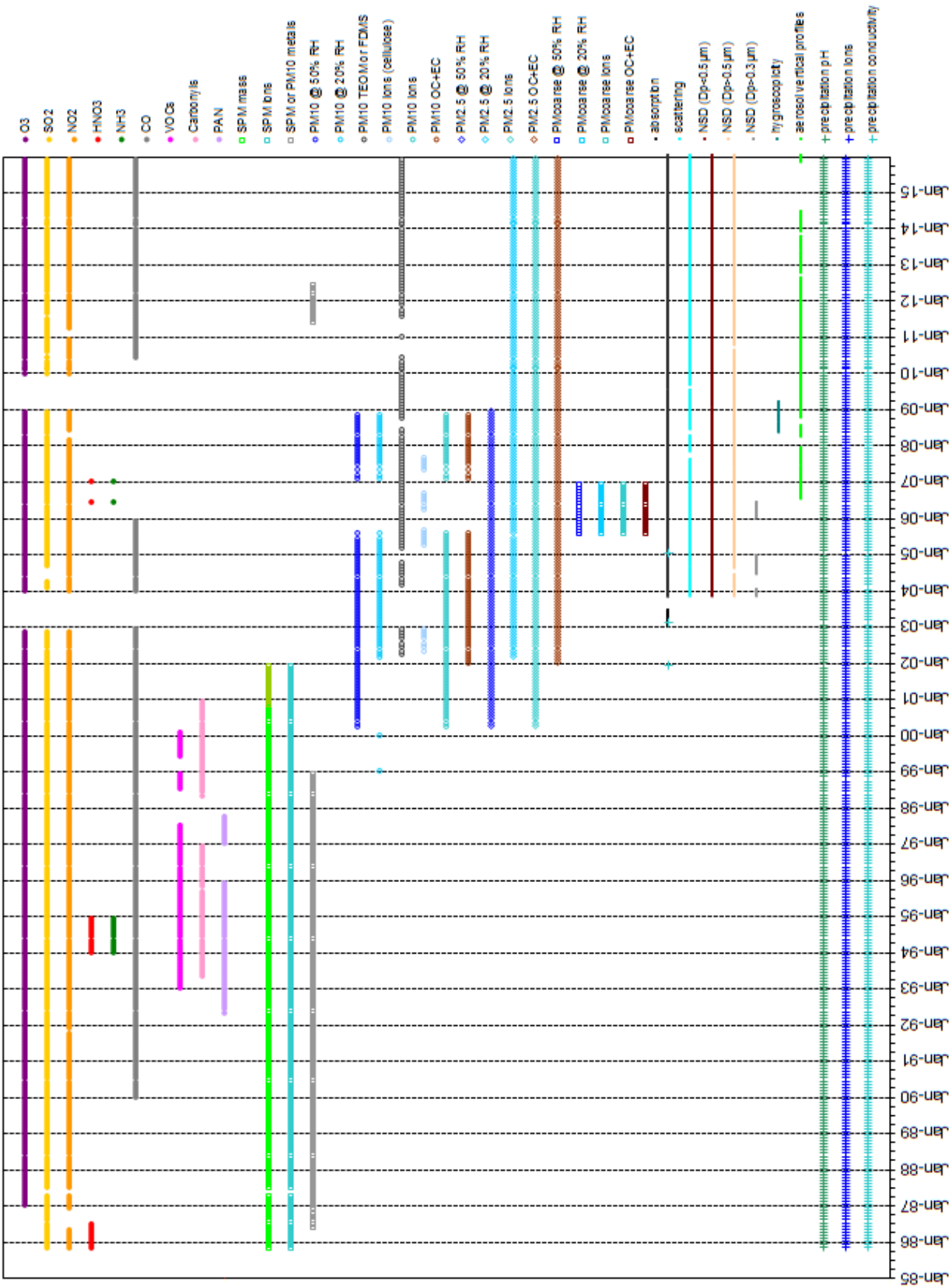

Fig. 12: Atmospheric short-lived species measurements performed at the JRC-Ispra station for atmospheric research since 1985.

4.1.2.3. The institutional program (http:/ec.europa.eu/jrc/en/research-topic/air-quality)

Since 2002, the measurement program of the air pollution monitoring station of JRC-Ispra has gradually been focused on short-lived climate forcers such as tropospheric ozone and aerosols, and their precursors (Fig. 12). Concretely, more sensitive gas monitors were introduced, as well as a set of new measurements providing aerosol characteristics that are linked to radiative forcing. The station contributed to the impact category "implementation, monitoring and evaluation of EU policies" as listed in the JRC institutional project work plan.

The site is also being used for research and development purposes. Regarding particulate organic and elemental carbon, techniques developed by the Air and Climate unit in Ispra have been implemented and validated by international atmospheric research networks (EUSAAR, ACTRIS), recommended in the EMEP sampling and analytical procedure manual, and adopted by the European Committee for Standardisation (CEN) as standard method (FprEN16909).

Additional information about the JRC-Ispra air monitoring station and other stations from the EMEP network can also be found in the following papers: Van Dingenen et al., 2004; Putaud et al., 2004; Mira-Salama et al., 2008; Putaud et al., 2010; Putaud et al., 2014. Nowadays, all validated monitoring data obtained at the JRC-Ispra station within the EMEP and the GAW program, and other past and current international projects (EUSAAR, ACTRIS) can be retrieved from the EBAS database (*http://ebas.nilu.no/*), selecting Ispra as the station of interest.

Table 1. Variables related to short-lived pollutants and radiative forcers measured in 2015

METEOROLOGY	Pressure, temperature, humidity, wind, solar radiation
GAS PHASE	SO_2, NO, NO_X, O_3, CO
PARTICULATE PHASE	For $PM_{2.5}$: PM mass, Cl^-, NO_3^-, SO_4^{2-}, $C_2O_4^{2-}$, Na^+, NH_4^+, K^+, Mg^{2+}, Ca^{2+}, OC, and EC content Number size distribution (10 nm - 10 µm) Aerosol light absorption, scattering and back-scattering coefficients Altitude-resolved aerosol light back-scattering and extinction
PRECIPITATION	Cl^-, NO_3^-, SO_4^{2-}, $C_2O_4^{2-}$, Na^+, NH_4^+, K^+, Mg^{2+}, Ca^{2+} pH, conductivity

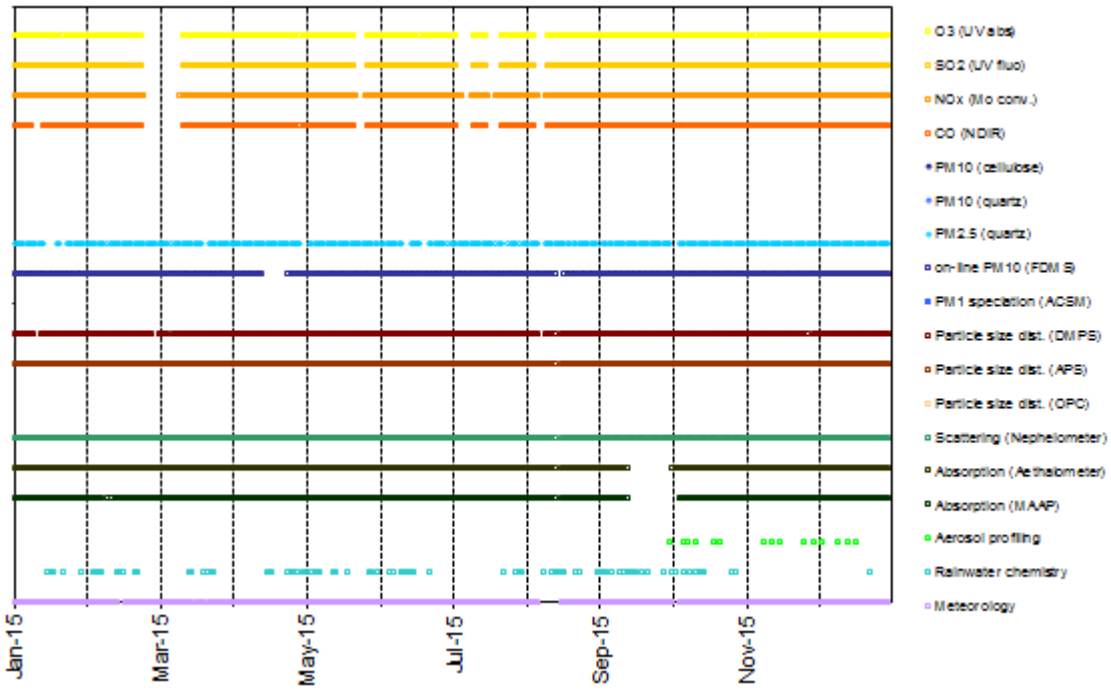

Fig. 13. Year 2015 data coverage at the JRC EMEP-GAW station.

4.2. Measurements and data processing

4.2.1. Air pollutant and short-lived radiative forcer measurements at the JRC- Ispra station in 2015

Since 1985, the JRC-Ispra air monitoring station program evolved significantly (Fig. 13). The measurements performed at the JRC-Ispra EMEP-GAW station in 2015 are listed in Table 1. *Fig. 13* shows the data coverage for 2015.

Meteorological variables were measured continuously, except from August 8th to July 16th. The values measured at the top of the JRC flux tower were used for gap filling.

SO_2, O_3, NOx and CO were measured almost continuously during the year 2015, except for the period 24 Feb. – 11. Mar. due to annual revision of the mobile laboratory and maintenance/linearity checks of all analysers, and for four 5 - 6 day gaps in May, Jul. and Aug., due to power fails.

Particulate matter ($PM_{2.5}$) samples were collected daily and analysed for $PM_{2.5}$ mass (at 20% RH), main ions, OC (organic carbon) and EC (elemental carbon), for the whole of 2015, except for 35 days (sampler breakdowns).

On-line PM_{10} measurements (FDMS-TEOM, Filter Dynamics Measurement System - Tapered Element Oscillating Microbalance) were carried out continuously, except for 14 days in total (breakdowns and maintenance).

Particle number size distributions (10 nm < Dp < 10 µm) and aerosol light scattering were measured almost continuously (> 96% coverage). Aerosol light absorption coefficients were measured almost continuously with a gap from Sep. 14th to Oct. 1st (calibration workshop at the WCAPC in Leipzig).

The Raymetrics Raman LiDAR was re-activated on Nov. 1st, 2015, after the laser was repaired by the manufacturer and reinstalled by the Lidar provider.

Precipitation was collected throughout the year and analysed for pH, conductivity, and main ions (collected water volume permitting).

4.2.2. Measurement techniques

4.2.2.1 On-line Monitoring

Meteorological Parameters

Meteorological data and solar radiation were measured directly at the EMEP station with the instrumentation described below.

WXT510 (S/N: A1410009 & A1410010)

Two WXT510 weather transmitters from Vaisala recorded simultaneously the six weather parameters temperature, pressure, relative humidity, precipitation and wind speed and direction from the top of a 10 m high mast.

The wind data measurements utilise three equally spaced ultrasonic transducers that determine the wind speed and direction from the time it takes for ultrasound to travel from one transducer to the two others. The precipitation is measured with a piezoelectric sensor that detects the impact of individual raindrops and thus infers the accumulated rainfall. For the pressure, temperature and humidity measurements, separate sensors employing high precision RC oscillators are used.

CM11 (S/N: 058911) & CMP 11 (S/N: 070289)

To determine the solar radiation, a Kipp and Zonen CM11 was used. From 23.06.2008 and onwards an additional CMP11 Pyranometer have been installed that measures the irradiance (in W/m^2) on a plane surface from direct solar radiation and diffuse radiation incident from the hemisphere above the device. Both devices were ca. 1.5 m above the ground till Apr 10th, 2013. From Apr. 22nd, the CMP11 S/N 070289 only is installed on the top of the container (3 m above ground). The measurement principle is based on a thermal detector. The radiant energy is absorbed by a black disc and the heat generated flows through a thermal resistance to a heat sink. The temperature difference across the thermal resistance is then converted into a voltage and precisely measured. Both the CM11 & CMP11 feature a fast response time of 12 s, a small non stability of +/-0.5 % and a small non linearity of +/-0.2 %.

Gas Phase Air Pollutants

Sampling

SO_2, NO, NO_x, O_3 and CO were measured from the mobile laboratory (plates number CM328CN), moved to EMEP/GAW provisional station at JRC-Ispra (see Fig. 1) about 500 meters from the old site.

The sampling line at the mobile lab. (inlet about 3.5 m above ground) consists of an inlet made of a stainless steel cylindrical cap (to prevent rain and bugs to enter the line), outside a stainless steel tube (diameter = about 4 cm), inside a Teflon tube (d = about 2.7 cm) and a "multi-channel distributor" tube, with ten ¼" connectors. This inlet is flushed by an about 45 L min^{-1} flow with a fan-coil (*measured with a gas-counter made by RITTER, sn. 11456*). Each instrument samples from the tube with its own pump through a 0.25 inch Teflon line and a 5 µm pore size 47 mm diameter Teflon filter (to eliminate particles from the sampled air). See also Fig. 14.

More details about the mobile lab and instruments (where exactly they were measuring and when) can be found in sections below.

SO_2: UV Fluorescent SO_2 Analyser

Thermo 43iTLE (S/N 1021443379): 01.01-31.12.2015: Provisional station, mobile lab.

At first, the air flow is scrubbed to eliminate aromatic hydrocarbons. The sample is then directed to a chamber where it is irradiated at 214 nm (UV), a wavelength where SO_2 molecules absorb. The fluorescence signal emitted by the excited SO_2 molecules going back to the ground state is filtered between 300 and 400 nm (specific of SO_2) and amplified by a photomultiplier tube. A microprocessor receives the electrical zero and fluorescence reaction intensity signals and calculates SO_2 based on a linear calibration curve.

Calibration was performed with a certified SO_2 standard at a known concentration in air. Zero check was done, using a zero air gas cylinder from Air Liquide, Alphagaz 1, CnHm < 0.5 ppm).

The specificity of the trace level Thermo instrument (TEI 43i-TLE) is that it uses a pulsed lamp. The 43i-TLE's detection limit is 0.05 ppb (about 0.13 µg m^{-3}) over 300 second averaging time, according to the technical specifications.

For more details about the instruments, manuals are available on \\ies.jrc.it\H02\ILargefacilities\ABC-IS\Quality_management\Manuals

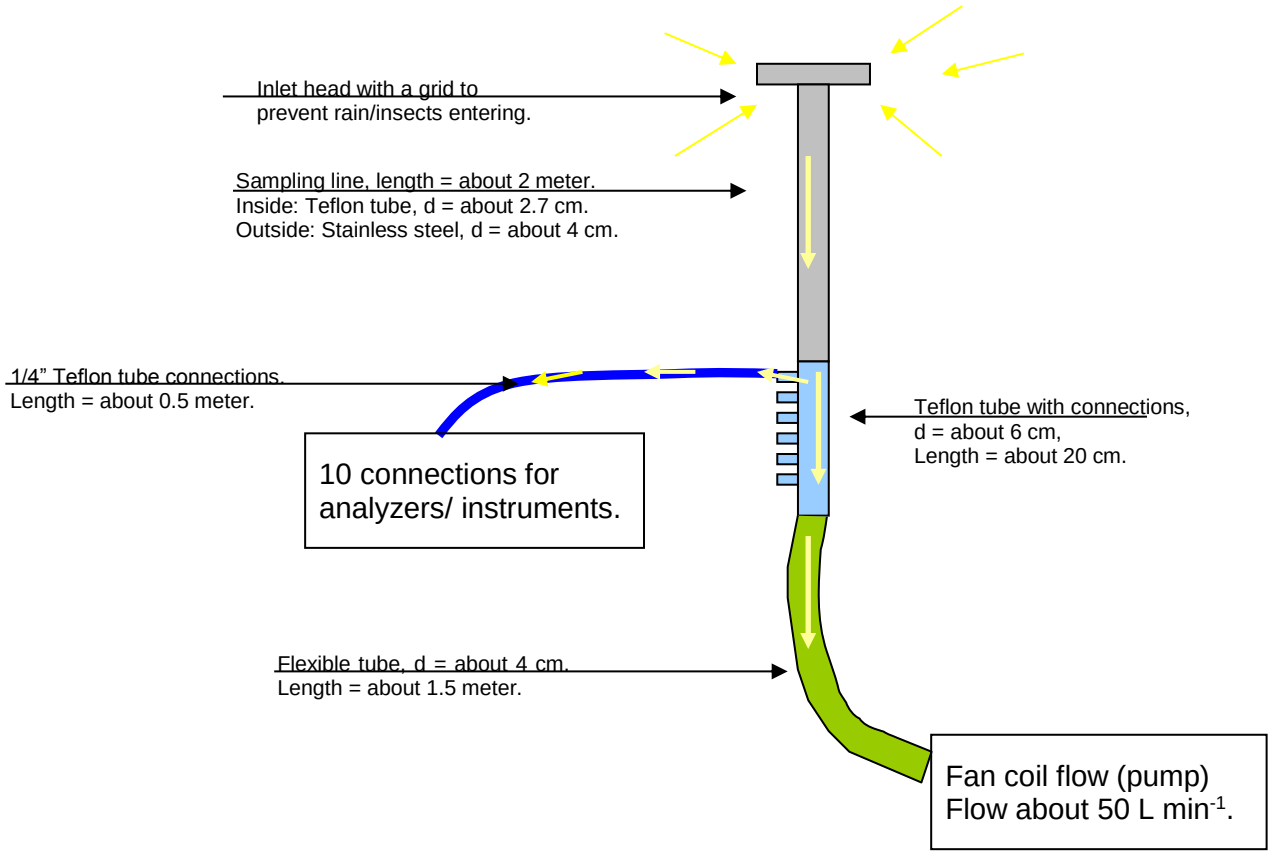

Fig. 14. Sampling inlet system for the gaseous air pollutant at the mobile lab. Inlet for the measurements is about 3.5 m above ground

NO + NO_X: Chemiluminescent Nitrogen Oxides Analyser (NO_2=NO_x-NO)

Thermo 42iTL (S/N 936539473) : 01.01-31.12.2015: Provisional station, mobile lab.

This nitrogen oxide analyser is based on the principle that nitric oxide (NO) and ozone react to produce excited NO_2 molecules, which emit infrared photons when going back to lower energy states:

$$NO + O_3 \rightarrow [NO_2]^* + O_2 \rightarrow NO_2 + O_2 + h\nu$$

A stream of purified air (dried with a Nafion Dryer for 42iTL) passing through a silent discharge ozonator generates the ozone concentration needed for the chemiluminescent reaction. The specific luminescence signal intensity is therefore proportional to the NO concentration. A photomultiplier tube amplifies this signal.

NO_2 is detected as NO after reduction in a Mo converter heated at about 325 °C.

The ambient air sample is drawn into the analyser, flows through a capillary, and then to a valve, which routes the sample either straight to the reaction chamber (NO detection), or through the converter and then to the reaction chamber (NO_X detection). The calculated NO and NO_X concentrations are stored and used to calculate NO_2 concentrations (NO_2 = NO_x - NO), assuming that only NO_2 is reduced in the Mo converter.

Calibration was performed using a zero air gas cylinder (Air Liquide, Alphagaz 1, CnHm<0.5 ppm) and a NO span gas. Calibration with a span gas was performed with a certified NO standard at a known concentration in N_2.

For more details about the instruments, the manuals are available on \\ies.jrc.it\H02\LargeFacilities\ABC-IS\Quality_management\Manuals

O_3: UV Photometric Ambient Analyser

Thermo 49C (S/N 0503110398): 01.01-31.12.2015: Provisional station, mobile lab.

The UV photometer determines ozone concentrations by measuring the absorption of O_3 molecules at a wavelength of 254 nm (UV light) in the absorption cell, followed by the use of Bert-Lambert law. The concentration of ozone is related to the magnitude of the absorption. The reference gas, generated by scrubbing ambient air, passes into one of the two absorption cells to establish a zero light intensity reading, I_0. Then the sample passes through the other absorption cell to establish a sample light intensity reading, I. This cycle is reproduced with inverted cells. The average ratio $R=I/I_0$ between 4 consecutive readings is directly related to the ozone concentration in the air sample through the Beer-Lambert law. Calibration is performed using externally generated zero air and external span gas. Zero air is taken from a gas cylinder (Air Liquide, Alphagaz 1, CnHm < 0.5 ppm). Span gas normally in the range 50 - 100 ppb is generated by a TEI 49C-PS transportable primary standard ozone generator (S/N 0503110396) calibrated/check by ERLAP (European Reference Laboratory of Air Pollution). A Nafion Dryer system is connected to the O_3 instrument.

For more details about the instruments, the manual is available on \\ies.jrc.it\H02\LargeFacilities\ABC-IS\Quality_management\Manuals

CO:Non-Dispersive Infrared Absorption CO Analyser

Horiba AMPA-370 (S/N WYHEOKSN) from 01.01 to 31.12.2015: Provisional station, mobile lab.

In 2015, carbon monoxide (CO) has been continuously monitored using a commercial Horiba AMPA-370 CO monitor based on the principle of non-dispersive infrared absorption (NDIR). The Horiba APMA-370 uses solenoid valve cross flow modulation applying the same air for both the sample and the reference, instead of the conventional technique to apply an optical chopper to obtain modulation signals. With this method the reference air is generated by passing the sample air over a heated oxidation catalyst to selectively remove CO which is then directly compared to the signal of the untreated sample air at a 1 Hz frequency. The result is a very low zero-drift and stable signal over long periods of time.

To reduce the interference from water vapour to about 1% the sample air was dried to a constant low relative humidity level of around 30% applying a Nafion dryer (Permapure MD-070-24P) tube in the inlet stream. The detection limit of the Horiba AMPA-370 is ~20 ppbv for a one minute sampling interval. The overall measurement uncertainty is estimated to be ± 7%.

For more details about the instrument, see the manual available from \\ies.jrc.it\H02\LargeFacilities\ABC-IS\Quality_management\Manuals

In 2015, the gas phase monitors were calibrated seven times with suitable span gas cylinders and zero air (see text for more details). Sampling flow rates are as follow:

Compounds	Flow rates ($L\ min^{-1}$)
SO_2	0.5
NO, NO_x	1.0/1.3
O_3	0.7
CO	1.5

Atmospheric Particles

Sampling conditions

Since 2008, all instruments for the physical characterization of aerosols (Multi-Angle Absorption Photometer, Aethalometer, Nephelometer, Aerodynamic Particle Sizer, Differential Mobility Particle Sizer) sample isokinetically from an Aluminium inlet pipe (diameter = 15 cm, length of horizontal part ~280 cm and vertical part ~220 cm) described in Jensen et al., 2010. The Tapered Element Oscillating Micro-balances (FDMS-TEOMs) used their own inlet systems. The MAAP sampled from the main inlet through Nafion dryers at a flow rate of 800 L hr^{-1} from Jan. to Oct, and 480 L hr^{-1} from Oct to Dec.

The size dependent particle losses along the pipe radius were determined by measuring the ambient aerosol size distribution with two DMPS at the sampling points P0 and P2 for different radial positions relative to the tube centre (0, 40 and 52 mm) at P2 (Gruening et al., 2009). Data show a small loss of particles towards the rim of the tube can be observed, but it stays below 15 %. The bigger deviation for particles smaller than 20 nm is again a result of very small particle number concentrations in this diameter range and thus rather big counting errors.

PM_{10} mass concentration: Tapered Element Oscillating Mass balance (TEOM), Series 1400a

Thermo FDMS – TEOM (S/N 140AB233870012 & 140AB253620409)

The Series 1400a TEOM® monitor incorporates an inertial balance patented by Rupprecht & Patashnick, now Thermo. It measures the mass collected on an exchangeable filter cartridge by monitoring the frequency changes of a tapered element. The sample flow passes through the filter, where particulate matter is collected, and then continues through the hollow tapered element on its way to an electronic flow control system and vacuum pump. As more mass collects on the exchangeable filter, the tube's natural frequency of oscillation decreases. A *direct* relationship exists between the tube's change in frequency and mass on the filter. The TEOM mass transducer does not require recalibration because it is designed and constructed from non-fatiguing materials. However, calibration is yearly verified using a filter of known mass.

The instrument set-up includes a Sampling Equilibration System (SES) that allows a water strip-out without sample warm up by means of Nafion Dryers. In this way the air flow RH is reduced to < 30%, when TEOM® operates at 30 °C only. The Filter Dynamic Measurement System (FDMS) is based on measuring changes of the TEOM filter mass when sampling alternatively ambient and filtered air. The changes in the TEOM filter mass while sampling filtered air is attributed to sampling (positive or negative) artefacts, and is used to correct changes in the TEOM filter mass observed while sampling ambient air.

Particle number size distribution: Differential Mobility Particle Sizer (DMPS)

DMPS "B, DMA serial no. 158", CPC TSI 3772 (S/N 70847419 and 3772133103), neutraliser ^{85}Kr 10 mCi (2007)

The Differential Mobility Particle Sizer consists of a home-made medium size (inner diameter 50 mm, outer diameter 67 mm and length 280 mm) Vienna-type Differential Mobility Analyser (DMA) and a Condensation Particle Counter (CPC), TSI 3772. Its setup follows the EUSAAR specifications for DMPS systems.

DMA's use the fact that electrically charged particles move in an electric field according to their electrical mobility. Electrical mobility depends mainly on particle size and electrical charge. Atmospheric particles are brought in the bipolar charge equilibrium in the bipolar diffusion charger (Eckert & Ziegler neutralizer with 370 MBq): a radioactive source (^{85}Kr) ionizes the surrounding atmosphere into positive and negative ions. Particles carrying a high charge can discharge by capturing ions of opposite polarity. After a very short time, particles reach a charged equilibrium such that the aerosol carries the bipolar Fuchs-Boltzman charge distribution. A computer program sets stepwise the voltage between the 2 DMA's electrodes (from 10 to 11500 V). Negatively charged particles are so selected according to their mobility. After a certain waiting time, the CPC measures the number concentration for each mobility bin. The result is a particle mobility distribution. The number size distribution is calculated from the mobility distribution by an inversion routine (from Stratmann and Wiedensohler, 1996) based on the bipolar charge distribution and the size dependent DMA transfer function. The DMPS measured aerosol particles in the range 10 – 600 nm during an 8 minute cycle until 12.06.2009 and afterwards in the range 10 to 800 nm with a 10 minute cycle. It records data using 45 size channels for high-resolution size information. This submicrometer particle sizer is capable of measuring concentrations in the range from 1 to 2.4 x 10^6 particles cm^{-3}. Instrumental parameters that are necessary for data evaluation such as flow rates, relative humidity, ambient pressure and temperature are measured and saved as well.

The CPC detection efficiency curve and the particle diffusion losses in the system are taken into account at the data processing stage.

Accessories include:

- FUG High voltage cassette power supplies Series HCN7E – 12500 Volts.

- Rotary vacuum pump vane-type (sampling aerosol at 1 LPM)

- Controlled blower (circulating dry sheath air)

- Sheath air dryer only using silica gel until 27.10.2009, thereafter sheath and sample air dryer using Nafion dryer; this mean that the DMPS started to sample in dry conditions from 27 October 2009 onwards.

- Mass flow meter and pressure transducer (to measure sheath air and sample flows).

Particle number size distribution: Aerodynamic Particle Sizer (APS)

APS TSI 3321 (S/N 70535014 & S/N 1243)

The APS 3321 is a time-of-flight spectrometer that measures the velocity of particles in an accelerating air flow through a nozzle.

Ambient air is sampled at 1 L min^{-1}, sheath air (from the room) at 4 L min^{-1}. In the instrument, particles are confined to the centre-line of an accelerating flow by sheath air. They then pass through two broadly focused laser beams, scattering light as they do so. Side-scattered light is collected by an elliptical mirror that focuses the collected light onto a solid-state photodetector, which converts the light pulses to electrical pulses. By electronically timing between the peaks of the pulses, the velocity can be calculated for each individual particle.

Velocity information is stored in 1024 time-of-flight bins. Using a polystyrene latex (PSL) sphere calibration, which is stored in non-volatile memory, the APS Model 3321 converts each time-of-flight measurement to an aerodynamic particle diameter. For convenience, this particle size is binned into 52 channels (on a logarithmic scale).

The particle range spanned by the APS is from 0.5 to 20 µm in both aerodynamic size and light-scattering signal. Particles are also detected in the 0.3 to 0.5 µm range using light-scattering alone, and are binned together in one channel. The APS is also capable of storing correlated light-scattering-signal. *dN/dLogDp* data are averaged over 10 min.

Particle scattering and back-scattering coefficient

Nephelometer TSI 3563 (S/N 1081 & S/N 142101)

The integrating nephelometer is a high-sensitivity device capable of measuring the scattering properties of aerosol particles. The nephelometer measures the light scattered by the aerosol and then subtracting light scattered by the walls of the measurement chamber, light scattered by the gas, and electronic noise inherent in the detectors.

Dried ambient air is sampled at 5.3 L min^{-1} since 18.11.2009 from a PM10 inlet. .

The three-color detection version of TSI nephelometer detects scattered light intensity at three wavelengths (450, 550, and 700 nm). Normally the scattered light is integrated over an angular range of 7–170° from the forward direction, but with the addition of the backscatter shutter feature to the Nephelometer, this range can be adjusted to either 7–170° or 90–170° to give total scatter and backscatter signals. A 75 Watt quartz-halogen white lamp, with a built-in elliptical reflector, provides illumination for the aerosol. The reflector focuses the light onto one end of an optical pipe where the light is carried into the internal cavity of the instrument. The optical pipe is used to thermally isolate the lamp from the sensing volume. The output end of the optical light pipe is an opal glass diffuser that acts as a *quasi*-cosine (Lambertian) light source. Within the measuring volume, the first aperture on the detection side of the instrument limits the light integration to angles greater than 7°, measured from the horizontal at the opal glass. On the other side, a shadow plate limits the light to angles less than 170°. The measurement volume is defined by the intersection of this light with a viewing volume cone defined by the second and fourth aperture plates on the detection side of the instrument. The fourth aperture plate incorporates a lens to collimate the light scattered by aerosol particles so that it can be split into separate wavelengths. The nephelometer uses a reference chopper to calibrate scattered signals. The chopper makes a full rotation 23 times per second. The chopper consists of three separate areas labelled "signal", "dark", and "calibrate".

The signal section simply allows all light to pass through unaltered. The dark section is a very black background that blocks all light. This section provides a measurement of the photomultiplier tube (PMT) background noise. The third section is directly illuminated this section to provide a measure of lamp stability over time. To reduce the lamp intensity to a level that will not saturate the photomultiplier tubes, the calibrate section incorporates a neutral density filter that blocks approximately 99.9 % of

the incident light. To subtract the light scattered by the gas portion of the aerosol, a high-efficiency particulate air (HEPA) filter is switched in line with the inlet for 300 s every hour. This allows compensation for changes in the background scattering of the nephelometer, and in gas composition that will affect Rayleigh scattering of air molecules with time. When the HEPA filter is not in line with the inlet, a small amount of filtered air leaks through the light trap to keep the apertures and light trap free of particles. A smaller HEPA filter allows a small amount of clean air to leak into the sensor end of the chamber between the lens and second aperture. This keeps the lens clean and confines the aerosol light scatter to the measurement volume only.

Nephelometer data are corrected for angular non idealities and truncation errors according to Anderson and Ogren, 1998. From 18.11.2009 onwards, a Nafion dryer has been installed at the inlet to measure dry aerosols. Internal RH generally ranges from 0 to 35 % (average 17%, 99th percentile 31% in 2014). At 35% RH, aerosol scattering would be on average increased by about 15% compared to 0% RH in Ispra (Adam et al., 2012). However, aerosol particle scattering coefficients presented in this report are **not** corrected for RH effects, except when specified.

Particle absorption coefficient

Aethalometer Magee AE-31 ('A' S/N 408:0303 & 'B' S/N 740:0609)

The principle of the Aethalometer is to measure the attenuation of a beam of light transmitted through a filter, while the filter is continuously collecting an aerosol sample. Suction is provided by an internally-mounted pump. Attenuation measurements are made at successive regular intervals of a time-base period. The objectives of the Aethalometer hardware and software systems are as follows:

(a) to collect the aerosol sample with as few losses as possible on a suitable filter material;

(b) to measure the optical attenuation of the collected aerosol deposit as accurately as possible;

(c) to calculate the rate of increase of the equivalent black carbon (EBC) component of the aerosol deposit and to interpret this as an EBC concentration in the air stream;

(d) to display and record the data, and to perform necessary instrument control and diagnostic functions.

The optical attenuation of the aerosol deposit on the filter is measured by detecting the intensity of light transmitted through the spot on the filter. In the AE-31, light sources emitting at different wavelengths (370, 470, 520, 590, 660, 880 and 950 nm) are also installed in the source assembly. The light shines through the lucite aerosol inlet onto the aerosol deposit spot on the filter. The filter rests on a stainless steel mesh grid, through which the pumping suction is applied. Light penetrating the diffuse mat of filter fibres can also pass through the spaces in the support mesh. This light is then detected by a photodiode placed directly underneath the filter support mesh. As the EBC content of the aerosol spot increases, the amount of light detected by the photodiode will diminish.

For better accuracy, further measurements are necessary: the amount of light penetrating the combination of filter and support mesh is relatively small, and a correction is needed for the 'dark response signal' of the overall system. This is the electronics' output when the lamps are off: typically, it may be a fraction of a percent of the response when the lamps are on. To eliminate the effect of the dark response, we take 'zero' readings of the system response with the lamps turned off, and subtract this 'zero' level from the response when the lamps are on.

The other measurement necessary is a 'reference beam' measurement to correct for any small changes in the light intensity output of the source. This is achieved by a second photodiode placed under a different portion of the filter that is not collecting the aerosol, on the left-hand side where the fresh tape enters. This area is illuminated by the same lamps. If the light intensity output of the lamps changes slightly, the response of this detector is used to mathematically correct the 'sensing' signal. The reference signal is also corrected for dark response 'zero' as described above.

The algorithm in the computer program (see below) can account for changes in the lamp intensity output by always using the ratio quantity [Sensing]/[Reference]. As the filter deposit accumulates EBC, this ratio will diminish.

In practice, the algorithm can account for lamp intensity fluctuations to first order, but we find a residual effect when operating at the highest sensitivities. To minimize this effect and to realize the full potential of the instrument, it is desirable for the lamps' light output intensity to remain as constant as possible from one cycle to the next, even though the lamps are turned on and off again. The computer program monitors the repeatability of the reference signal, and issues a warning message if the fluctuations are considered unacceptable. When operating properly, the system can achieve a reference beam repeatability of better than 1 part in 10000 from one cycle to the next. The electronics circuit

board converts the optical signals directly from small photocurrents into digital data, and passes it to the computer for calculation. A mass flow meter monitors the sampled air flow rate. These data and the result of the EBC calculation are written to disk and displayed on the front panel of the instrument.

Aethalometer data are corrected for the shadowing effect and for multiple-scattering in the filter to derive the aerosol absorption coefficient (Arnott et al., 2005) with a correction factor C = 3.60, 3.65, and 3.95 for green 450, 550 and 660 nm, respectively.

Multi Angle Absorption Photometer (S/N 4254515)

A new Multi Angle Absorption Photometer (MAAP) model 5012 from Thermo Scientific has been installed at the EMEP station in September 2008 and provides equivalent black carbon concentrations (EBC) and aerosol absorption (α) data at a nominal wavelength of 670 nm. Note that during a EUSAAR workshop (www.eusaar.org) in 2007 it has been observed that the operating wavelength of all MAAP instruments present at that workshop was 637 nm with a line width of 18 nm fwhm. The operating wavelength of this MAAP instrument has not been measured yet, therefore it is assumed to work at 670 nm as stated by the manufacturer.

The MAAP is based on the principle of aerosol-related light absorption and the corresponding atmospheric equivalent black carbon (EBC) mass concentration. The Model 5012 uses a multi angle absorption photometer to analyse the modification of scattering and absorption in the forward and backward hemisphere of a glass-fibre filter caused by deposited particles. The internal data inversion algorithm of the instrument is based on a radiation transfer model and takes multiple scattering processes inside the deposited aerosol and between the aerosol layer and the filter matrix explicitly into account (see Petzold et al., 2004).

The sample air is drawn into the MAAP and aerosols are deposited onto the glass fibre filter tape. The filter tape accumulates the aerosol sample until a threshold value is reached, then the tape is automatically advanced. Inside the detection chamber (Fig. 15), a 670-nanometer light emitting diode is aimed towards the deposited aerosol and filter tape matrix. The light transmitted into the forward hemisphere and reflected into the back hemisphere is measured by a total of five photo-detectors. During sample accumulation, the light intensities at the different photo-detectors change compared to a clean filter spot. The reduction of light transmission, change in reflection intensities under different angles and the air sample volume are continuously measured during the sample period. With these data and using its proprietary radiation transfer scheme, the MAAP calculates the equivalent black carbon concentration (EBC) as the instruments measurement result.

Using the specific absorption cross section $\sigma_{\square BC}$ = 6.6 m^2/g of equivalent black carbon at the operation wavelength of 670 nm, the aerosol absorption (α) at that wavelength can be readily calculated as:

$$\alpha = EBC \times \sigma_{BC} \qquad Eq.\ 1$$

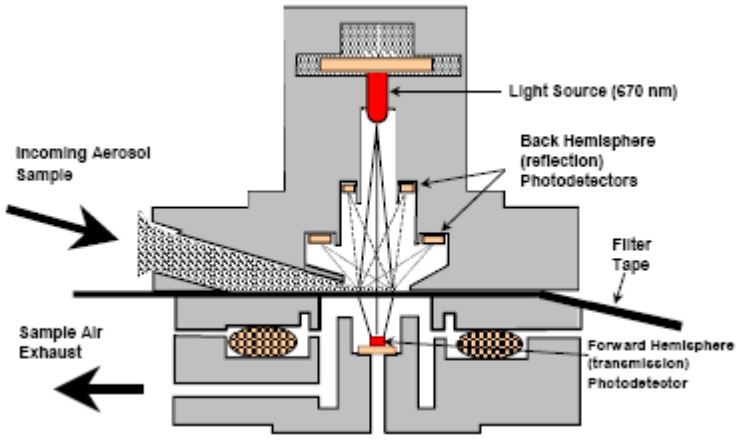

Fig. 15: MAAP detection chamber (sketch from the manual of the instrument).

Range-resolved aerosol light backscattering and extinction

Raymetrics Aerosol Raman Lidar (S/N 400-1-12, QUANTEL Brilliant B Laser and cooler S/N 120059004 and S/N 120034401, LICEL Transient Recorder & Hi Voltage Supply S/N BS3245 and BS3245b, industrial PC S/N TPL-1571H-D3AE)

LIDAR measurements are based on the time resolved detection of the backscattered signal of a short laser pulse that is sent into the atmosphere (for an introduction see Weitkamp, 2005). Using the speed of light, time is converted to the altitude where the backscattering takes place. Utilising some assumptions about the atmospheric composition, aerosol backscattering and extinction coefficients as well as aerosol optical thickness can be derived using the LIDAR equation. The received power P of the detector is therein given as a function of distance and wavelength by *Eq. 2*:

$$P(R,\lambda) = P_0 \, c\tau/2 \, A\eta \frac{O(R)}{R^2} \beta(R,\lambda) \exp\left(-2\int_0^R \alpha(r,\lambda) dr \right)$$

Eq. 2: P_0: Power of the laser pulse, c: speed of light, τ: laser pulse length, A: area of the telescope, η: system efficiency, R: distance, O: overlap function (between laser beam and receiving optics field of view), λ: wavelength, β: backscatter coefficient, α: absorption coefficient

The instrument itself was installed on October 8-11th, 2012, and accessories (including radar) on December 11-13, 2012. This lidar emits at 3 wavelengths from IR to UV (1064 nm, polarised-532 nm, 355 nm) and records at 5 wavelengths, namely the emission wavelengths and two vibrational Raman channels at 387 and 607 nm. Measurements at 1064 nm, 532 nm, and 355 nm provide aerosol backscatter profiles, while measurements at 687 nm, and 387 nm provide aerosol extinction profiles during the dark hours of the day. The 532 nm signal depolarisation is also measured. In 2015, the instrument was run with a 5 min integration time during time slots covering noon (Mondays) and sunset (Mondays and Thursdays) according to the ACTRIS schedule, and during Calipso overpasses (about once every 8 days at 01:40 or 12:30). Data are inverted using the online Single Calculus Chain developed by EARLINET. Data are being processed to cope with new requirements for submitting data to the ACTRIS-EARLINET data bank.

Page left intentionally blank

4.2.2.2 Sampling and off-line analyses

Particulate Matter

Particle sampler: Partisol 2025 S/N 2025B22156220203
Micro-balance: MC5 S/N 50208287
Ion Chromatographs: ICS 2000 S/N 07101404 and 07101405 and DX-120 (Jan.-Feb.)
OC-EC analyser: Sunset Lab OCEC analyser S/N 173 and S/N 200 (Jan.)

$PM_{2.5}$ was continuously sampled at 16.7 L min^{-1} on quartz fibre filters with a Partisol sampler equipped with a carbon honeycomb denuder. The sampled area is 42 mm. Filters were from PALL Life Sciences (type TISSUEQUARTZ 2500QAT-UP). Filter changes occurred daily at 08:00 UTC.

Filters were weighed at 20 % RH before and after exposure with a microbalance Sartorius MC5 placed in a controlled (dried or moisture added and scrubbed) atmosphere glove box. They were stored at 4 °C until analysis.

Main ions (Cl^-, NO_3^-, SO_4^{2-}, $C_2O_4^{2-}$, Na^+, NH_4^+, K^+, Mg^{2+}, Ca^{2+}) were analysed by ion chromatography with electrochemical eluent suppression (ICS2000 for the whole year and Dionex DX 120 for Jan. and Feb.) after extraction of the soluble species in an aliquot of 16 mm Ø in 10 ml 18.2 MOhm cm resistivity water (Millipore mQ).

Organic and elemental carbon (OC+EC) were analysed using a Sunset Dual-optical Lab Thermal-Optical Carbon Aerosol Analyser (S/N 173-5 and S/N 200 for Jan.). $PM_{2.5}$ samples were analysed using the EUSAAR-2 thermal protocol that has been developed to minimize biases inherent to thermo-optical analysis of OC and EC (Cavalli et al., 2010), which is described in the table below.

No measurement of PM_{10} or PM_{coarse} was performed in 2015.

Table 2: Parameters of the EUSAAR-2 analytical protocol

Fraction Name Sunset Lab.	Plateau Temperature (°C)	Duration (s)	Carrier Gas
OC 1	200	120	He 100%
OC 2	300	150	He 100%
OC 3	450	180	He 100%
OC 4	650	180	He 100%
cool down		30	He 100%
EC1	500	120	He:O_2 98:2
EC2	550	120	He:O_2 98:2
EC3	700	70	He:O_2 98:2
EC4	850	110	He:O_2 98:2

Wet-only deposition

Precipitation sampler: Eigenbrodt *Model NSA 181/KS* S/N 3313 and 3312
Conductimeter and pH-meter: Sartorius Professional Meter PP-50 S/N 16350322.
Ion Chromatographs: ICS 2000 S/N 07101404 and 07101405

For precipitation collection, two wet-only samplers were used that automatically collect the rainfall in a 1 L polyethylene container. The collection surface is 550 cm^2. 24-hr integrated precipitation samples (if any) are collected every day starting at 8:00 UTC. All collected precipitation samples were stored at 4 °C until analyses (ca. every 3 months).

Analyses include the determinations of pH and conductivity at 25 °C and principal ion concentrations (Cl^-, NO_3^-, SO_4^{2-}, $C_2O_4^{2-}$, Na^+, NH_4^+, K^+, Mg^{2+}, Ca^{2+}) by ion chromatography with electrochemical eluent suppression.

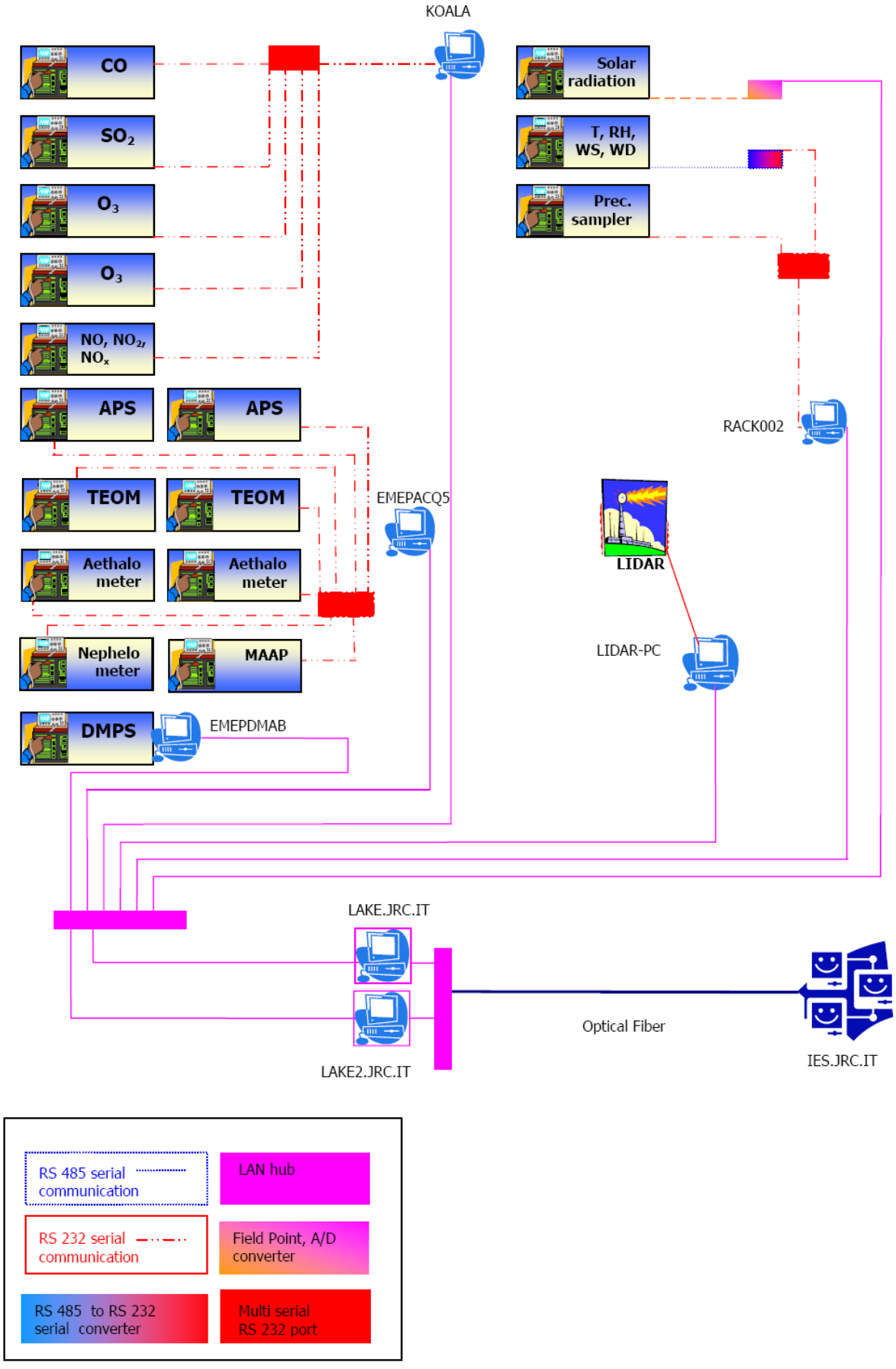

Fig. 16: Set-up of the EMEP- GAW station Data Acquisition System.

4.2.3. On-line data acquisition system/data management

The JRC EMEP-GAW station Data Acquisition System (DAS) is a specifically tailored set of hardware and software (developed by the Air and Climate unit, in collaboration with NOS s.r.l), designed to operate instruments, acquire both analogue and digital output from instruments and store pre-processed measurement data into a database for further off-line evaluation. The DAS operated and controlled the instrumentation during 2015. No updates were implemented.

The software environment of the DAS is Labview 7.1 from National Instruments and the database engine for data storage is Microsoft SQL Server 2008.

The DAS is designed to continuously run the following tasks:

- Start of the data acquisition at a defined time (must be full hour);
- Choose the instruments that have to be handled;
- Define the database path where data will be stored (primary in the network, secondary local on the acquisition machine);
- Define the period (10 minutes currently used) for storing averaged data, this is the data acquisition cycle time;
- Obtain data (every 10 seconds currently set) for selected instruments within the data acquisition cycle:
  - For analogue instruments (currently only the CM11 and CMP11 Pyranometers), apply the calibration constants to translate the readings (voltages or currents) into analytical values;
  - Send commands to query instruments for data or keep listening the ports for instruments that have self-defined output timing;
  - Scan instruments outputs to pick out the necessary data;
- Calculate average values and standard deviations for the cycle period;
- Query instruments for diagnostic data (when available), once every 10 minutes;

- Store all data in a database
  - With a single timestamp for the gas analysers, FDMS-TEOM and Nephelometer
  - With the timestamp of their respective measurement for all other instruments.

The following instruments are managed with the DAS (Fig. 16), using three PCs (currently called Emepacq5, Koala and Rack002):

Emepacq5:

- Number size distribution for particles diameter >0.500 µm, APS
- On-line FDMS-TEOMs
- Aerosol light absorption, Aethalometer
- Aerosol light absorption, MAAP
- Aerosol light scattering, Nephelometer

Koala:

- Reactive gases: CO, SO2, NO, NO_2, NO_x, O_3

Rack002:

- Solar radiation
- Weather transmitter (temperature, pressure, relative humidity, wind speed and direction, precipitation)
- Precipitation data

Data acquired are stored in a Microsoft SQL Server 2008 database on the central database ***emep_db*** hosted on the pc **Lake2.jrc.it**. If local network is not available, data are stored in a local database on the acquisition pc itself. Each pc has a software for the synchronisation of **emep_db** with **local db.**

The PC "**Lake.jrc.it**" connects the laboratory to the JRC network (*ies.jrc.it* domain) via optical lines. The schematic setup of the data acquisition system is shown in Fig. 16.

The acquisition time is locally synchronized for all PCs via a network time server running on lake and is kept at UTC, without adjustment for summer/winter time. Data are collected, called ***emep_db*** that runs on "**Lake2.jrc.it**".

Lake is the user gateway for the Station user, to allow granted staff to remotely access the acquisitions computers. This PC is also used to share information (life cycle sheets, lidar data) between IES domain and the Station network.

In the web site the projects to which ABC-IS contributes and contact persons can also be retrieved.

The web site runs over two machines. The first is the web server, **ccuprod2**, in the DMZ (demilitarized zone), where the web page code runs and is managed by the Air and Climate Unit IT staff. The development environment was Python and Ajax. The second computer, **emepimag.jrc.it,** in the JRC network, queries the database for data, generate plots and store plots in a folder in ccuprod2, to make them available to the internet. This second machine is managed by ABC-IS data management team and the software has been developed in C-sharp.

4.2.4. Data evaluation

The structured data evaluation system (EMEP_Main.m) with a graphic user interface (see Fig. 17) has been used with Matlab Release R2007b (www.mathworks.com) as the programming environment. The underlying strategy of the program is:

1) Load the necessary measurement data from all selected instruments from the data acquisition database as stored by the DAS (source database).
2) During the weekly data evaluation, the data are export into excel sheets for a first data process and flag.
3) Calculate outputs that require data from more than one instrument..
4) The files flagged are then imported into the database.
5) Generate the Level 1 data.
6) Perform the calculation of hourly averages for all parameters.
7) Store hourly averages (Level 2 data) of all results into the data base, organized into different tables for gas phase, aerosol phase and meteorological data.
8) With the new data evaluation system, at the end of each year, data are ready for the data submission.

Only the evaluation of gas phase data has an automatic removal algorithm for outliers / spikes implemented: d_i = 10 minute average value at time i, std_i = standard deviation for the 10 minute average (both saved in the raw data)

if $std_i > 100 \cdot \overline{std}$ and $|d_i - d_{i\pm1}| > 10 \cdot \overline{std}$

$\Rightarrow$ $d_i = 1/2\left(d_{i-1} + d_{i+1}\right)$ for d_{i-1} **and** d_{i+1} **no** outliers,

otherwise $d_i = missig\ data$.

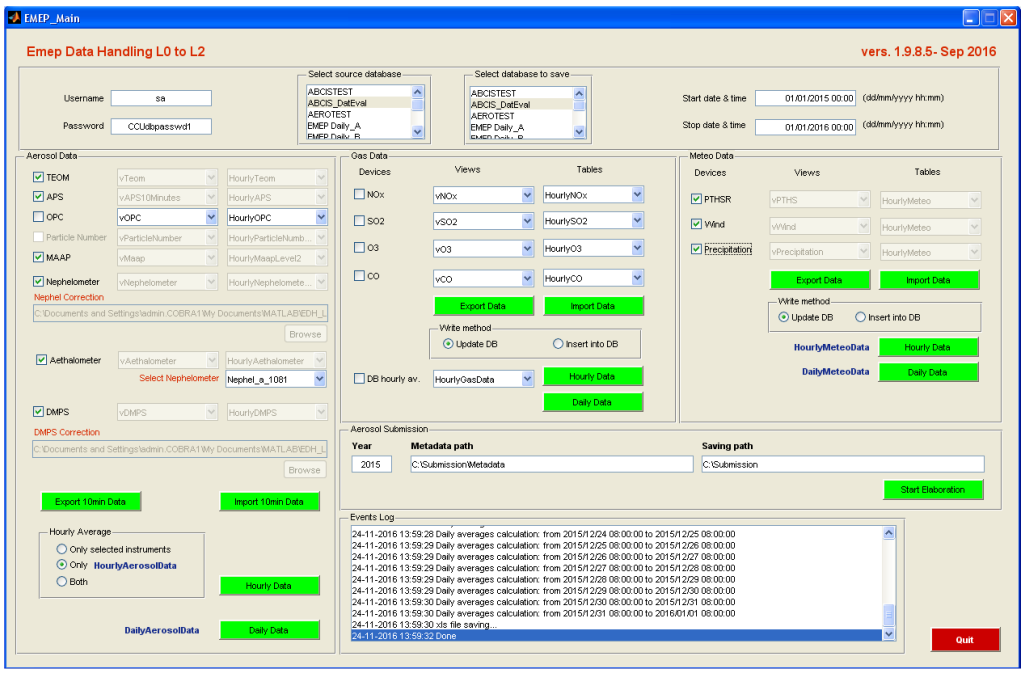

Fig. 17. Graphic user interface of the EMEP-GAW station data evaluation.

This algorithm corrects for single point outliers and removes double point outliers. All other situations are considered correct data. To check these data and to exclude outliers for all other measurements, a visual inspection of the 10 min data needs to be performed.

In addition, quick looks of evaluated data for selected time periods can be produced as well as printed timelines in the pdf-format for the evaluated data. All database connections are implemented via ODBC calls (Open DataBase Connectivity) to the corresponding Microsoft SQL server 2008.

Daily averages ($8:00 < t \leq 8:00 +1$ day) of all parameters stored in the hourly averages database can be calculated and are subsequently stored in a separate Microsoft SQL Server 2008 database.

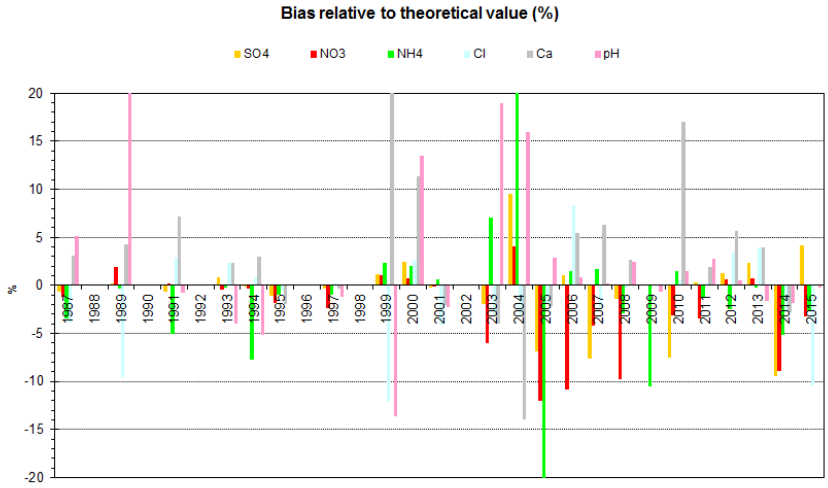

Fig. 18. EMEP inter-laboratory comparisons for rainwater analyses (1987-2015): JRC-IES results.

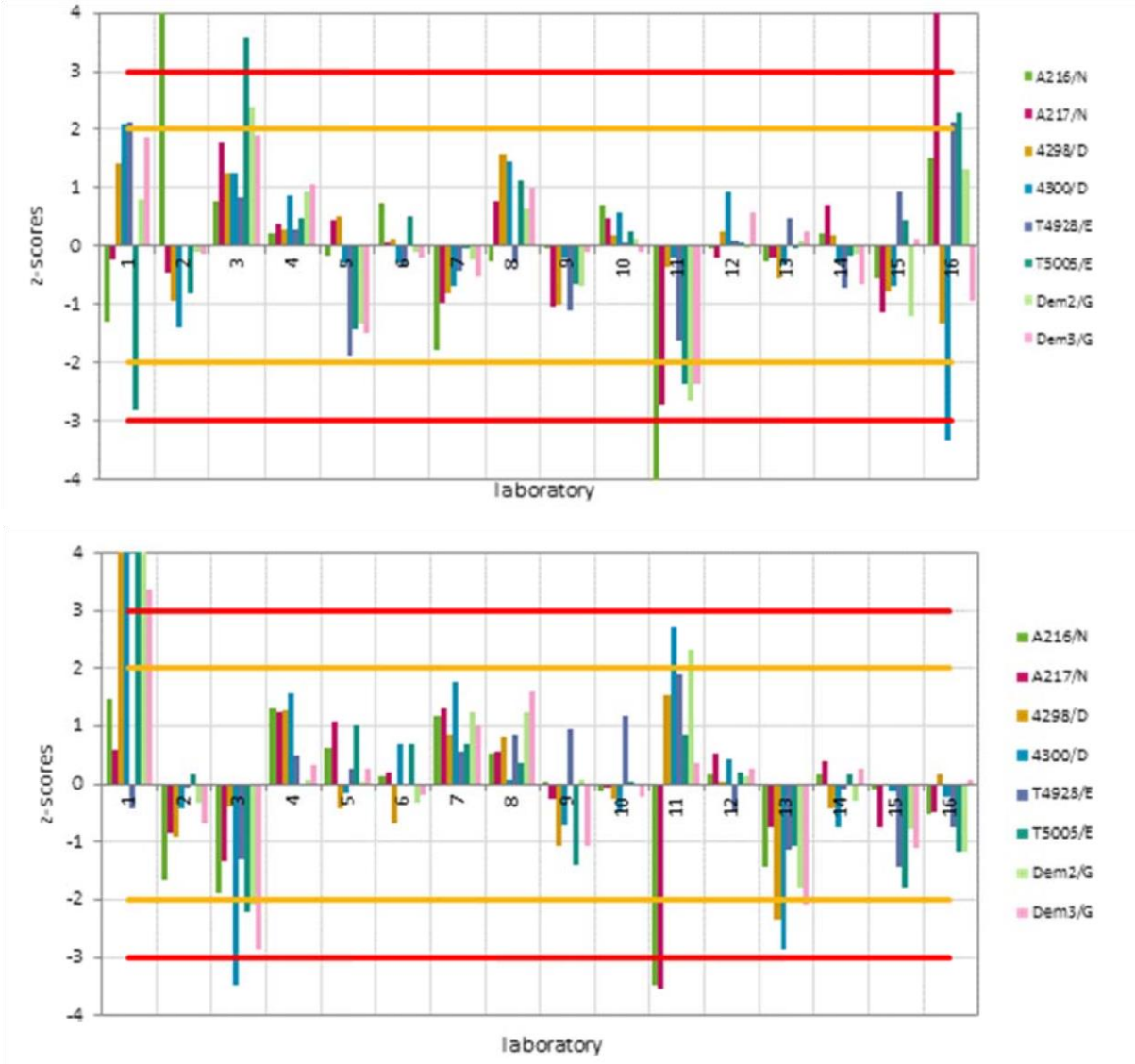

Fig. 19. JRC-IES instruments' (15) performance for the determination of (top) total carbon (TC) and (bottom) elemental carbon (EC/TC ratio) during the ACTRIS inter-laboratory comparison 2015.

4.3. Quality assurance

At JRC level the quality system is based on the Total Quality Management philosophy the implementation of which started at the Environment Institute in December 1999. We have been working under ISO 9001 and ISO 14001 since 2010 (more information about our QMS system can also be found in the chapter "Quality management system"). Lacking personnel to specifically follow this business, the JRC-Ispra station for atmospheric research did not renew the accreditation for the monitoring of SO_2, NO, NO_2 and O_3 under EN 45001 obtained in 1999. However, most measurements and standardized operating procedures are based on recommendations of the EMEP manual (1995, revised 1996; 2001; 2002; 2014), WMO/GAW 153, ISO and CEN standards. Moreover, the JRC-Ispra gas monitors and standards are checked by the European Reference Laboratory for Air Pollution (ERLAP) regularly. This includes annual preventive maintenance, linearity check and Gas Phase Titration (for NO_x). For on-line aerosol instruments, the only inter-comparison workshop took place in Sep. 2015 (absorption spectrometers) at the world calibration centre for aerosol physics (WCCAP) in Leipzig (D) under ACTRIS (www.actris.net). In addition, the EMEP-GAW station was favourably audited on March 22-24.03, 2010, in the frame of EUSAAR (www.eusaar.net) by Dr. T. Tuch, World Calibration Centre for Aerosol Physics (WCCAP) as described in a specific report.

Ion analysis quality was checked through the 31th annual EMEP inter-laboratory comparison (Fig. 18). In the 2015 exercise, all ions measured in the rain water synthetic samples provided by NILU were determined with an error ≤10%, except K^+ (-17%). The mean error for pH measurements was -0.2%. The data quality objective within EMEP is 10% accuracy or better for NO_3^- and SO_4^{2-} and 15% accuracy or better for other components.

The inter-laboratory comparison for organic and elemental carbon analyses organized in the frame of the competitive project ACTRIS in 2015 indicate no systematic bias for the determination of total carbon, and a slight systematic negative bias in the determination of EC compared to the average of the participants (Fig. 19).

Data quality for other measurements is also checked whenever possible through comparison among different instruments (for gases), mass closure (for PM) and ion balance (for precipitation) exercises.

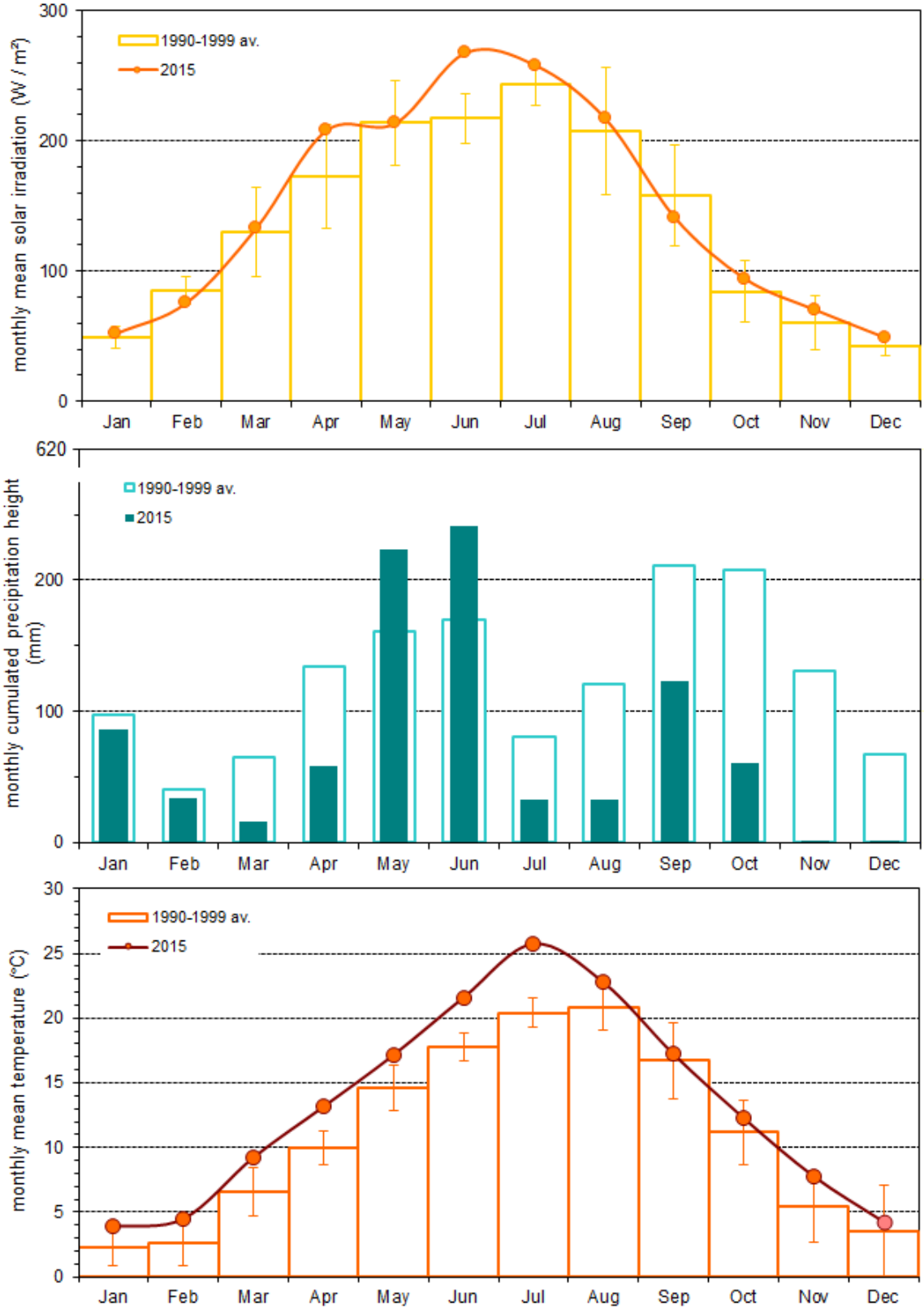

Fig. 20. Solar global irradiation, precipitation amount, and temperature monthly values observed at the EMEP-GAW station of the JRC-Ispra in 2015, compared to the 1990-1999 period ± standard deviations.

4.4. Results of the year 2015

4.4.1. Meteorology

Meteorological data were acquired directly at the EMEP site using a Pyranometer (solar radiation) and a weather transmitter (T, P, RH, precipitation) located at the provisional site at 4 and 5 m above the ground, respectively. For 16 days (of which 9 in August) meteorological data were obtained from the ABC-IS forest flux tower top measurements. In Fig. 20, monthly values of these meteorological variables for 2015 are compared to the 1990-1999 average used as reference period.

April and June were significantly sunnier compared to average. 2015 as a whole was warmer compared to the reference period, especially from March to July.

March, August, October and above all November and December were particularly dry, while May and June were a little wetter than usual. The total yearly rainfall was 1190 mm, i.e. much less than the 1990-1999 average (1484 mm).

4.4.2. Gas phase air pollutants

SO_2, CO, NOx and O_3 were measured almost continuously during the year 2015, except for a few gaps in Feb.-March, May, July and August (annual data coverage > 87%). Expanded uncertainties were calculated to be 8% for SO_2, 7% for CO, 12% + 1.0 ppb for NO, 9% +1.4 ppb for NO_2 and 7% for O_3, which is in line with the *European Directive 2008/50/EC* (less than 15 % at the limit value). To render the time series comparable to the historical data acquired at the EMEP-GAW site at Bd 77p, *10 min NOx data were flagged for local contamination (8% of the data points), and hourly (and daily) averages were computed excluding the data points for which local contamination was identified*.

In 2015, the seasonal variations in SO_2, NO, NO_2, NO_x and O_3 were similar to those observed over the 1990-1999 period (Fig. 21). Concentrations are generally highest during wintertime for primary pollutants (SO_2, CO, NO_x), and in summertime for O_3. The higher concentrations of SO_2, CO, NO_x in winter result mainly from a least dispersion of pollutant during cold months (low boundary layer height and stagnant conditions), whereas the high concentration of O_3 during summer is due to enhanced photochemical production.

SO_2 concentrations (average = 0.7 µg/m³) were not much greater compared to 2014, and about 6 times less compared to the reference period (1990-1999).

Daily mean CO concentrations ranged from 0.13 to 1.0 µg m^{-3} (~0.1 – 0.9 ppmv), which are typical values in a regional background station like the ABC-IS station in Ispra. The lowest values were observed in very clean air masses during Föhn events and windy summer days, and the highest values during cold winter nights.

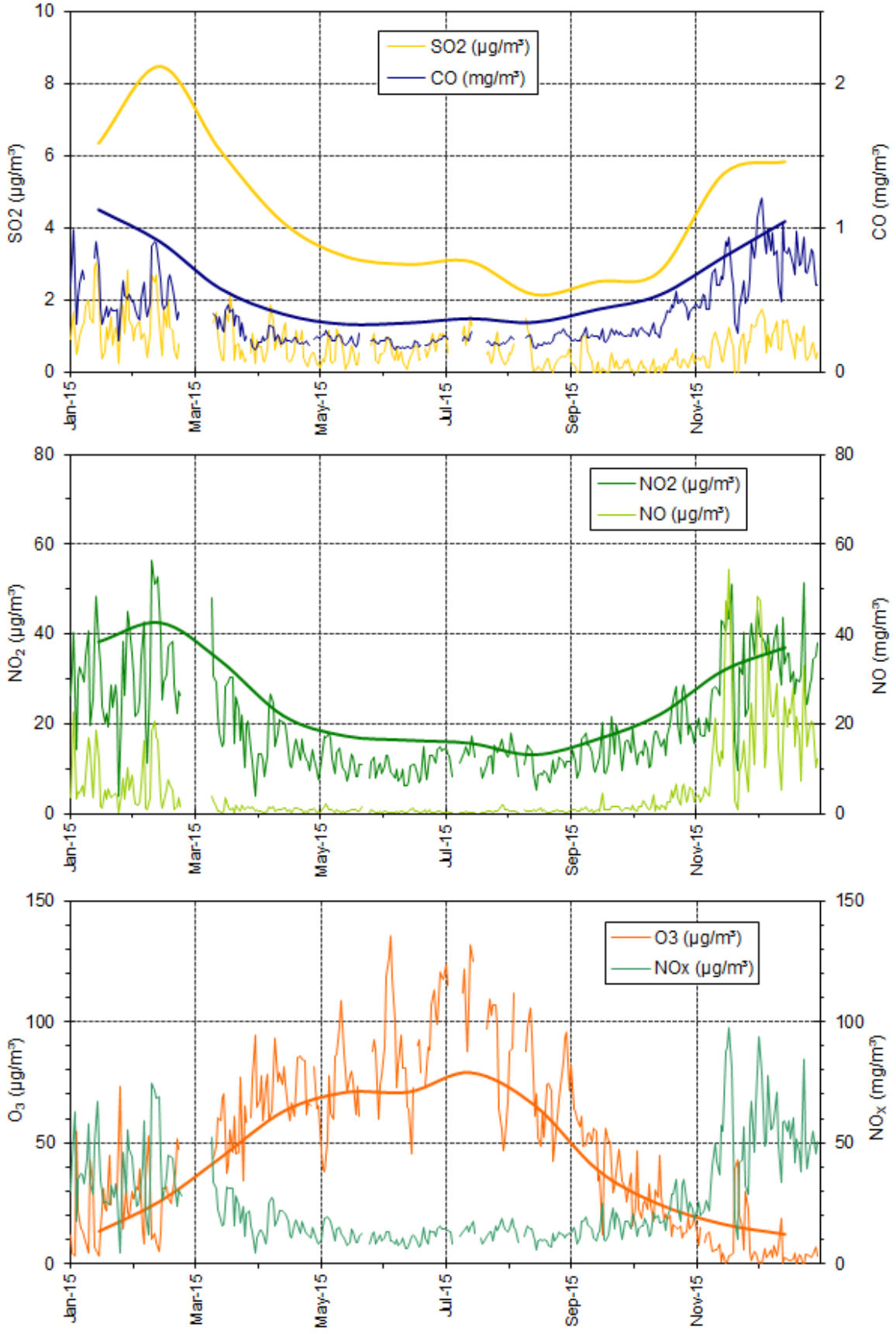

Fig. 21. Seasonal variations of the 24 hr averaged concentrations of SO_2, CO, NO_2, NO, O_3 and NO_x in 2015 (thin lines) and 1990-1999 monthly averages (thick lines: yellow=SO_2, blue=CO, green=NO_2, orange=O_3).

Local contamination screened NO_2 concentrations (annual average = 20 µg m^{-3}) were on average 20% lower than during 1990-1999 but 10% more than the 2014 levels, while local-contamination screened NO concentrations (annual average = 4.8 µg m^{-3}) were very similar to 2014 (4% less).

The temporal coverage for O_3 measurements was only 88% in 2015, and measurements are lacking for several days in May, July and August (Fig. 13), when high levels are expected (Fig. 21). Caution should therefore be taken when comparing the O_3 indices for 2015 with previous years. The annual average O_3 concentration in *2015* (50 µg m^{-3}, 25 ppb) was 5% higher than in 2014, and similar to 2013, i.e. in line with the relatively high O_3 concentrations observed since the early 2010's.

The vegetation exposure to above the ozone threshold of 40 ppb (AOT 40 = Accumulated dose of ozone Over a Threshold of 40 ppb, normally uses for "crops exposure to ozone") was 29100 ppb h in 2015, i.e. about twice as much as the 15100 ppb h of 2014 (cloudy and wet summer), and similar to the 32300 ppb h observed in 2013 (with a data coverage for O_3 of 98 % in 2013). A rough attempt of gap filling led to an estimate of AOT40 = 37200 ppb h in 2015, i.e. even higher than in 2013.

For quantification of the health impacts (population exposure), the World Health Organisation uses the SOMO35 indicator (Sum of Ozone Means over 35 ppb, where means stands for maximum 8-hour mean over day), i.e. the accumulated ozone concentrations dose over a threshold of 35 ppb (WHO, 2008). In 2015, SOMO35 was 4030 ppb day (Fig. 22), 5060 ppb day after a rough gap filling, i.e. again higher than in 2014 data and during the 2007-2011 period, and comparable to 2012-2013. As much as 17 extreme O_3 concentrations (>180 µg m^{-3} over 1 hour) were observed in 2015, to be compared to 8, 18, and 2 extreme events in 2012, 2013, and 2014 respectively. The value 180 µg m^{-3} over 1 hour corresponds to the threshold above which authorities have to inform the public (European Directive 2008/50/EC on ambient air quality and cleaner air for Europe).

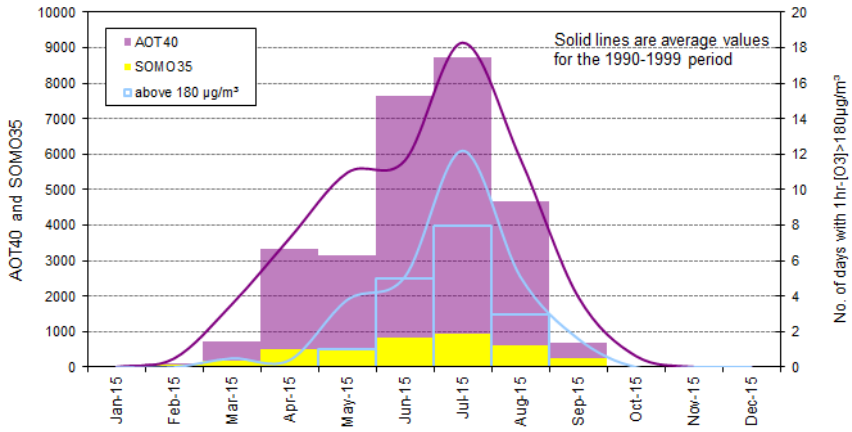

Fig. 22: AOT 40 (ppb h), SOMO35 (ppb day) and number of exceedances of the 1-hour averaged 180 µg/m³ threshold values in 2015 (bars), and reference period values 1990-1999 (lines).

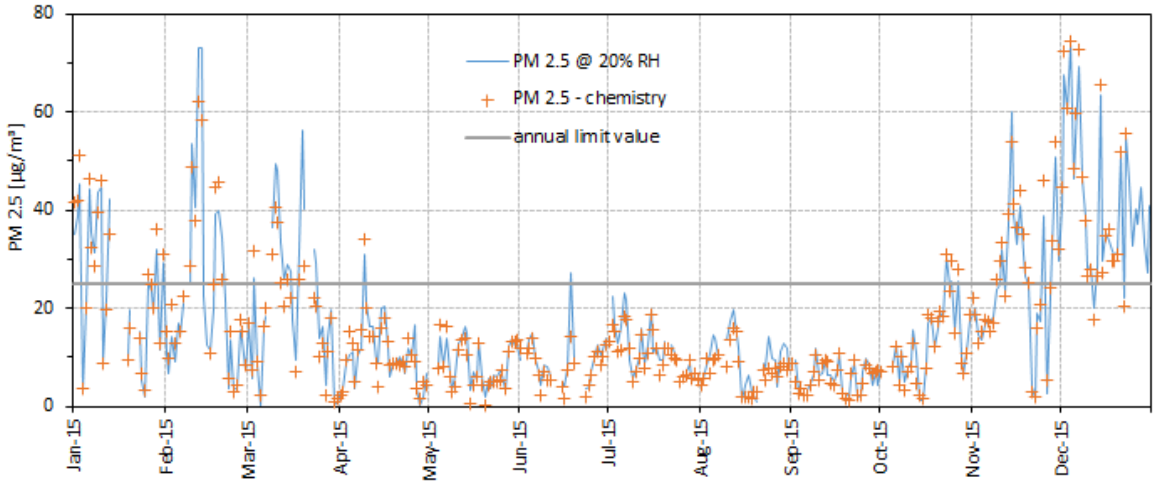

Fig. 23: 24hr-integrated $PM_{2.5}$ mass concentrations from off-line gravimetric measurements at 20 % RH and chemical determination of main constituents in 2015.The grey line indicates the annual limit value of 25 µg/m³ to be reached by 2015 (European directive 2008/50/EC).

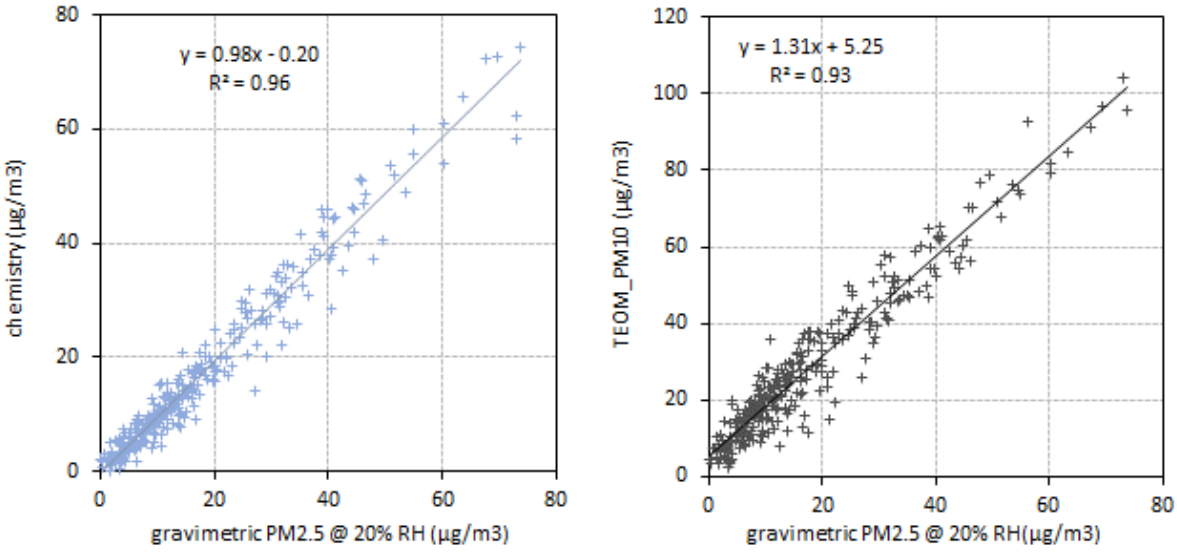

Fig. 24. Regressions between gravimetric $PM_{2.5}$ measurements at 20 % RH and sum of the $PM_{2.5}$ chemical constituents (left), and between FDMS-TEOM PM10 and gravimetric $PM_{2.5}$ measurements at 20 % RH (right) in 2015.

During the reference period 1990-1999, the information level of 180 µg m^{-3} had been exceeded 29 times per year on average. The other "protection of human health factor" mentioned by the European Directive 2008/50/EC (120 µg m^{-3} as maximum daily 8-hour average) was exceeded 76 times in 2015, leading to a 3-year average of 50 exceedances per year, well above the Directive threshold (25 exceedances per year).

4.4.3. Particulate phase

4.4.3.1 Particulate matter mass concentrations

$PM_{2.5}$ concentrations (Fig. 23) measured gravimetrically at 20 % relative humidity (RH) averaged 17.3 µg m^{-3} over 2015 (data coverage = 90%). This was the 4th lowest value observed since this measurement was started in 2002 (lowest value = 13.0 µg m^{-3} in 2014, 2nd lowest value = 16.1 µg m^{-3} in 2013), well below the European annual limit value of 25 µg m^{-3} to be reached by 2015 (European directive 2008/50/EC). Gravimetric measurements of $PM_{2.5}$ mass at 20% RH and the sum of $PM_{2.5}$ mass constituents determined from chemical analyses are well correlated (Fig. 24).

Based on FDMS-TEOM measurements of PM_{10} (96% annual data coverage), 21 exceedances of the 24-hr limit value (50 µg m^{-3}) were observed in 2015, to be compared to the 16, 38 and 51 exceedances observed in 2014, 2013 and 2012, respectively. The annual PM_{10} average (27.6 µg m^{-3}) was much bigger than in 2014 (19.5 µg m^{-3}), but still far below the 40 µg m^{-3} annual average EC limit value.

The correlation between gravimetric $PM_{2.5}$ and PM_{10} concentrations measured with a TEOM-FDMS (Fig. 24, right hand) was acceptable (R^2=0.93) in 2015.The regression suggests an offset of about 5 µg m^{-3} from the TEOM, and a ratio between PM_{10} and $PM_{2.5}$ of 1.3 on average.

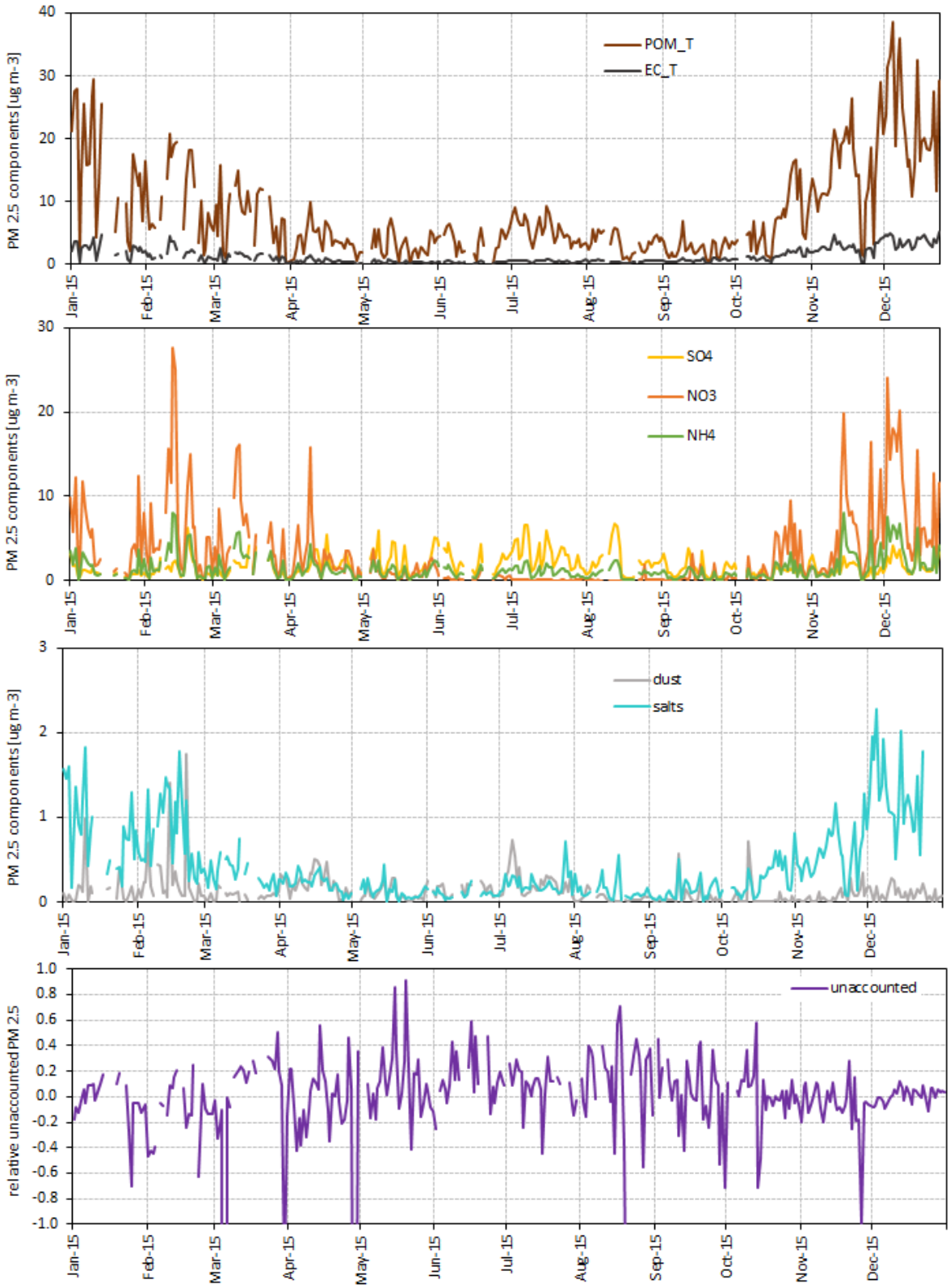

Fig. 25. 24-hr integrated concentrations of the main $PM_{2.5}$ constituents in 2015, and relative unaccounted mass.

4.4.3.2 PM2.5 chemistry:

Main ions (Cl^-, NO_3^-, SO_4^{2-}, $C_2O_4^{2-}$, Na^+, NH_4^+, K^+, Mg^{2+}, and Ca^{2+}), OC and EC were determined from the quartz fibre filters collected for PM mass concentration measurements for the whole of 2015 (data coverage = 90%).

Fig. 25 shows the temporal variations in the $PM_{2.5}$ main components derived from these measurements. Particulate organic matter (POM) is calculated by multiplying OC (organic carbon) values by the 1.4 conversion factor to account for non-C atoms contained in POM (Russell et al., 2003). "Salts" include Na^+, K^+, Mg^{2+}, and Ca^{2+}. Dust is calculated from Ca^{2+} concentrations and the regression (slope = 4.5) found between ash and Ca^{2+} in the analyses of ash-less cellulose filters (Whatman 40) in previous years. Most components show seasonal variations with higher concentrations in autumn and winter, and lower concentrations in summer, like $PM_{2.5}$ mass concentrations. This is mainly due to changes in pollutant horizontal and vertical dispersion, related to seasonal variations in meteorology (e.g. lower boundary layer in winter). The amplitude of the POM, NH_4^+ and NO_3^- seasonal cycles may be enhanced due to equilibrium shifts towards the gas phase, and/or to enhanced losses (negative artefact) from quartz fibre filters during warmer months. Indeed, historical data (May – Sept. 2013) show that the concentration of NH_4NO_3 in $PM_{2.5}$ determined from filters (0.2 µg / m³) can be 1/5 of the concentration measured in the submicron aerosol (1.0 µg / m³) with an ACSM (see 2013 annual report).

NH_4^+ follows NO_3^- + SO_4^{2-} very well as indicated by the regression shown in Fig. 26. This correlation results from the atmospheric reaction between NH_3 and the secondary pollutants H_2SO_4 and HNO_3 produced from the oxidation of SO_2 and NO_x, respectively. The slope of this regression is very close to 1, which means that NH_3 was sufficiently available in the atmosphere to neutralise both H_2SO_4 and HNO_3. This furthermore indicates that $PM_{2.5}$ aerosol was generally not very acidic in 2015.

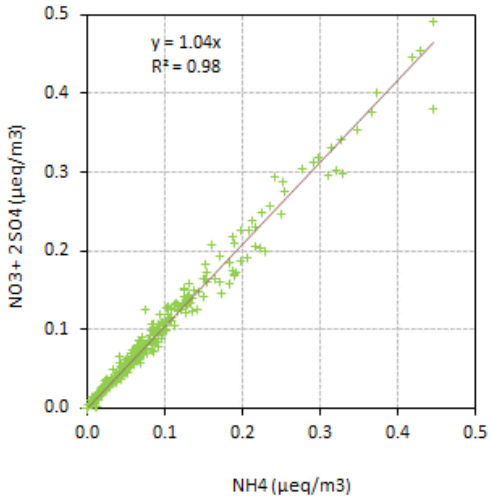

Fig. 26. SO_4^{2-} + NO_3^- vs. NH_4^+ (µeq/m³) in $PM_{2.5}$ for 2015

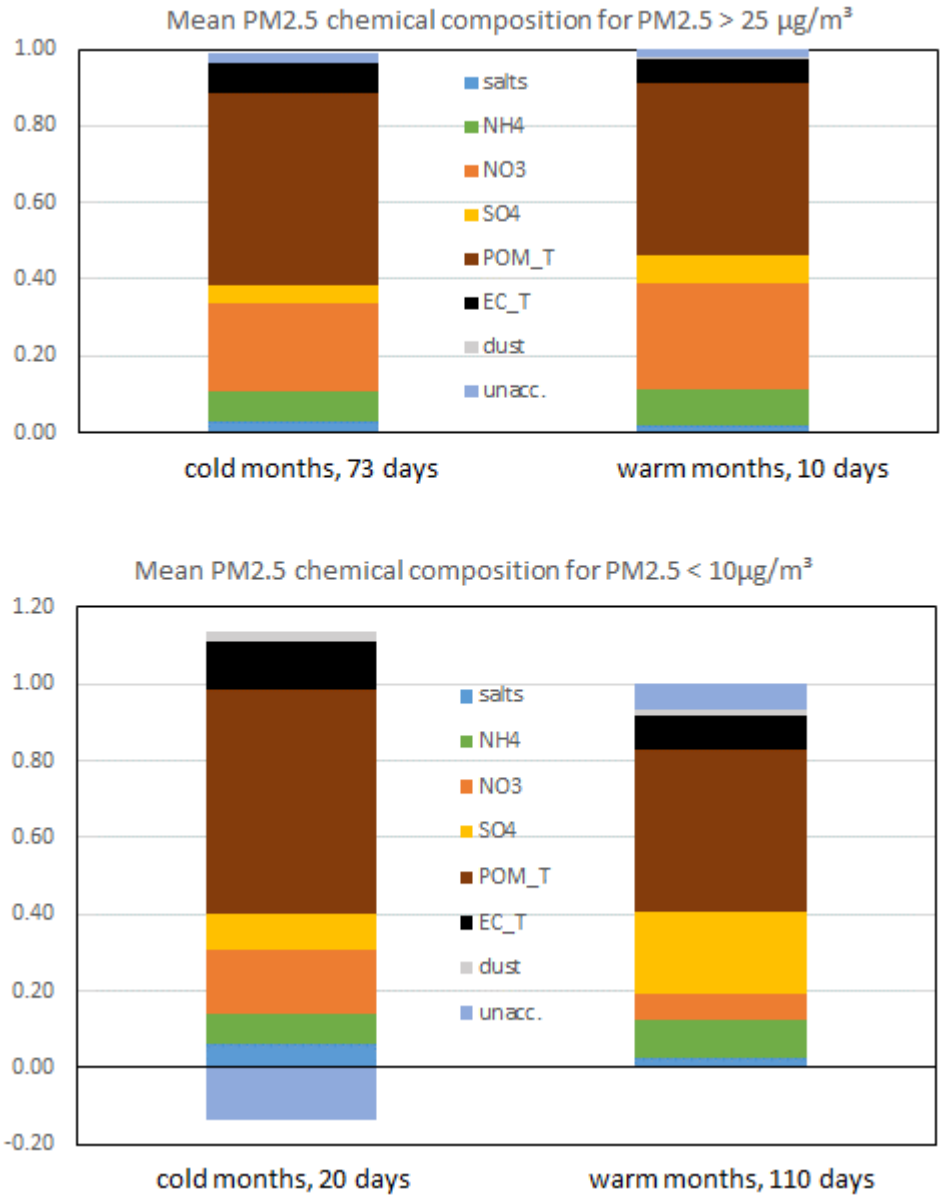

Fig. 27: Average composition of $PM_{2.5}$ in 2015 for days on which $PM_{2.5}$ > 25 µg/m³ (top) and PM2.5 < 10 µg/m³ (bottom), over cold (Jan., Feb., Mar., Nov., Dec.) and warm (Apr. – Oct.) months.

4.4.3.3 Contribution of the main aerosol constituents to $PM_{2.5}$

The contributions of the main aerosol components to $PM_{2.5}$ are presented in Table 3 (annual averages) and in Fig. 27 (a) for days on which the "24-hr limit value for $PM_{2.5}$ of >25 µg/m³ was exceeded" during the cold months (Jan., Feb., March, Nov. and Dec., 73 cases) and the warm months (Apr. to Oct, 10 cases) and (b) for days on which 24-hr integrated $PM_{2.5}$ concentration was below 10 µg / m³ during cold (20 cases) and warm months (110 cases).

These $PM_{2.5}$ compositions may not always represent accurately the actual composition of particulate matter in the atmosphere (mainly due to possible negative sampling artefacts), but are suitable to assess which components contributed to the $PM_{2.5}$ mass collected by a quartz fibre filter downstream of a 20 cm-long carbon monolith denuder.

Over the whole year 2014, carbonaceous species accounted for 62% of $PM_{2.5}$ (EC: 10%, POM: 52%), and secondary inorganics for 40% (NH_4: 9%, NO_3: 15%, and SO_4: 16%). In both the cold and the warm seasons, particulate air pollution days are characterised by a strong increase in NO_3 contribution. Considering low $PM_{2.5}$ concentration days, summertime is characterised by higher SO_4^{2-} concentrations (faster SO_2 photochemical conversion) and lower POM and NO_3^- concentrations (equilibriums shifted towards the gas phase as temperatures increase). Dust and salts do not contribute significantly to the $PM_{2.5}$ mass. Their contribution is larger on cleanest days compared to most polluted days.

Table 3: Annual mean concentrations and contributions of major $PM_{2.5}$ constituents in 2015

constituent	salts Cl^-, Na^+, K^+, Mg^{2+}, and Ca^{2+}	NH_4^+	NO_3^-	SO_4^{2-}	POM	EC	dust	unaccounted
Mean conc. (µg m^{-3})	0.42	1.50	3.14	1.78	8.31	1.31	0.13	0.62
Mean cont. (%)	3.4	9.4	14.9	15.9	51.6	10.1	1.5	-8.2

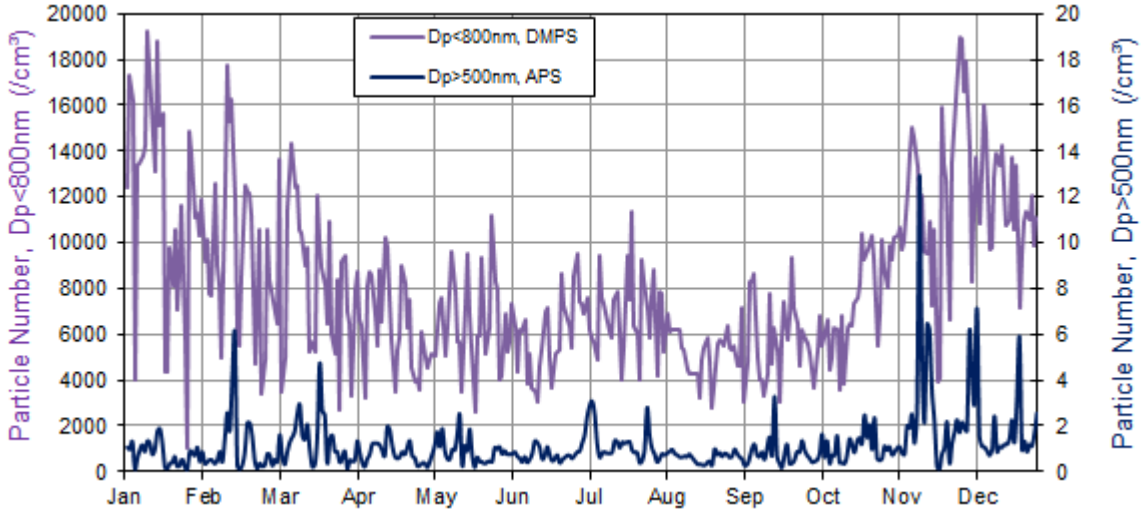

Fig. 28. 24 hr – mean particle number concentrations for Dp < 600 nm and Dp >500 nm.

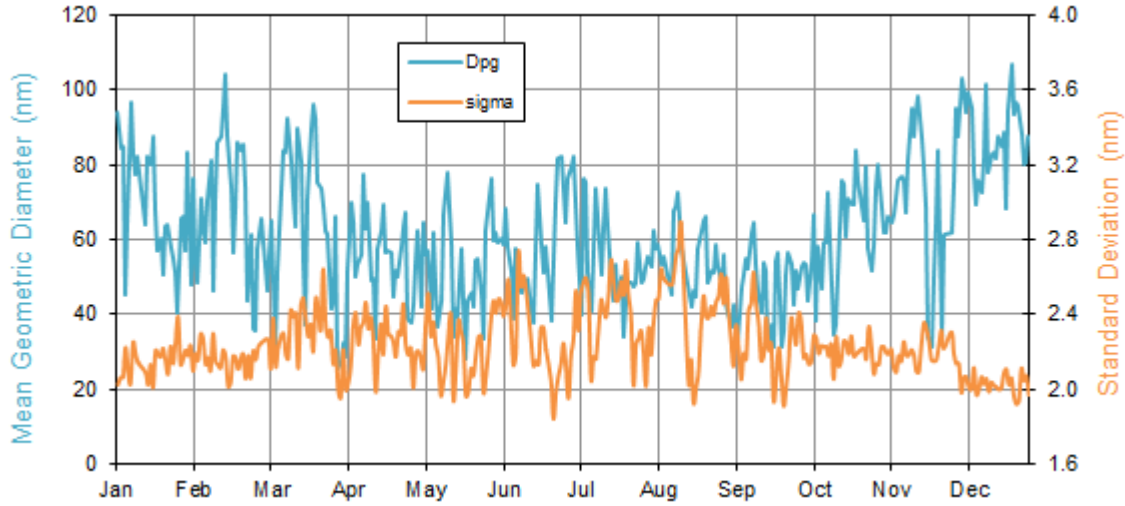

Fig. 29. 24 hr - averaged particle geometric mean mobility diameter (from the DMPS) and standard deviation

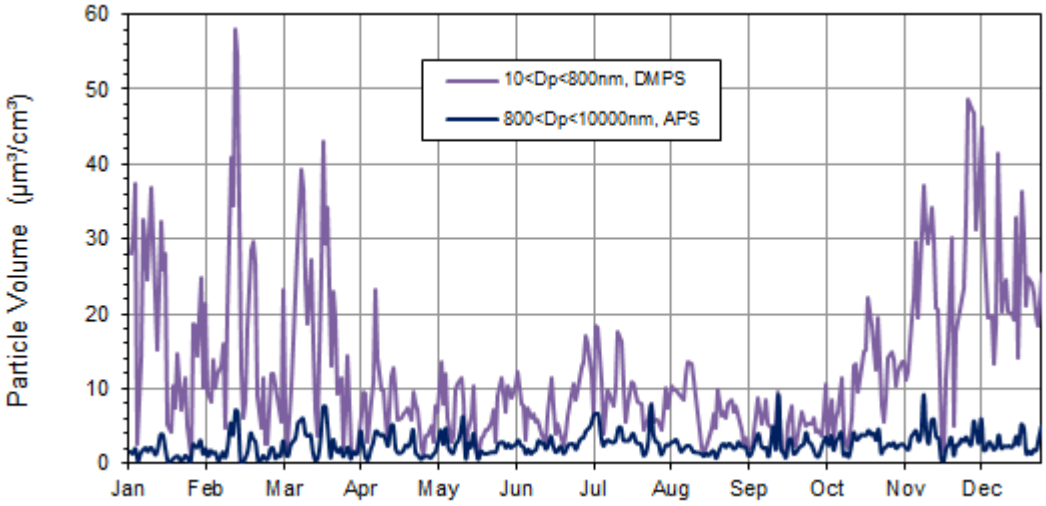

Fig. 30. 24 hr - averaged particle volume concentrations for Dp< 800 nm and Dp > 800 nm.

4.4.3.4 Aerosol micro-physical properties

Measurements of the particle number size distributions smaller than 800 nm diameter were carried out using a Differential Mobility Particle Sizer almost continuously in 2015, except for a few breakdowns resulting in a data coverage of 96%.

Particle number concentrations averaged over 24 hr (from 08:00 to 08:00 UTC) ranged from 1010 to 19200 cm^{-3} (average: 8040 cm^{-3}) and followed a seasonal cycle similar to that of PM mass concentrations, with maxima in winter and minima in summer (Fig. 28). It should be mentioned, that the DMPS data presented here have not been corrected for inlet diffusion losses and CPC efficiency, but those normally account for only a few percent on particle number and have no impact on the other variables. The vicinity of internal and external roads led to numerous episodes of local contamination, which were flagged during the data analysis process. Excluding the data points affected by local contamination (10% of the data), the annual mean particle number drops by 8%.

The mean mode diameter at RH < 30 % ranged between 26 and 107 nm (average = 62 nm) in 2015. The variations in particle size distributions characteristics (Fig. 29) show seasonal patterns as well: the mean geometric diameter is generally larger in winter (about 60-90 nm) than in summer (about 40- 60 nm, with peaks at 80 nm), whereas the standard deviation of the distribution follows an opposite trend (larger in summer than in winter).

The size distribution of particles larger than 500 nm was measured using an Aerodynamic Particle Sizer almost continuously over 2015 (data coverage: 99%). Aerodynamic diameters were converted to geometric diameter assuming a particle density of 1.50. As previously observed, particles larger than 500 nm generally (90^{th} percentile) accounted for <0.03% of the total particle number only (Fig. 28), but for more than 30 % of the total particle volume on average (Fig. 30). The seasonal variations in particle volume concentration reflect the changes in particle number and mean geometric diameter, with larger volumes in winter than in summer.

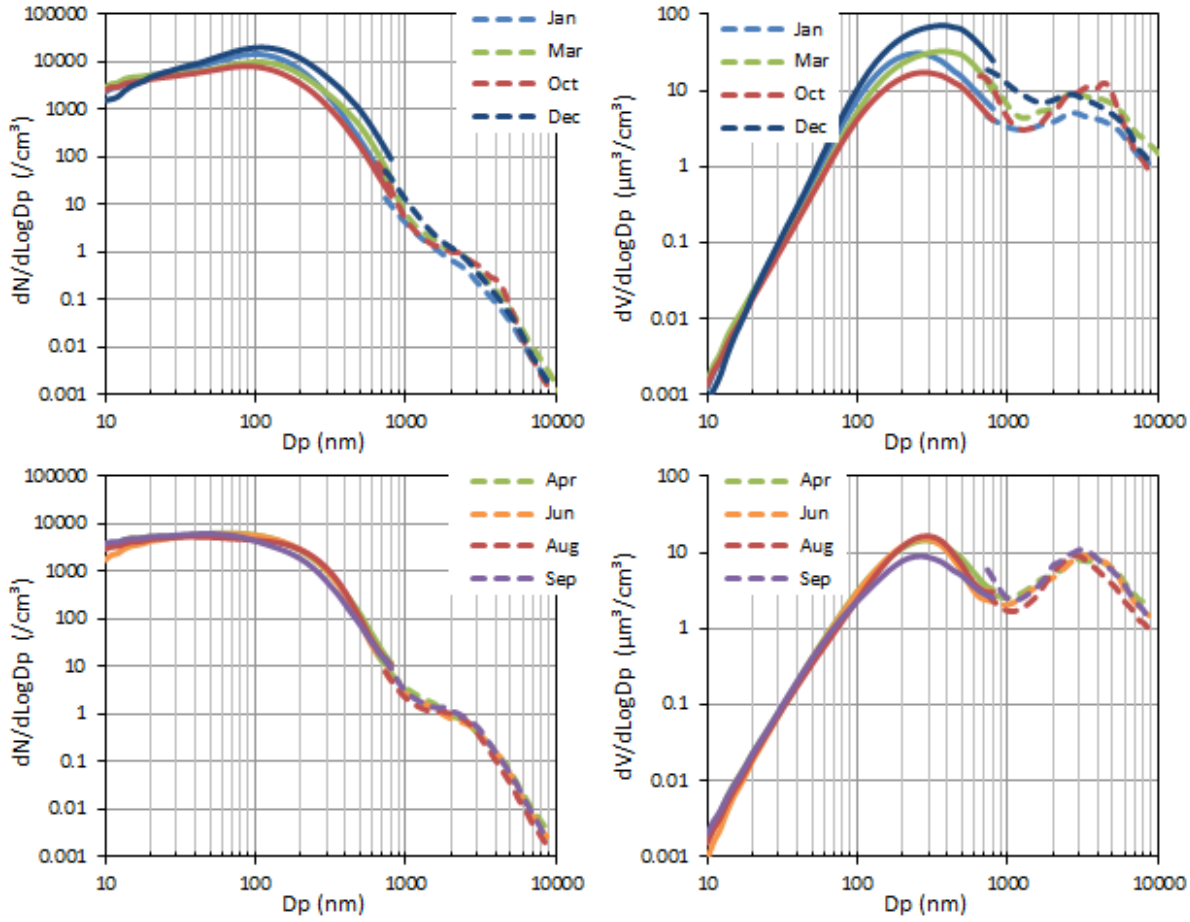

Fig. 31. Monthly mean particle number (left) and volume (right) size distributions measured in 2015 with a DMPS (10-800 nm, solid lines) and an APS (0.85-10 µm, dashed lines).
*A density of **1.25 g cm**$^{-3}$ was used to convert aerodynamic to geometric diameters.*

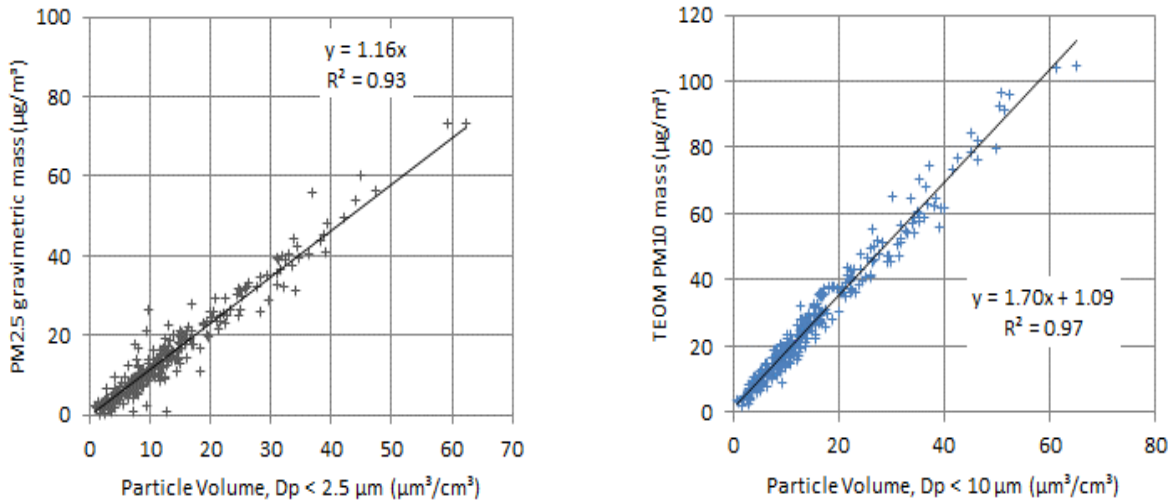

Fig. 32. 2015 regressions between (left) $PM_{2.5}$ mass concentrations determined from gravimetric measurements at 20 % RH and particle volume (Dp < 2.5 µm) calculated from DMPS and APS measurements (about 20% RH), and (right) between PM_{10} mass concentrations measured with the TEOM-FDMS at 30 % RH and particle volume (Dp < 10 µm) at about 20% RH.

The apparent good agreement between particle number size distributions (Fig. 31) measured with the DMPS and the APS actually reveals a marginal consistency between these two instruments, since the aerosol density (1.25 g cm^{-3}) used to convert aerodynamic diameters (measured by the APS) to mobility diameters (measured by the DMPS) is out of the range (1.6 ± 0.1 g cm^{-3}) expected for atmospheric particles (McMurry et al., 2002).This aerosol density appears even to be too big for January and December. This was already observed previously, and may be due to over-counting by the DMPS of particles larger than 300 nm, as also suggested by the 2013 DMPS inter-comparison at the WCCAP in Leipzig.

Both comparisons between PM mass and aerosol particle volume concentrations show a good correlation (Fig. 32). The slope of the regression between $PM_{2.5}$ at 20 % RH and particle volume suggests an aerosol density of 1.16 (to be compared to 1.24, 1.20, 1.31, 1.38 and 1.37 in 2014, 2013, 2012, 2011 and 2010, respectively), while the regression between PM_{10} mass and aerosol volume concentration (for Dp < 10 µm) suggests a density of 1.7, larger than the nominal value of 1.5 g cm^{-3} assumed to convert aerodynamic diameters to mobility diameters for particle volume calculation. This (together with the comparison between $PM_{2.5}$ mass and chemistry) might indicate that $PM_{2.5}$ gravimetric measurements were underestimated.

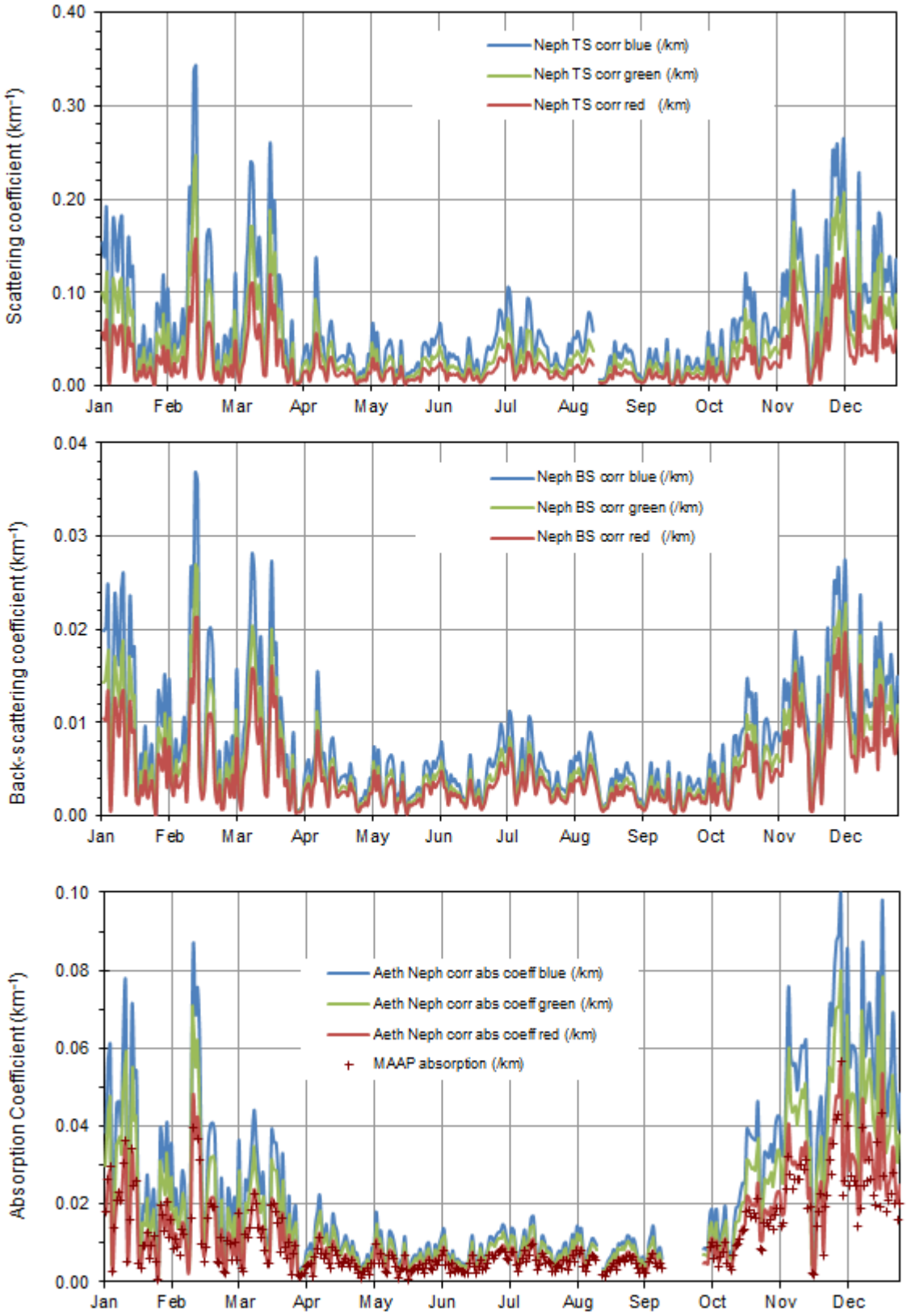

Fig. 33. Daily mean atmospheric particle light scattering (top), backscattering (middle), and absorption (bottom) coefficients at three wavelengths, derived from Nephelometer, Aethalometer and MAAP measurements (not corrected for RH) performed in 2015.

4.4.3.5 Aerosol optical properties

Aerosol optical properties have been monitored continuously during 2015 (data coverage = 99% for light scattering, 94% for light absorption measurements). Data from the Nephelometer (Fig. 33 a and b) have been corrected for angular non idealities (truncation to 7 – 170°, slightly not cosine-weighted distribution of illumination) according to Anderson and Ogren (1998), but not for RH effects. Thanks to the implementation of a Nafion dryer and the reduction of the sampling flow rate to 6-12 L min^{-1}, the Nephelometer internal RH was maintained below 35% for more than 95% of the time, with exception occurring mainly in July and August. At 35% RH, aerosol scattering is on average increased by about 15 % compared to 0% RH in Ispra (Adam et al., 2012).

Atmospheric particle absorption coefficients at 7 wavelengths (Fig. 33 c) were derived from the Aethalometer AE-31 data corrected for the shadowing and multiple scattering effects when Nephelometer data were available, according to Weingartner et al. (2003), making use of coefficients derived from Schmid et al. (2006), i.e. 3.60, 3.65 and 3.95 at 470, 520, and 660 nm, respectively.

Both scattering and absorption coefficients follow seasonal variations (Fig. 33) in line with PM mass variations, mainly controlled by pollutant dispersion rates.

The uncertainty in the multiple scattering correction factor may introduce a quite large uncertainty in the aerosol absorption coefficient values, since correction factors ranging from 2 to 4 have been proposed (Weingartner et al., 2003; Arnott et al., 2005). The use of the correction factors listed above leads to an aerosol absorption coefficient at 660 nm somewhat greater than the absorption coefficient obtained from the Multi Angle Absorption Photometer (MAAP) for 670 nm, above all with the instruments settings set at the calibration workshop in Sept. 2015 (Fig. 34). NB: in December 2015, it was recommended by ACTRIS that the coefficient 3.5 should be used for all wavelengths without any correction for the filter loading.

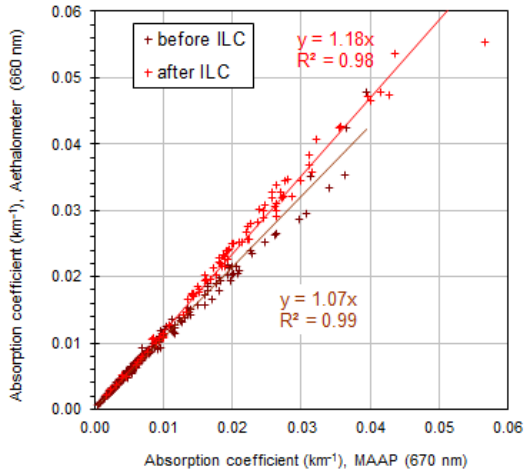

Fig. 34. Comparison between the Aethalometer and MAAP derived light absorption coefficients at 660 and 670 nm, respectively. Data points are daily averages (2015).

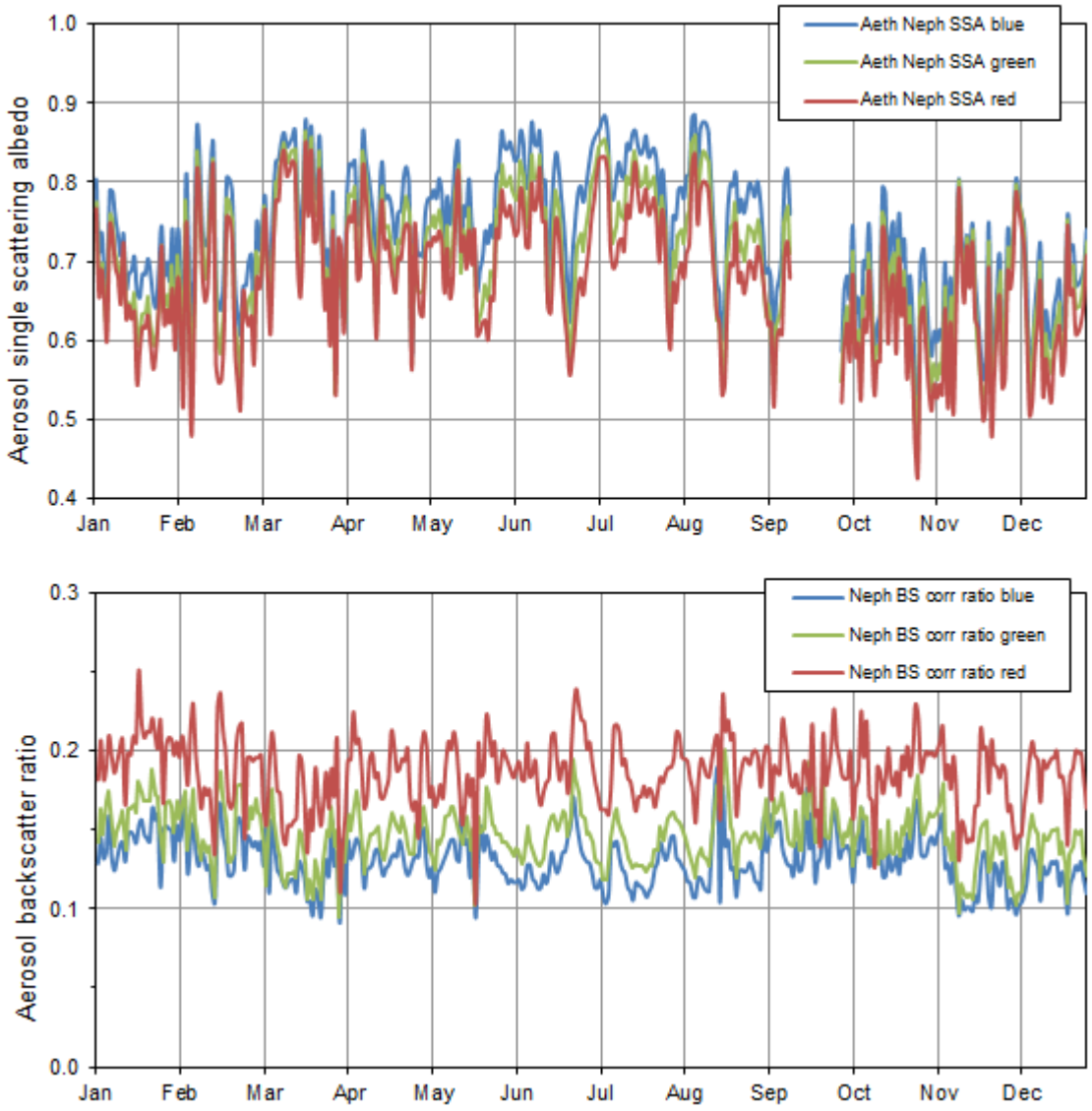

Fig. 35. Aerosol 24-hr averaged single scattering albedo and backscatter to total scatter ratio at three wavelengths corresponding to blue, green and red, as calculated for 2015 (RH < 40%).

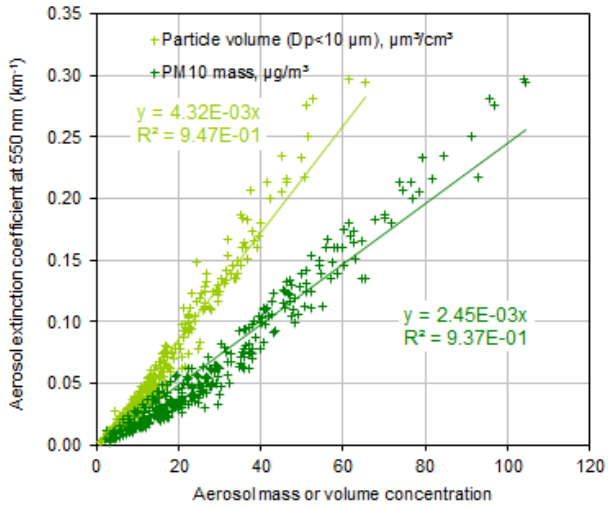

Fig. 36. Regression between the aerosol extinction coefficient and PM_{10} mass (FDMS-TEOM) and volume (DMPS + APS) concentrations in 2015.

The 24 hr-averaged aerosol single scattering albedo (SSA) at λ = 550 nm (at RH generally < 40 %) ranged from 0.46 to 0.87 (annual average 0.70), with generally higher values in summer compared to winter (Fig. 35, top). In 2015, the lowest aerosol single scattering albedo values were affected by the proximity of the provisional measurement site to the internal and external roads of the JRC. As a consequence, the mean SSA was lower than in 2010-2012 (0.75-0.79), but also lower than in 2013 (0.76). Excluding the values clearly affected by local influences, the mean single scattering albedo was 3% bigger. The absorption coefficients were flagged for local submission before submission to the WDCA data bank (EBAS).

The backscatter / total scatter ratio at 550 nm (Fig. 35, bottom) ranged from 0.09 to 0.20 (average 0.15), with no significant change compared to previous year.

The aerosol extinction coefficient and particle mass or volume concentrations are rather well correlated (Fig. 36). The slope of the regression between extinction and mass shows that the extinction mass efficiency is on average 2.5 $m^2\,g^{-1}$ (vs 2.8 in 2014, and 3.4 in 2012 and 2013), i.e. low compared with 4.7 $m^2\,g^{-1}$, the value calculated based on the aerosol mean chemical composition during 2015, and mass cross section coefficients for the various constituents found in the literature (see Table 4). The agreement between these two estimates of the aerosol extinction cross section deteriorated compared to 2010 – 2012 and suggest that the TEOM-FDMS mass concentration data and the estimate of the aerosol volume from the DMPS and APS measurements are overestimated.

Table 4. Mean aerosol chemical composition ($PM_{2.5}$) in 2015 and extinction cross section.

	2015 $PM_{2.5}$ comp. (%)	σ_{ext} (m^2/g)	Reference (for σ_{ext})
"sea salt"	3	1.3	Hess et al., 1998
NH_4^+, NO_3^- and SO_4^{2-}	38	5.0	Kiehl et al., 2000
organic matter	49	3.6	Cooke et al., 1999
elemental carbon	10	11	Cooke et al., 1999
Dust	1	0.6	Hess et al., 1998
Total	**100**	**4.7**	

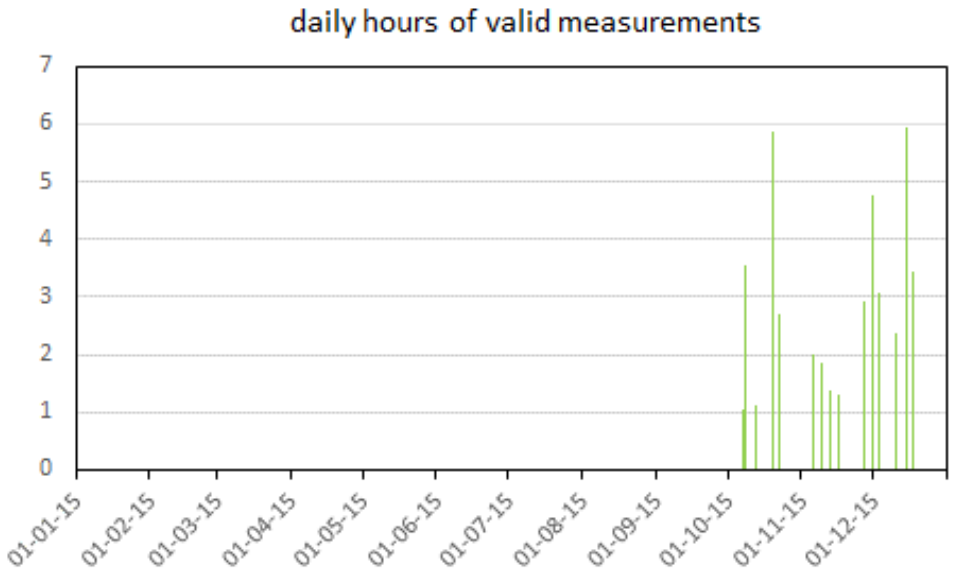

Fig. 37. Aerosol vertical profiling measurements performed daily with the Raman Lidar in 2015.

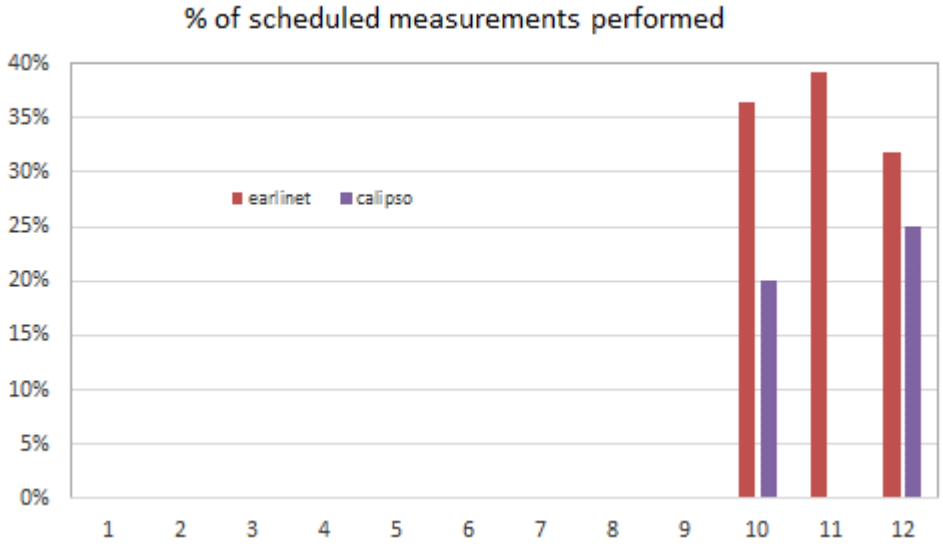

Fig. 38. Scheduled aerosol vertical profiling measurements performed monthly during the EARLINET climatology and Calipso overpass time slots in 2015.

4.4.3.6 Aerosol *vertical profiles*

The Raman LiDAR from Raymetrics was operated for measuring aerosol vertical profiles from Oct. 2015, when the laser was sent back from the manufacturer's and re-installed by the provider.

From that time, the LiDAR was operated automatically for 1 to 2 periods per day: noon (2hr) and sunset (4-5 hr) on Mondays, and sunset (4-5 hr) on Thursdays (EARLINET climatology), plus Calipso overpasses (every 16 days at about 01:40 and 12:35 UTC), weather permitting (Fig. 37). These scheduled measurements were covered at 36% and 15% (Fig. 38), respectively, while ACTRIS' target is 50%.

Fig. 39 shows an example of range corrected backscatter signal at 532 nm (no data inversion applied) recorded on October 19th, 2015, from 10:15 to 19:10 UTC. The "low value" area at the bottom of the chart is due to the overlap function dropping to 0 at the ground. Pollution particles are observed up to 1 km in the morning, afternoon and evening.

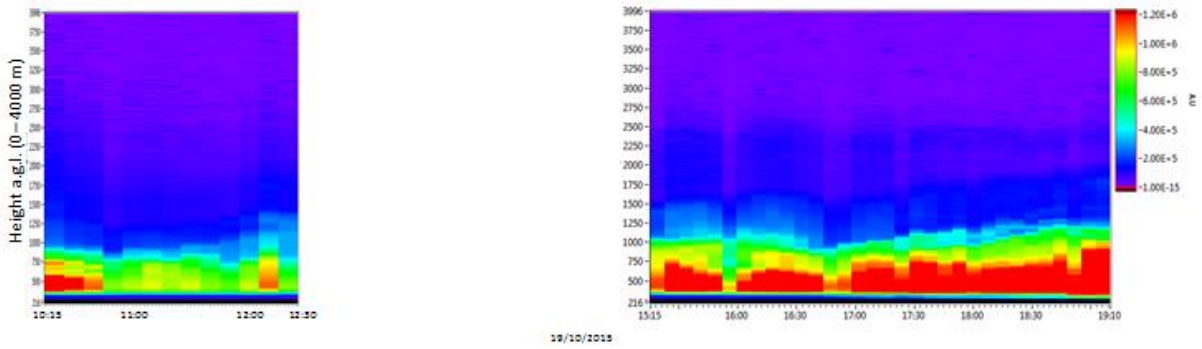

Fig. 39: Lidar range corrected signal obtained at ABC-IS on October 19th, 2015, illustrating the aerosol mixed layer height, and the accumulation of pollution in the evening (UTC time).

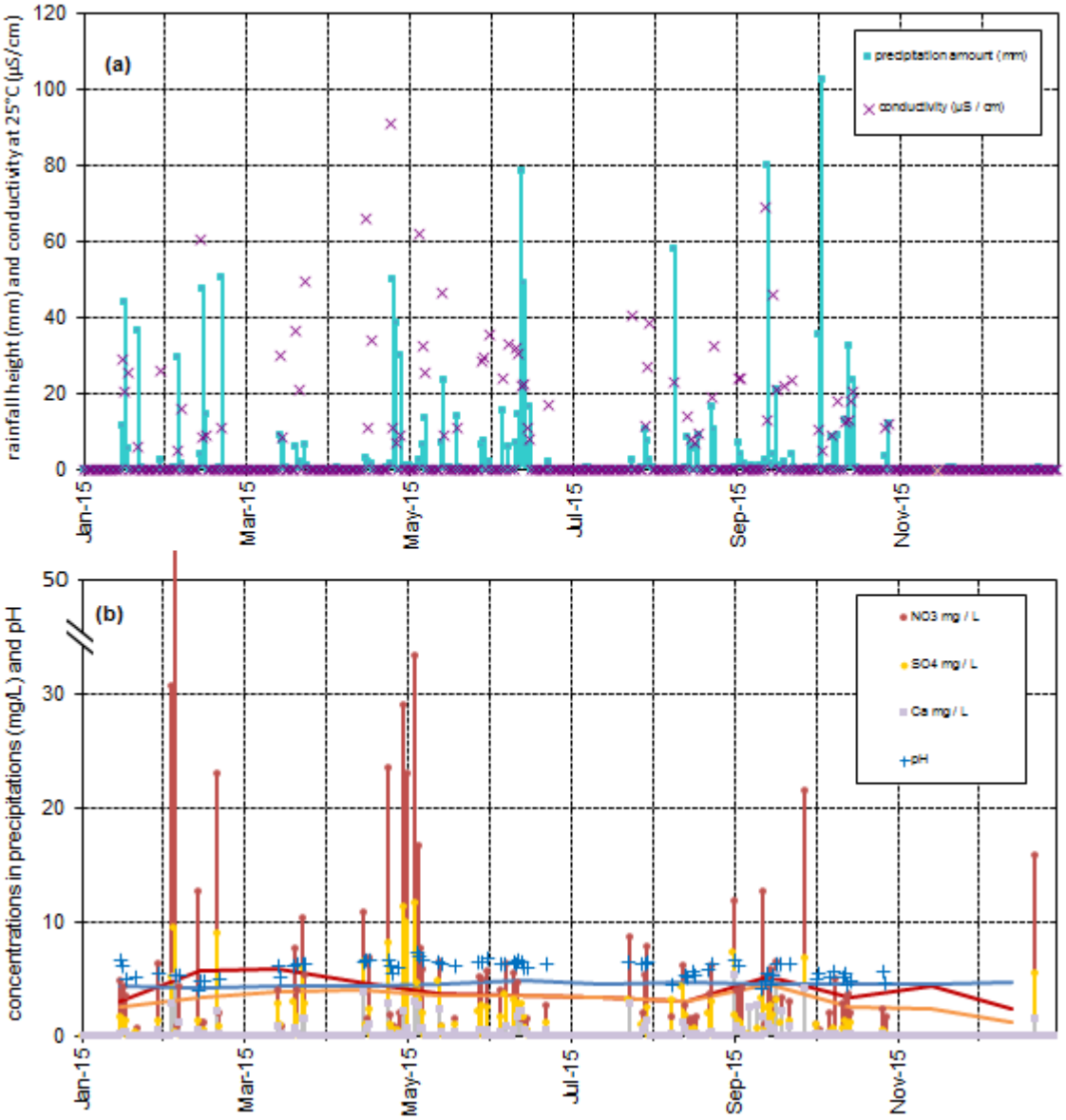

Fig. 40 (a) *Precipitation amount, conductivity and (b) concentrations of 3 major ions in precipitation (bars) and pH (crosses) in 2015, and during the 1990-99 period (lines).*

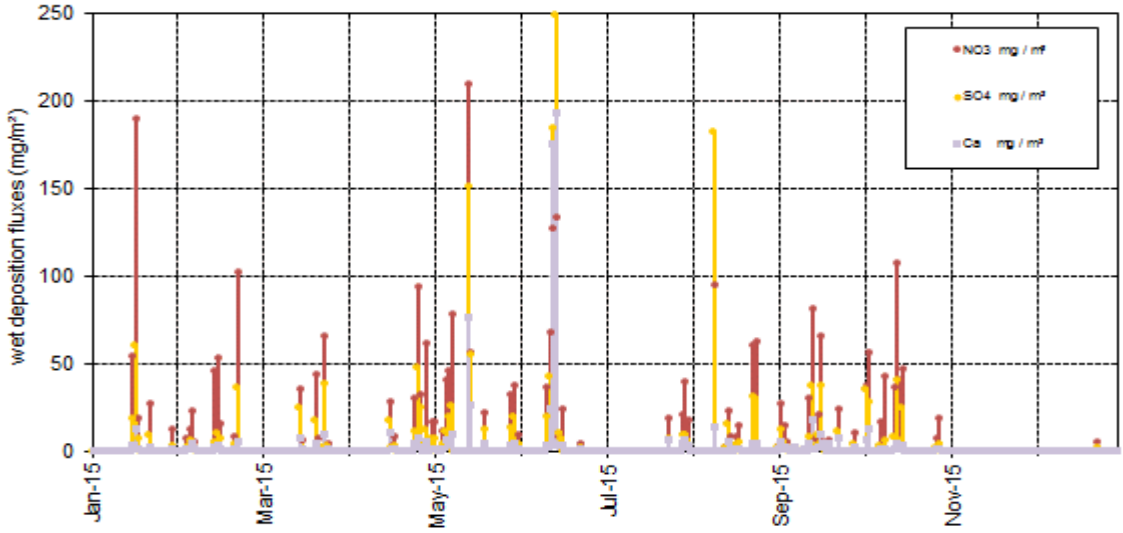

Fig. 41. Wet deposition fluxes of 3 main components in rain water in 2015.

4.4.4. Precipitation chemistry

In 2015, 107 precipitation samples were collected and their ion content determined. Acidity (pH) and conductivity were also measured in 73 of those samples (those where the water volume was sufficient). The precipitation measured during the collected events ranged from 0.05 to 102 mm (Fig. 40a) for a total of 1190 mm *vs.* 1410 mm detected by the rain sensor at the ABC-IS forest flux tower. Two major rain events (3 and 9 mm on May 18th and 19th) were not sampled due to a sampler failure.

The ranges of concentrations measured in these samples are indicated in Table 5. Volume weighted mean concentrations of the anthropogenic species NO_3^- and SO_4^{2-} in 2015 were less than the 1990-1999 averages, while concentrations of all the marine or crustal components were greater. All precipitation samples collected in 2015 but 1 were acidic (pH < 7.0), and 43 had a pH<5.6 (equilibrium with atmospheric CO_2), compared to 58 in 2014, 43 in 2013, 28 in 2012 and 17 in 2011. As much as 18 samples had a pH < 4.6 (compared to 9 in 2014 and 2013).

Wet deposition was evenly distributed over January - October, while almost no wet deposition occurred in November - December (Fig. 41). The annual wet deposition flux of the main acidifying and eutrophying species was 1.8, 3.1, and 1.4 g m^{-2} for SO_4^{2-}, NO_3^-, and NH_4^+, respectively, i.e. equal (NO_3^- & NH_4^+) or greater (SO_4^{2-}) than in 2013 and 2014, and greater than in 2012 and 2011, despite the little precipitation observed in 2015 (see also section 4.6 next page).

Table 5. Statistics relative to the precipitation samples collected in 2015 (averages are volume weighted)

	pH	cond. µS/cm	Cl- mg/L	NO3- mg/L	SO42- mg/L	Na+ mg/L	NH4+ mg/L	K+ mg/L	Mg2+ mg/L	Ca2+ mg/L
Average	5.23	13.2	0.45	3.69	1.70	0.50	1.59	0.14	0.08	0.60
Min	3.94	4.65	0.04	0.01	0.04	0.03	0.01	0.01	0.01	0.05
Max	7.18	91.0	15.1	52.1	11.5	13.5	10.4	1.13	1.19	5.42
1990-1999	4.40	24.9	0.44	3.94	3.07	0.23	1.25	0.09	0.06	0.45

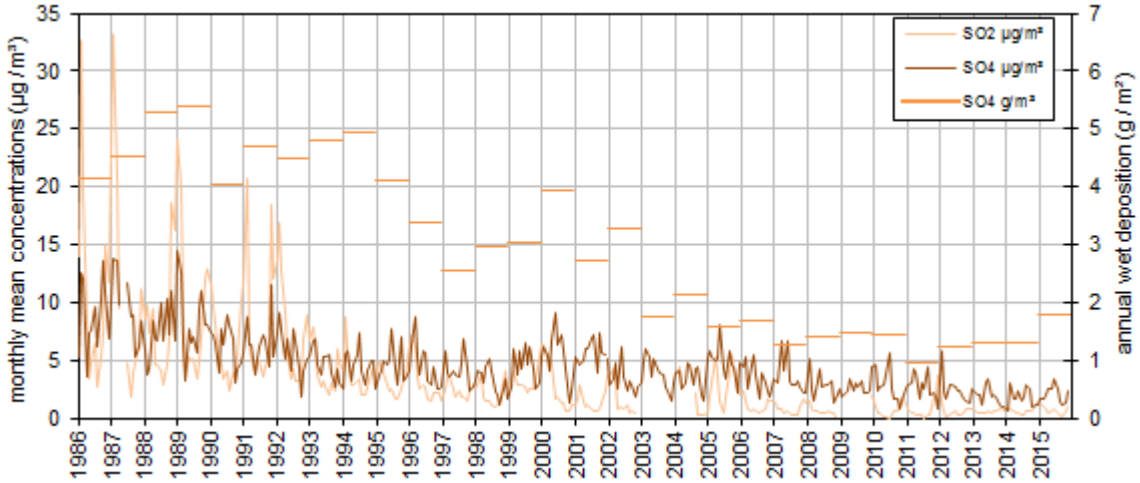

Fig. 42. Oxidized sulfur species monthly mean concentrations and yearly wet deposition.

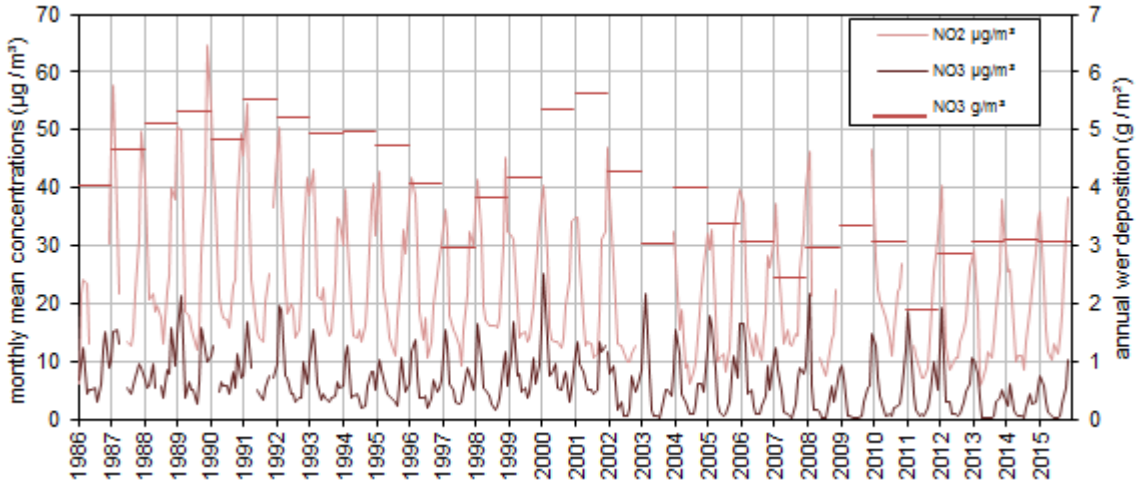

Fig. 43. Oxidized nitrogen species monthly mean concentrations and yearly wet deposition.

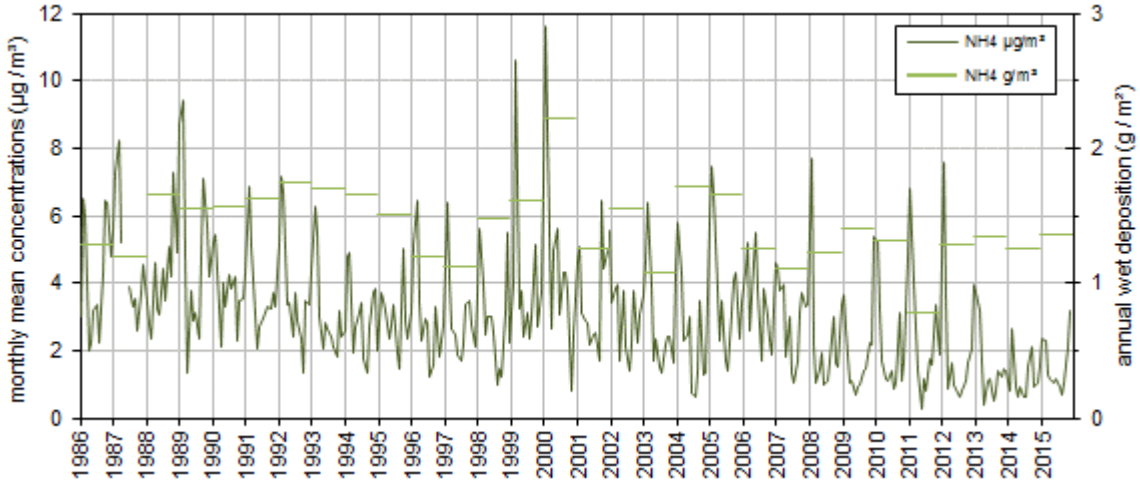

Fig. 44. Reduced nitrogen species monthly mean concentration and yearly wet deposition.

4.5. Results of year 2015 in relation to ~ 30 years of measurements

4.5.1. Sulfur and nitrogen compounds

The annual mean SO_2 concentration in 2015 was slightly greater than in 2014, but in line with the range of values (0.6 – 0.8 µg/m³) observed at our station in the 2010's. SO_2 concentrations are nowadays ~10 times smaller than in the 90's, and less than half compared to the 2000's. Annual mean particulate SO_4^{2-} concentration slightly (10%) increased compared to the historical minimum of 2014 (when summer was exceptionally wet), but 2015 remains the 2nd lowest record (slightly beating 2013 and 2012). In 2015, SO_4^{2-} concentrations were on average less than half compared to the 2000's, and 1/3 compared to the 90's. It should be kept in mind that SO_4^{2-} concentrations were measured in PM_{10} or in $PM_{2.5}$ from 2002 onwards, whereas it was measured in TSP (Total Suspended Particulate) from 1986 to 2001. However, simultaneous sampling of PM_{10} and TSP over 14 months showed that SO_4^{2-} in PM_{10} is generally less than 5 % lower than in TSP. SO_4^{2-} is mainly present in the $PM_{2.5}$ fraction at our site (see Fig. 24 of the ABC-IS annual report 2010). From 2005 onwards the calculations were as follows:

$$SO_4^{2-}(PM_{10}) = SO_4^{2-}(PM_{2.5}) \times \langle SO_4^{2-}(PM_{10})/\ SO_4^{2-}(PM_{2.5})\rangle$$

the average $\langle SO_4^{2-}(PM_{10})/\ SO_4^{2-}(PM_{2.5})\rangle$ being calculated based on the simultaneous PM_{10} and $PM_{2.5}$ samples collected in 2010-2012.

Particulate SO_4^{2-} concentrations decreased much less than SO_2 concentrations, which suggests that locally produced SO_2 decreased much more than possibly long-range transported SO_4^{2-} over the past 25-30 years. SO_4^{2-} wet deposition in 2015 was 40% more than the values of 2013 and 2014, mainly due to large fluxes in May, June and August.

In 2015, NO_2 concentrations were 20% greater than the 2010's mean value, but still 20% less compared to the 90's. Monthly mean concentrations of nitrogen dioxide (NO_2) do not show such a pronounced decreasing trend as seen for SO_2 over the past 29 years (Fig. 43). Over the last decade, NO_2 maxima are not significantly lower than during the previous one, which does not reflect the 30 % abatement in NO_x emissions reported in the emission inventories for this period. In contrast, particulate NO_3^- annual mean concentration observed in 2015 was the 2nd lowest record observed at our station (just after the 2014 low record associated with exceptional precipitation) , and half of the average over 1990 – 2010. It should be noted that since October 2000, NH_4^+ and NO_3^- have been measured mostly from quartz fibre filters, which are known to lose NH_4NO_3 at temperatures > 20 °C, as demonstrated e.g. by the comparison with the ACSM measurements we performed in Ispra in 2013. This might contribute significantly to the fact that NO_3^- summertime minima are particularly low since 2002. Furthermore, NO_3^- was measured from PM_{10} or in $PM_{2.5}$ from 2002, and no more from TSP, as over the 1986 to 2001 period. However, simultaneous sampling of PM_{10} and TSP over 14 months showed that NO_3^- in PM_{10} is generally less than 5 % lower than in TSP, like SO_4^{2-}. From 2005 and onwards the calculations were as follows

$$NO_3^-(PM_{10}) = NO_3^-(PM_{2.5}) \times \langle NO_3^-(PM_{10})/\ NO_3^-\ (PM_{2.5})\rangle$$

the average $\langle\ NO_3^-(PM_{10})/\ NO_3^-(PM_{2.5})\rangle$ being calculated based on the simultaneous PM_{10} and $PM_{2.5}$ samples collected in 2010-2012. NO_3^- wet deposition annual flux observed in 2015 was among the 10 lowest ever recorded since 1986 in Ispra, equal to the 2013 and 2014 values, i.e. slightly greater than the average over the last decade.

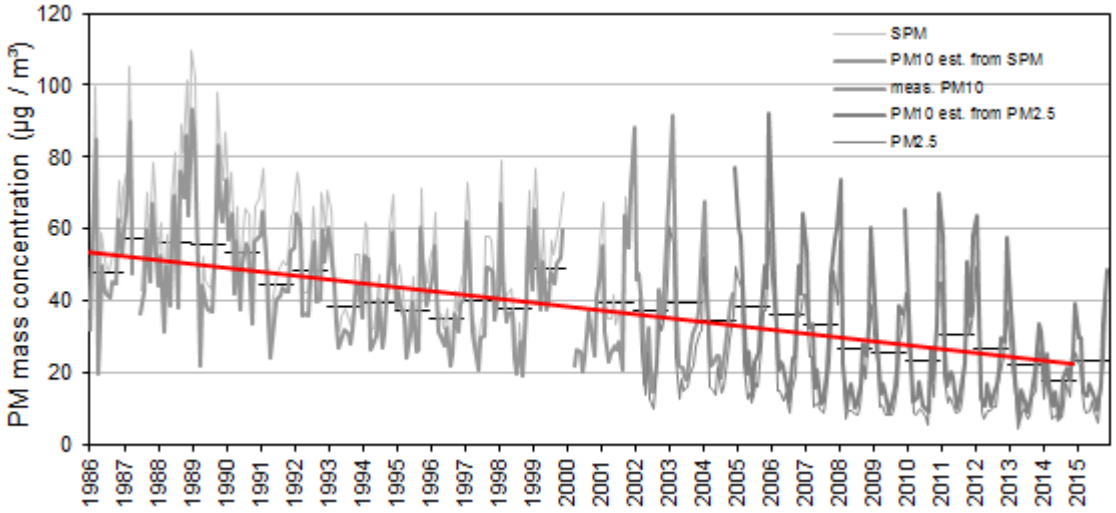

*Fig. 45***.** *Particulate matter mass concentration monthly (grey) and annual (black) averages. The red line is the long term trend over annual averages. All values are gravimetric measurements or estimated from gravimetric measurements.*

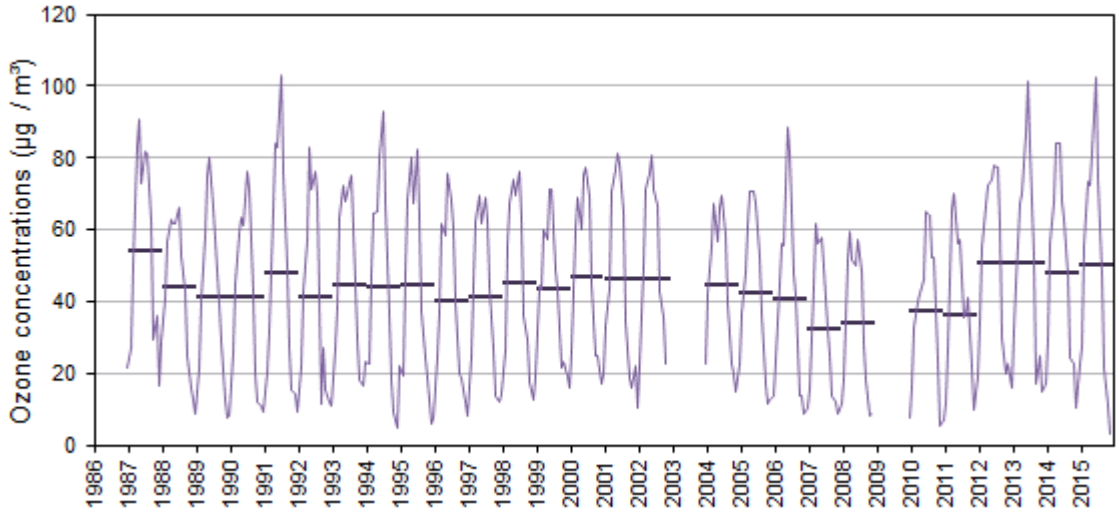

Fig. 46. Ozone yearly and monthly mean concentrations at JRC-Ispra.

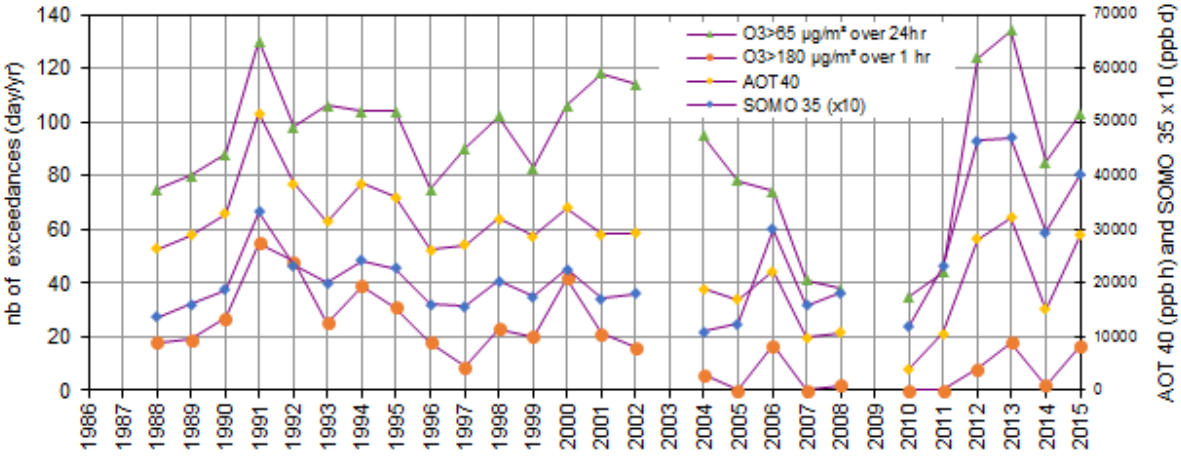

Fig. 47. AOT40, SOMO35 values, and number of O_3 limit value exceedances.

Although the annual mean concentration of NH_4^+ in particulate matter was in 2015 30% greater than the historical minimum reached in 2014 (Fig. 44), it was still the 2nd lowest value observed since 1986, i.e. twice less compared to the 1990 – 2010 period. As for particulate NO3-, November and December concentrations were particularly greater in 2015 compared to 2014 (dry vs. wet weather).

It should be noted that from the year 2002, NH_4^+ was measured in the PM_{10} or in the $PM_{2.5}$ fraction. From 2005 and onwards, NH_4^+ concentrations in PM_{10} were calculated as follows:

$$NH_4^+(PM_{10}) = NH_4^+(PM_{2.5}) \times \langle NH_4^+(PM_{10})/\ NH_4^+(PM_{2.5})\rangle$$

where the average $\langle NH_4^+(PM_{10})/\ NH_4^+(PM_{2.5})\rangle$ is calculated based on simultaneous PM_{10} and $PM_{2.5}$ measurements performed in 2010-2012. On average, NH_4^+ can neutralize nearly 100% of the acidity associated with NO_3^- and SO_4^{2-} in the particulate phase (see Fig. 26). NH_4^+ is also quite well correlated with $NO_3^- + SO_4^{2-}$ in rainwater. NH_4^+ annual wet deposition in 2015 was close to 10% greater than the average recorded in Ispra over the last decade.

4.5.2. Particulate matter mass

The 2015 annual mean $PM_{2.5}$ concentration measured at 20% RH (17.3 µg/m³) was 30% more than in 2014 but still among the 4 lowest values obtained since 2002. The annual value for PM_{10} at 50% RH estimated from $PM_{2.5}$ measurements is however in line with the general decreasing trend of - 1.1 µg m^{-3} yr^{-1} over the 3 last decades (Fig. 45). It should however be kept in mind that PM_{10} concentrations were estimated from TSP mass concentration measurements (carried out by weighing at 60 % RH and 20 °C cellulose acetate filters sampled without any particle size cut-off and "dried" at 60 °C before and after sampling) over 1986-2000, based on a comparison between TSP and PM_{10} over the Oct. 2000 - Dec. 2001 period (R^2 = 0.93, slope = 0.85), and based on measured $PM_{2.5}$ values for years 2005-2014. After the historical low winter concentrations observed in winter 2013 – 2014, winter concentrations increased again in winter 2014 and 2015, at least partly due to the exceptionally dry Dec. 2014 and 2015. Summertime PM minima showed a robust decreasing trend over 1986 – 2005, but remained rather constant over the last decade at about 10 µg/m³.

4.5.3. Ozone

Fig. 46 shows monthly and yearly mean O_3 concentrations observed since 1987. Ozone was not measured in 2009 and there was a major data acquisition breakdown in 2003. Annual average O_3 concentrations have been consistently high since 2012 – higher than during any previous year except 1986. Summertime peaks' magnitude regularly increased since 2008, with the exception of 2014 (very wet summer). In contrast, wintertime values decreased between 2013 and 2015, while they were increasing from 2010 to 2013.

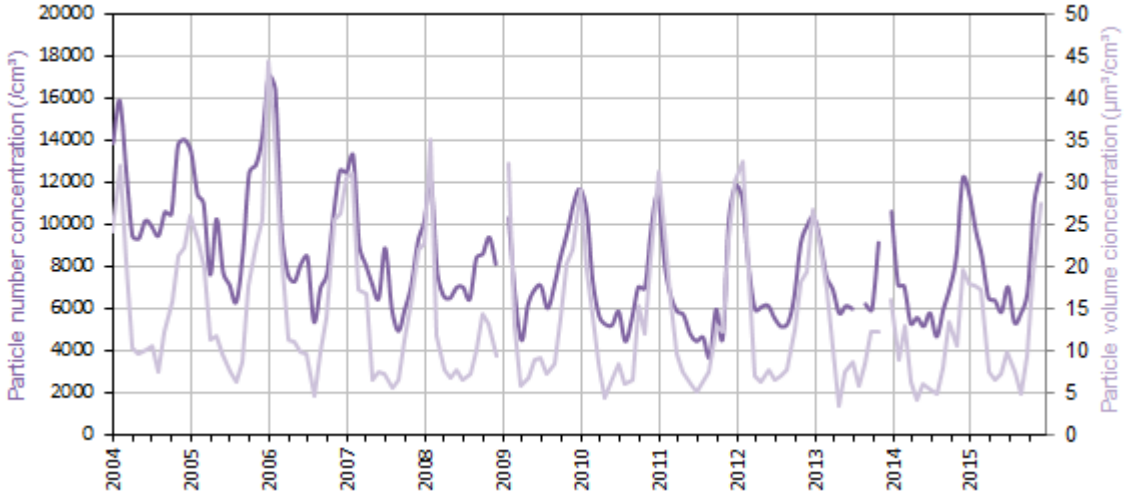

Fig. 48. Particle number (left) and volume (right) monthly mean concentrations.

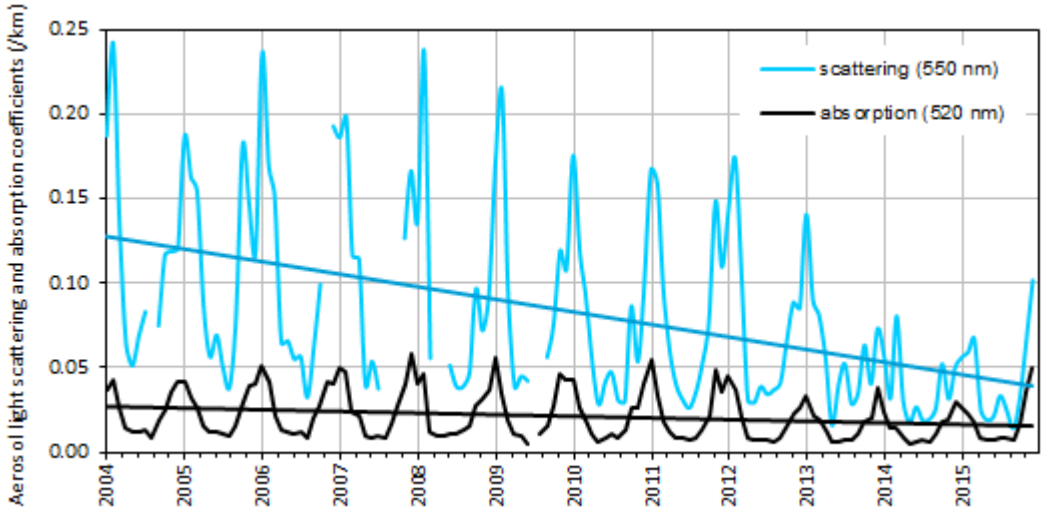

Fig. 49. Aerosol green light scattering and absorption monthly mean coefficients

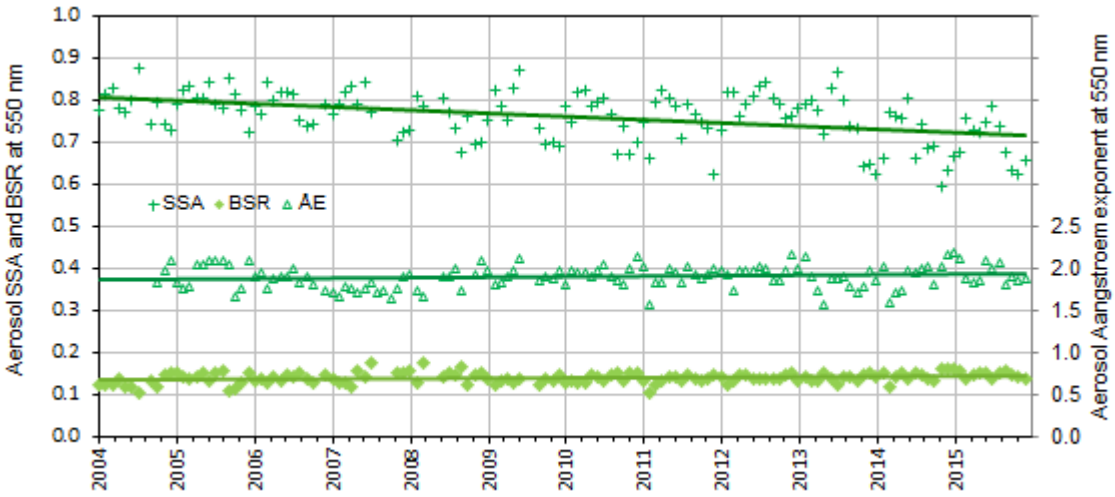

Fig. 50. Aerosol optical characteristics at 550 nm (monthly means): single scattering albedo and backscatter ration (left hand axis) and scattering Ångström exponent (right hand axis).

Ozone indicators (Fig. 47) for 2015 increased again after the minimum observed in 2014 linked to the unusual summertime weather conditions. The number of days with extreme O_3 concentrations (limit of 180 µg/m³ over 1hr exceeded), as well as both indicators for the vegetation protection (number of days with a 24-hour mean O_3 concentration > 65 µg/m³, vegetation protection limit, and the AOT40, Accumulated Ozone exposure over a Threshold of 40 ppb), were in 2015 back to values observed in the 1990's.

The population exposure indicator SOMO 35 (Sum of Ozone Means Over 35 ppb, where means stands for maximum 8-hour mean over day) remained in 2015 even higher than ever observed in the past, except in 2012 and 2013. Values for these indicators tentatively corrected for the missing data (gap filling) can be found on page 45.

4.5.4. Aerosol micro-physical and optical properties

Measurements of the aerosol microphysical properties started at the atmospheric research station of the JRC-Ispra site in 2004. We present here for the first time the 12-year long time series for these variables.

Aerosol particle volume concentrations have clearly decreased over the past 12 years (Fig. 48), in line with the decrease in PM_{10} and $PM_{2.5}$ mass concentrations (Fig. 45). It is interesting to note that also the particle number concentrations also decreased both during summer and winter months, but only until about 2010. Since then, no clear trend in the particle number concentration can be observed.

The aerosol light scattering coefficient has also clearly decreased over the past 12 years (Fig. 49), consistently with the decrease in PM mass and particle volume (or surface) concentrations. Simultaneously, the aerosol absorption coefficient has also decreased slightly, but much less rapidly that the scattering coefficient. As a consequence, the aerosol single scattering albedo (SSA = scattering/(scattering + absorption) significantly decreased over the past 12 years, while the aerosol backscatter ratio only slightly increased (Fig. 50). This could be explained by a decrease in the mean particle diameter, also suggested by the increase in the scattering Ångström exponent. The impact of these changes on the direct radiative forcing by atmospheric particles was discussed elsewhere (Putaud et al., 2014).

4.6. Conclusions

The data coverage in 2015 ranged from 87 to 99% for the various instruments measuring near surface (3 to 4.5 m agl) concentrations. In contrast, the remote aerosol vertical profiling was resumed in October, and data are available for the last 25% of the year only.

2015 as a whole was warmer (especially from March to July) and dryer (in March, August, October and above all in November and December) compared to the reference period (1990 – 1999), and April and June were significantly sunnier than usual. These exceptional weather

conditions can probably explain at least part of the changes in atmospheric pollution observed in 2015 compared to the previous years.

They probably explain why various indicators for O_3 pollution were worse in 2015 compared to 2014, during which the weather was exceptionally bad in summer. They cannot however explain why O_3 was that high compared to 1988-2011, since high O_3 levels were also recorded in 2012-2013. The concentrations of SO_2, NOx and CO also increased compared to 2014, but remained within the range of the concentrations observed during the 2010s, and do not affect the general trend of improvement in these air quality indicators over the last 3 decades.

Daily $PM_{2.5}$ aerosol sampling on quartz fibre filter, using a Partisol sampler equipped with a carbon monolith denuder, and subsequent gravimetric and chemical analyses, showed that the concentration of $PM_{2.5}$ mass and of most of its components (SO_4^{2-}, NO_3^-, NH_4^+, POM and EC) increased in 2015 compared to 2014. Weather differences between 2014 and 2015 can again probably explain most of the differences observed, and the data from 2015 still confirm the mitigation of particulate air pollution observed since 1986. $PM_{2.5}$ average chemical composition was dominated by carbonaceous species (POM: 52%, EC: 10%), followed by secondary inorganics (NH_4^+: 9%, NO_3^-: 15%, SO_4^{2-}: 16%). It should be noted that on average the mass balance was over-reached by 8%. As previously observed, there was a clear increase of NO_3^- contribution to $PM_{2.5}$ when shifting from cleaner ($PM_{2.5}$ < 10 µg/m³) to more polluted periods ($PM_{2.5}$ > 25 µg/m³) during both cold and warmer months. $PM_{2.5}$ (from gravimetric analyses) and PM_{10} (from FDMS-TEOM measurements) annual mean mass concentrations (17 and 27 µg/m³respectively) were both below the EU annual limit value (25 and 40 µg/m³, respectively), and only 21 exceedances of the 24-hr limit value (50 µg/m³) were observed. The long term time series still suggests a trend of decreasing PM_{10} mass concentration of - 1.1 µg m^{-3} yr^{-1} over the last 3 decades.

The annual mean particle number concentration (average: 8040 cm^{-3}) was in (dry) 2015 greater than in (wet) 2014 (~ 6650 cm^{-3}), but less than in 2013 (8220 cm^{-3}). The 12-yr time series shows that the particle number annual mean concentration seem to be rather constant since 2010, while it clearly decreased from 2004 to 2010. Particle number size distributions were in 2015, as usual, generally broadly bimodal, with a submicron mode at ca. 100 nm (dry) and a less pronounced coarse mode around 2 µm. However, both the light backscatter ratio and the Ångström exponent suggest that the mean particle diameter tends to decrease slowly. The atmospheric aerosol scattering and absorption coefficients derived from Nephelometer and Aethalometer measurements in dried atmosphere (generally lower than 40%) also show a decreasing trend over the past 12 years. However, the absorption coefficient does not decrease as fast as the scattering coefficient, and as a consequence, the aerosol single scattering albedo (0.70) was in 2015 significantly less compared to recent years also (0.76 in 2013, 0.79 in 2012 and , 0.77 in 2011), with a possible impact on the climate cooling effect of the aerosol. Filter-based measurement of the light absorption by aerosols remain difficult and prone to

uncertainties. Such measurements would be better constrained if a light extinction monitor based on the cavity attenuated phase shift (CAPS) technique could be implemented.

All aerosol extensive variables measured at JRC-Ispra (at ground level) follow comparable seasonal variations with minima in summer. These variables are generally well correlated and lead to variable degrees of chemical, physical, and optical closure. In 2015, a reasonable overlap between the particle size distributions as measured with the DMPS and the APS was obtained for a particle density of 1.25 g/cm³. This value is in agreement with the average sub-2.5 µm aerosol density of 1.2 g/cm^3 determined from the regression between the gravimetric $PM_{2.5}$ mass and the DMPS + APS volume. However, it is even lower than in 2014, and remains too low compared to 2010 - 2012 (1.3 – 1.4 g/cm^3). In contrast, the ratio between the PM_{10} mass concentration measured with the FDMS-TEOM and the aerosol volume DMPS + APS volume leads to a density of 1.7 g/cm^3, a bit too high considering the chemical composition of the particulate matter at our site. This might indicate that $PM_{2.5}$ gravimetric measurements were underestimated in 2015. However, the extinction-to-mass ratio of 2.5 m^2 g^{-1} (vs. 2.8 m^2 g^{-1} in 2014, 3.4 m^2 g^{-1} in 2012-2013 and 3.9 m^2 g^{-1} in 2011), is also low compared to the value that can be calculated from the mean $PM_{2.5}$ chemical composition, which averages to 4.7 m^2 g^{-1} in 2015 like in 2014, which suggests that whether the aerosol volume and PM_{10} concentrations were overestimated, or the extinction coefficient calculated as scattering + absorption was underestimated. Again, a direct measurement of the aerosol light extinction would be very useful to address this issue.

Aerosol vertical profiles were obtained with the Raymetrics Raman LiDAR from October to December, after the laser was re-installed by the manufacturer. Mainly due to unsuitable meteorological conditions, only 35% of the profiles scheduled by EARLINET could be measured. The data have to be processed using the ACTRIS Single Calculus Chain and submitted to the ACTRIS/EARLINET data base by the end of 2016.

Concentrations of all the ions measured in rainwater in 2015 (Cl^-, NO_3^-, SO_4^{2-}, Na^+, NH_4^+, K^+, and Mg^{2+}, and Ca^{2+}) were higher than in 2014 (due in part to the fact that precipitation was considerably lower in 2015). The concentrations of SO_4^{2-} and NH_4^+ were also greater than the 1990 -1999 averages. The annual wet deposition fluxes of the main acidifying and eutrophying species (1.8, 3.1, and 1.4 g m^{-2} for SO_4^{2-}, NO_3^-, and NH_4^+, respectively) were equal or greater than during the previous years, despite the low volume of precipitation recorded in 2015. Also, twice as much rain samples with pH<4.6 (i.e. 10 times more acidic than due to the equilibrium with atmospheric CO_2) were observed in 2015 (18) compared to 2014 and 2013 (9).

Ground-level 2015' data listed by EMEP and ACTRIS as core variables have all been reported to EBAS in 2016, as requested by these programs. They can be freely downloaded from these web sites.

Page left intentionally blank

Fig. 51: The flux tower of 24 m at the Pinus pinea site in San Rossore

5. Atmosphere – Biosphere flux monitoring at the forest station of San Rossore

5.1. Location and site description

The measurement site 'San Rossore' (43°43.9205'N, 10°17.45817E, 12 m a.s.l.), operated by the Air and Climate Unit, is located in the Parco San Rossore (www.parcosanrossore.org), approximately 9 km west of Pisa and 1200 m east of the seashore in a Mediterranean forest ecosystem (Fig. 51). The Climate Change and Air Quality Unit began to operate the predecessor site in the Parco San Rossore site in 1999, the present location is running since 2013.

The measurement site is situated in an almost flat area with a morphology characterized by the presence of sandy dunes. The vegetation in the direct vicinity is a pinewood established in 1921 following artificial seeding and it is dominated by the evergreen tree Pinus pinea with very sparse Quercus ilex. The average canopy height is approximately 19 m whereas the needles start at about 16.5 m. The understory vegetation is confined to the forest edges and canopy gaps and is very sparse as well.

The area has a Mediterranean – type climate within the sub-humid zone, with a mean annual rainfall of 876 mm yr^{-1} and a range of 534 – 1270 mm for the period 1980 – 2005. The long term data were obtained from a meteorological station located at a distance of approximately 10 km and managed by the Regional Hydrologic Service of Tuscany. Rain falls mainly during autumn and winter with about 50% occurring between September and November, while the driest months are July and August. The average annual temperature is approximately 14.2 °C with the average temperature of the coldest month (January) being 7 °C and that one of the warmest month (August) being 25 °C. The wind regime is characterized by a sea – land breeze circulation, i.e. the air flows quite predictable from the west (sea) during day and from east (land) during night.

The scientific activities were at that moment primarily embedded into the ICOS initiative. ICOS (Integrated Carbon Observation System, www.icos-ri.eu) is one of the pan-European research infrastructure projects identified by the European Strategy Forum on Research Infrastructures (ESFRI) for implementation. After its preparatory phase planned for 2008 until 2013 with an extension towards 2015, during which monitoring infrastructure and technical procedures are developed, its operational phase will run for 20 years from 2016 onwards.

Table 6: ICOS class 2 Ecosystem Station core parameters.

Core variables continuous	**Core variables daily to monthly**	**Core variables yearly**
CO_2, H_2O and energy fluxes	leaf area index	biomass (above ground)
wind speed and direction		soil carbon
CO_2 concentration vertical profile, normal precision		stem diameter
net radiation: • incoming/reflected global radiation • incoming/outgoing longwave radiation • Albedo		above-ground Net Primary Production (NPP)
diffuse global radiation		litter fall
incoming / reflected under canopy Photosynthetic Active Radiation (PAR)		land-use history
temperature and relative humidity vertical profile		managements and natural disturbances
air pressure		C and N import and export on managed sites
precipitation, through-fall, snow depth		
soil heat flux		
ground water level		
soil temperature profile		
water content profile		

Table 7: ICOS variables measured continuously during 2015 in San Rossore

FLUXES	CO_2, latent heat, sensible heat continuously
METEOROLOGY	3D wind speed, temperature, relative humidity, pressure, precipitation
RADIATION	short & long wave incoming & outgoing, direct & diffuse photosynthetic active radiation
SOIL	temperature profile, water content profile, heat flux, water table height

Once in operational mode, greenhouse gas concentrations and fluxes will be monitored on a routine basis following a very strict quality controlled protocol, both in terms of measurement instrumentations required to be used and procedures to be followed. The JRC plans to contribute with a class 2 Atmospheric Station (AS) for the high precision monitoring of greenhouse gas concentrations (at the JRC-Ispra site) and a class 2 Ecosystem Stations (ES), the San Rossore forest flux tower, for the monitoring of ecosystem fluxes. Class 2 stations provide data for less parameter compared to class 1 stations and thus require less investment for instrumentation and have lower running costs in terms of instruments and staff. The mandatory variables to be monitored at the class 2 Ecosystem Station are shown in Table 6.

With regards to data reporting as in the previous years, quality checked data for 2015 have been submitted for the measurement site under the station name IT-SR2 to the Fluxnet database at the European Fluxes Database Cluster at www.europe-fluxdata.eu.

5.2. Measurements in 2015

Despite being still in the upgrading phase of the measurement site to comply with ICOS class 2 requirements, the monitoring program at the new Pinus pinea site continued well. The main parameters measured are summarized in Table 7. In addition, ozone (O_3) concentrations have been measured from the middle of May until the end of the year.

Fluxes of CO_2, H_2O and sensible heat were measured with eddy covariance technique using EddyMeas (Olaf Kolle, www.bgc-jena.mpg.de) for data acquisition and evaluated with the EdiRe software package from the University of Edinburgh (www.geos.ed.ac.uk/abs/research/micromet). The ancillary parameters (meteorology, radiation and soil) were obtained with respective sensors and the data quality checked for instrument malfunctioning, obvious outliers and consistency. In the following chapters, first the instruments used are described and then daily averages of the different parameters measured during the course of 2015 are presented.

5.3. Description of the instruments

5.3.1. Infrastructural:

5.3.1.1 Sensor location

The instruments for eddy covariance flux system, i.e. sonic anemometer and fast gas analyser, solar radiation and meteorological parameters are mounted on the top of the guided wire tower at a height of 24 m above ground, 5 m above the canopy top at 19 m.

Soil parameters are measured at an undisturbed soil plot approximately 20 m west of the tower.

A wooden hut complements the installation hosting IT and communication equipment, a UPS system and is also used for storage.

5.3.1.2 Data acquisition

Eddy covariance flux data are stored with high frequency, i.e. 10 Hz, as chunks of 30 minutes on a local laptop connected to the sonic anemometer. Data from the sensors located on the tower top are read every 10 s and averaged and stored every 30 minutes by a CR3000 data logger from Campbell (www.campbellsci.co.uk) also installed on the tower top. Soil measurements are handled the very same way by a CR3000 installed on the ground.

For eddy covariance flux data, the start time of every 30 minutes measurement period is saved as the reference time, whereas for all other data, the end of the 30 minutes measuring period is used. The time reference used for all San Rossore measurements is has been changed in October 2015 to local solar time (UTC+1) to comply with ICOS requirements.

5.3.1.3 Power supply, IT & communication infrastructure

The fixed line power supply of approx. 4 kW is locally backed up by an UPS system MSM 10 from Riello (www.riello-ups.de) to protect the system for transient power outages and provide an autonomous running time of approx. 19 hours for the installation. Computers and data loggers are connected via a local TCP/IP network. In addition, a cellular router TK704U from Welotec (www.welotec.com) provides internet access via the mobile 3G network. For safety reason at the remote site, a 3G repeater provides mobile phone coverage also on the forest ground in the vicinity of the site.

Measurement data is automatically transferred from San Rossore via ftp to a server (sanrosso@ftp-ccu.jrc.it) in Ispra at 6:00 local solar time. Remote connection to a computer at the site can be established as well.

5.3.2. Ecosystem fluxes:

5.3.2.1 Sonic Anemometer for 3D wind direction Gill HS-50

Sonic anemometers determine the three dimensional wind vectors at high frequency using the speed of sound. The Gill HS-50 (www.gill.co.uk) emits ultrasonic pulses between its pairs of transducers, measures the flight time of the pulses to the paired transducer and calculates the wind speed in the direction of the transducer pair (see Fig. 52). Combining the results from the three transducer pairs, the 3 dimensional wind speed is calculated at a frequency of 10 Hertz. After a rotation of the coordinate system during the data processing to align it with the north direction, horizontal and vertical wind speeds and the wind direction are calculated besides their use for flux calculations. As the speed of sound measured with the anemometer depends on the temperature, the so-called sonic temperature is reported by the instrument as well.

Due to the absence of moving parts and the fact that no calibration is required, the instrument is very robust and reliable. Instrument servicing is done at the manufacturer.

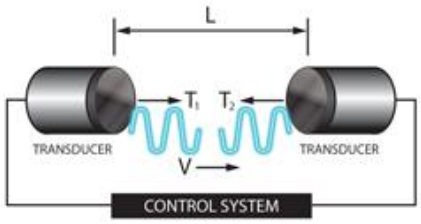

$$T_2 = \frac{L}{C - V} \quad \text{and} \quad T_1 = \frac{L}{C + V}$$

therefore

$$V = \frac{L}{2}\left\{\frac{1}{T_1} - \frac{1}{T_2}\right\} \qquad C = \frac{L}{2}\left\{\frac{1}{T_1} + \frac{1}{T_2}\right\}$$

Fig. 52: Measurement principle of sonic anemometers, T: travelling time of sound pulses, L: distance between transducers, C: speed of sound, V: wind speed in direction of transducers (sketch from www.gill.co.uk)

5.3.2.2 Fast infrared gas analyser (IRGA) for CO_2 & H_2O concentration LI-7200 FM from Licor

For the determination of CO_2 and H_2O fluxes with the eddy covariance technique, fast analysers (10 to 20 Hertz) for concentration measurements of the gases of interest are obligatory. At the San Rossore forest flux tower, a LI-7200 FM system from LI-COR (www.licor.com) has been installed, consisting of the LI-7200 enclosed CO_2/ H_2O analyser, the LI-7550 analyser interface unit and the LI-7200-101 flow module.

The LI-7200 is a high performance, non-dispersive, enclosed open path infrared CO_2/H_2O analyser based on the infrared absorption of CO_2 and H_2O at ambient conditions that provides concentration measurements at a frequency of up to 20 Hertz. With the flow module, ambient air is drawn into to analyser through the sample inlet at a set flow rate of 15 l/min. In the sample volume of 16.09 cm^3 (see Fig. 53), light from the infrared source is absorbed at characteristic wavelengths for CO_2 and H_2O. This specific absorption is a function of the gas concentration in the sample volume. Using the absorption measurements at the CO_2 & H_2O wavelengths, at a non-absorbing wavelength plus calibration factors and measured temperature and pressure, the LI-7200 reports molar densities, mass densities or mole fraction of the two gases.

Zero and span checks and calibrations are done regularly using zero gas from a cylinder plus a dew point generator (RH CAL from EdgeTech) and a CO_2 standard from a cylinder.

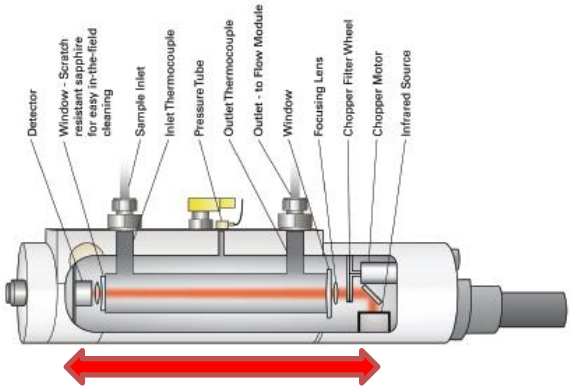

Fig. 53: LI-7200 analyser head (from www.licor.com), arrow indicates sampling volume

5.3.3. Radiation instruments

5.3.3.1 Net radiometer Kipp & Zonen CNR1& CNR4

The net radiometers CNR1 & 4 from Kipp & Zonen (www.kippzonen.com) measures the energy balance between incoming and reflected radiation in the short (305 – 2800 nm) and long (5-50 µm) wavelength range to obtain the net radiation at the earth's surface. The short wavelength range is measured with two CM3 pyranometers, one facing upwards and one downwards. For the long range, two CG3 pyrgeometers facing opposite directions are used. The design of the instrument ensures a field of view of 180° upwards and downwards for the respective sensors. The CNR 4 is an improved version of the CNR1 featuring a blower and heating system to minimize the influence of dew and frost on the radiation measurements. The CNR 4 replaced the CNR 1 in San Rossore from 2nd of March 2015.

The energy E_{short} of the short wave or so-called global (solar) radiation is calculated from the voltages provided by the CM3's using their sensitivity C_{CM3}: $E_{short} = V / C_{CM3}$. To calculate the energy E_{long} of the long wave radiation from the reported voltages, besides the sensitivities of the CG3's C_{CG3}, also the sensor temperature T measured with a PT-100 is needed: $E_{long} = V / C_{CG3} + 5.67 \cdot 10^{-8} \cdot T^4$. The net radiation over all wavelengths is then easily calculated by adding the respective energies: $E_{net} = E_{short}^{up} + E_{long}^{up} - E_{short}^{down} - E_{long}^{down}$. In addition, the Albedo of the earth's surface defined as the ratio of outgoing to incoming solar radiation can be obtained with the instrument as well: $Albedo = E_{short}^{downt} / E_{short}^{up}$.

Calibration and instrument checks at the factory are recommended every two years according to the manufacturer.

5.3.3.2 Photosynthetic active radiation Delta-T BF3 & BF5

With the Sunshine Sensor BF3 from Delta-T (www.delta-t.co.uk), total (in the sense of direct plus diffuse) solar radiation, diffuse radiation and the sunshine state is measured as photosynthetic active radiation (PAR) of the solar spectrum, i.e. from 400-700 nm. The BF5 is an improved version of the BF3 featuring a heating system to prevent condensation and replaced the BF3 in San Rossore from 2nd of March 2015 onwards. To distinguish between direct and diffuse radiation, a set of seven photodiodes (PD) is arranged under a patterned hemispherical dome with 50% black bands such that at any position of the sun in the sky at least one photodiode is completely in the shade and at least one is fully exposed to direct sunlight. This design eliminates the necessity of frequent alignment of the shading parts to the position of the sun. The diffuse radiation is then given by $PAR_{diffuse} = 2 \cdot PD_{\min}$ and the direct radiation by $PAR_{direct} = PD_{\max} - PD_{\min}$

The instrument reports $PAR_{diffuse}$, $PAR_{total} = PAR_{diffuse} + PAR_{direct}$ and sunshine state. The latter one indicates sunshine if

$PAR_{total} / PAR_{diffuse} > 1.25$ and $PAR_{total} > 50\ \mu mol \cdot m^{-2} \cdot s^{-1}$.

5.3.4. Meteorological sensors

5.3.4.1 Temperature & relative humidity UMS KPK1/5-ME

To measure ambient temperature and relative humidity, a combined sensor KPK1/5-ME from UMS (www.ums-muc.de) is installed into a passive radiation shield.

5.3.4.2 Ambient air pressure Keller Druckmesstechnik PAA-41

Ambient air pressure is measured with a PAA-41 capacitive pressure sensor from Keller Druckmesstechnik (www.keller-druck.com) using a ceramic measurement cell for enhanced reliability.

5.3.4.3 Rain sensor UMS ARG 100/std

The ARG 100/std from UMS (www.ums-muc.de) is a tipping bucket type of rain gauge. It features a collecting funnel with a surface area of 500 cm^2 and a resulting resolution of 0.2 mm of rain fall per tip.

5.3.5. Gas sensors

5.3.5.1 Dual beam ozone monitor model 205 from 2B Technologies

To measure the ozone concentration, a dual beam Ozone Monitor from 2B Technologies (www.twobtech.com) is used. The underlying measurement principle is the UV (λ=254 nm) absorption of ozone and the Lambert-Beer law that relates the absorption to concentration. Using two measurement cells in this dual beam monitor, one with a scrubber to remove all ozone and one unfiltered allows to directly calculate ozone concentrations and to compensate for intensity variations in the UV light source.

Zero measurements are periodically performed using an external ozone scrubber, calibration measurements more infrequent with a Model 306 Ozone Calibration Source from 2B Technologies that is checked against a primary standard ozone generator (TEI 49C-PS from Thermo).

5.3.6. Soil instruments

5.3.6.1 Soil heat flux sensors HFP01 from Hukseflux

Three thermal sensors HFP01 from Hukseflux (www.hukseflux.com) have been buried ten centimetres underground in the undisturbed soil around the tower to obtain a good spatial averaging of the soil heat flux. The determination of the heat flux is based on measuring the temperature difference of two sides of a plate that is exposed to a heat flow using a number of thermocouples connected in series (see Fig. 54) with the convention that positive values indicate a heat flux into the soil, a negative one heat flux out of the soil. Ignoring possible errors, the temperature difference between the hot and cold side of the sensor is proportional to the heat flow. As the thermocouples provide a voltage proportional to the temperature, the voltage output of the sensor is proportional to the heat flow across the sensor.

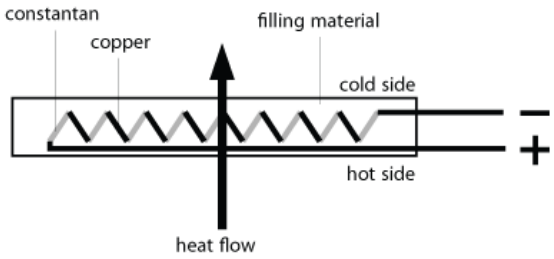

Fig. 54: Sketch of a soil heat flux sensor (drawing from www.wikipedia.org)

5.3.6.2 Soil water content vertical profile with TRIME-TDR from IMKO

Profile measurements of soil water content are performed using the TRIME-TDR (Time domain Reflectometry with Intelligent MicroElements with) from IMKO (www.imko.de). Based on Time-Domain-Reflectometry, the sensor generates high frequency electromagnetic pulses that propagate along a wave guide and reflected back into the sensor. Depending on the dielectric constant of the material surrounding the waveguide, the round trip time of the hf-pulses varies between some tens and thousand picoseconds. As the dielectric constant of soil and thus the round trip time strongly depends on the soil moisture content, measuring this time gives the water content of the soil surrounding the sensor. Burying several sensors at depths of 5, 30, 50, 100 cm below ground provides the soil humidity profile.

5.3.6.3 Soil temperature profile with Th3-v probe from UMS

For the measurement of soil temperatures at different depths, a Th3-v probe from UMS (www.ums-muc.de) is used. This probe features a convenient set of 6 temperature probes in a profile system buried at 5, 10, 20, 30, 50 and 100 cm below ground.

Table 8: Processing steps for flux calculations using the EdiRe Software package.

EdiRe Process	**brief description**
Preprocessed Files	data from input file, gas concentrations as molar densities
Extract	all high speed data
Despike	all high speed data
Linear	conversion of raw data from voltages into physical variables
1 chn statistics	averages of 3D wind, sonic temperature and gas concentration
Gas conversion	conversion of molar densities to molar fraction
Filter – detrend	linear detrending of gas concentrations
Wind direction	align with geographic direction
Rotation coefficients	perform 3D coordinate rotation
Cross Correlate	gas concentrations with vertical wind speed
Remove Lag	remove time lag between anemometer and gas analyser
Friction Velocity	calculate u*
Sensible heat flux coefficient	
Latent heat of evaporation	
2 chn statistics	calculate covariances, i.e. uncorrected fluxes
Sonic T - heat flux correction	
Stability - Monin Obhukov	calculate z/L stability parameter
Frequency response	calculate high frequency correction for all fluxes
Webb correction	calculate water density fluctuation correction for all fluxes
Stationarity	perform stationarity test
Integral Turbulence	calculate integral turbulence
Cospectra	calculate co-spectra for all fluxes
Storage	calculate storage term
User defined	determine quality flag (0,1,2) for all flux data according to Carboeurope methodology

5.3.6.4 Ground water level CS456-SA from Campbell Scientific

The ground water level is monitored with a Diver from Campbell Scientific (www.campbellsci.co.uk). The device is placed in a water filled hole, 1.9 m below ground, and logs autonomously the pressure. Combining the measurement with the barometric pressure at the site gives the height of the water column above the sensor. Together with the known sensor depth below ground, the water table height can be easily calculated (see also Fig. 55):

$$WL = TOC - CL - WC \text{ with } WC = 9806.65 \cdot \left(p_{Diver} - p_{baro}\right) / \rho \cdot g \; ;$$

g = 9.81 m/s^2, ρ = 1.00 kg/m^3

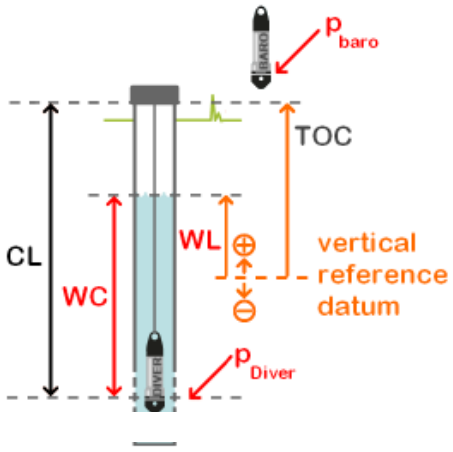

Fig. 55: Principle of water level calculation using the Diver (sketch from www.swstechnology.com). CL: cable length, TOC: top of container, WC: water column, WL: water level relative to a reference, p: pressure.

5.3.7. Flux data processing

Data evaluation for flux data is done using the free EdiRe software package developed at the micrometeorology group from the University of Edinburgh (www.geos.ed.ac.uk/abs/research/micromet/EdiRe/). As input data, EdiRe uses the 30 min raw flux data files in the binary *.slt format plus 30 minute averaged pressure, temperature and relative humidity data in ASCII format. As time convention, the start of the measurement period has to be assigned to the input data, the middle of the measurement period is assigned to the output data.

The main processing steps used within EdiRe to arrive at final, 30 minute averaged flux data that are corrected for various effects are listed in Table 8.

.

In order to obtain budgets from e.g. annual datasets that unavoidably contain gaps in the data, a gap filling procedure must be established to calculate the missing values based on drivers for the respective parameter. In addition, partitioning of the measured CO_2 flux (that is the Net Ecosystem Exchange, NEE), into Gross Primary Production (GPP, the gross carbon uptake) and respiration of the Ecosystem (Reco) enables a better understanding of the underlying ecosystem exchange processes. Gap-filling and partitioning of the data measured at the ABC-IS station is done with the online tool at:

www.bgc-jena.mpg.de/bgi/index.php/Services/REddyProcWeb.

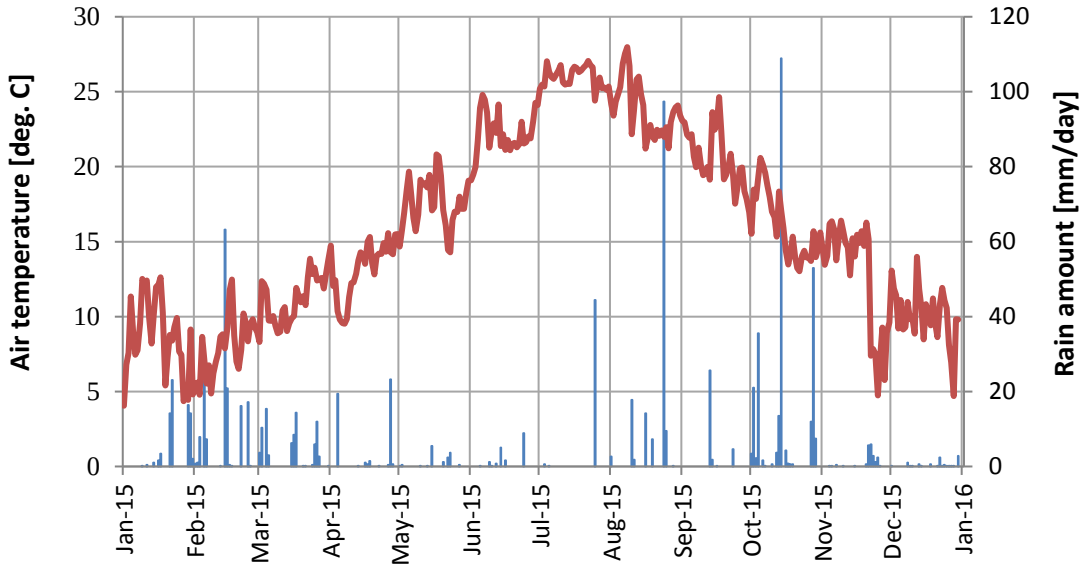

Fig. 56: Daily averages of air temperature (top) and daily sum of precipitation (bottom) as measured in the Parco San Rossore.

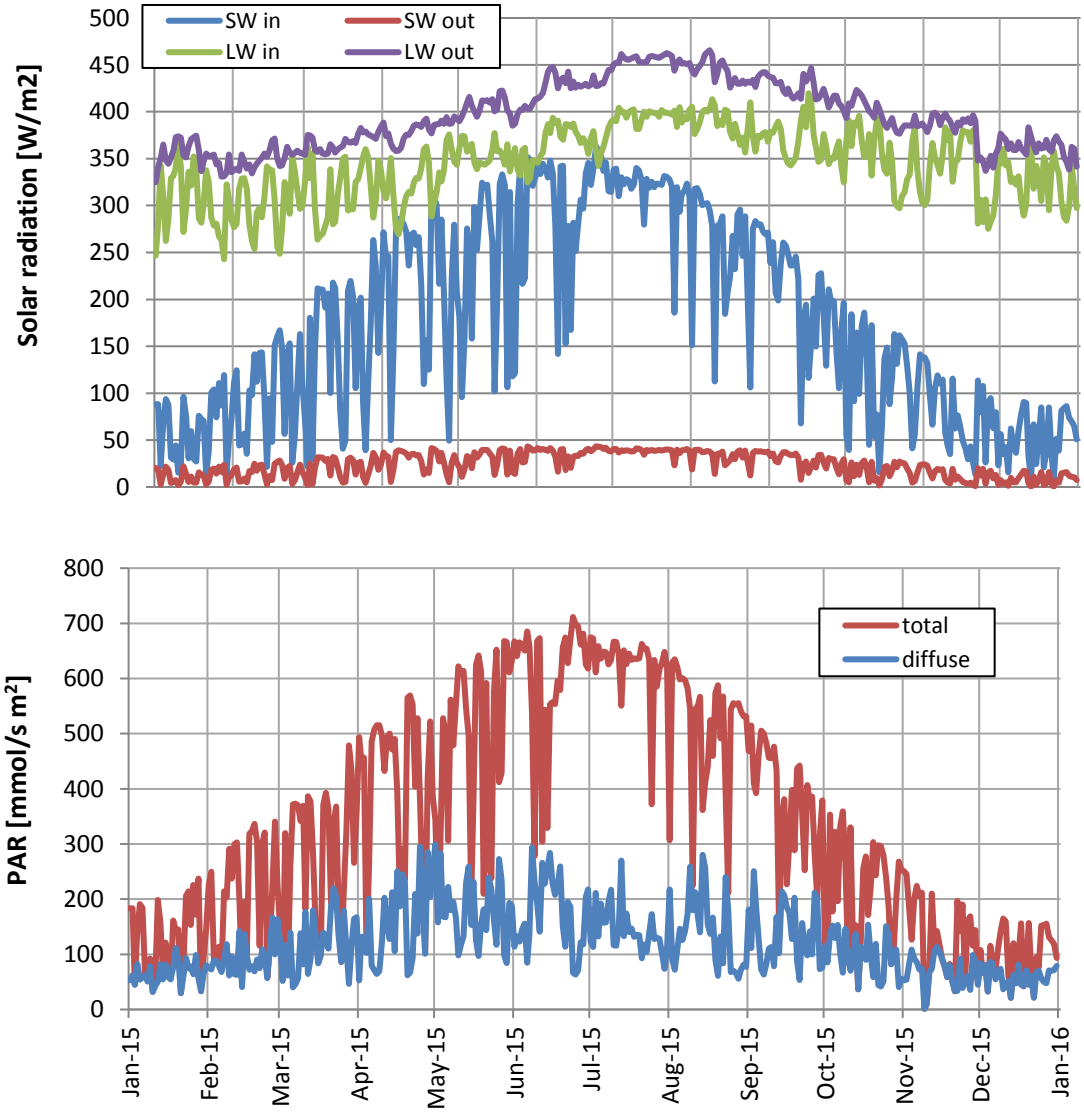

Fig. 57: Daily averages of short wave incoming radiation (top) and incoming photosynthetic active radiation (bottom).

5.4. Results of the year 2015

5.4.1. Meteorology

Daily averages for the annual cycle of air temperature and precipitation are shown in Fig. 56. The annual mean temperature for 2015 was 15.9° C (15.9° C for 2014), 1.7° C above the long term average of 14.2° C. With a total measured rainfall of 924 mm (1525 mm in 2014), 2015 was a normal year for San Rossore with a mean annual rainfall of 876 mm yr^{-1}. Also regarding rainfall pattern, 2015 was an average year with most precipitation in spring / autumn and a rather dry first half of summer.

The predominant sea – land breeze wind circulation can be seen from the statistical evaluation of the 3D wind direction measurements and is shown in Fig. 58. The red plot shows the frequency distribution of the wind for winds speed > 0.5 m/s in terms of its origins; the blue line indicates the average wind speed per directional bin. The average annual wind speed was 1.5 m/s.

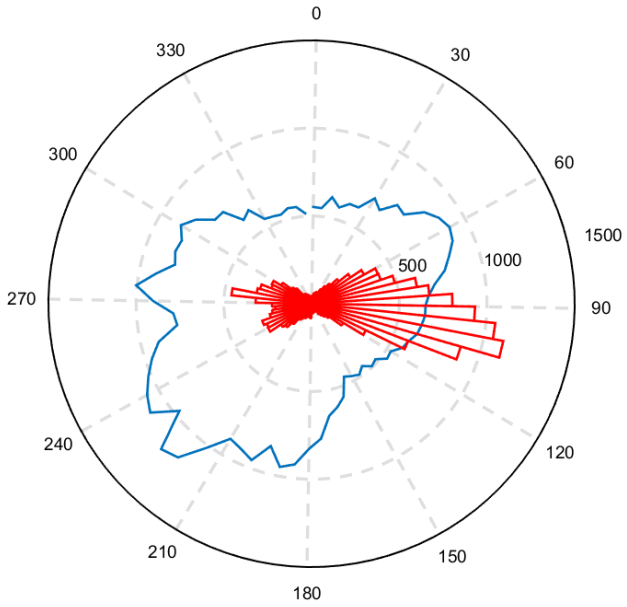

Fig. 58: Wind rose for 30 min. averages of wind measurements with wind speed >0.5 m/s. Red: directions of the wind origin, blue: average wind speeds per direction interval in a.u.

5.4.2. Radiation

In Fig. 57 , the annual cycle of short & long wavelength incoming & outgoing radiation are plotted as measured with the CNR1 and CNR4 net radiometers above the forest canopy at 24 m. The surface albedo, i.e. the ratio between SWout and SWin (305 – 2800 nm) averages to approximately 0.13 for the summer period and 0.16 for the winter period of the measurement. On the bottom part of Fig. 57, the photosynthetic active radiation (PAR) part of the solar spectrum (approx. 400 – 700 nm) is shown as total and diffuse incoming radiation.

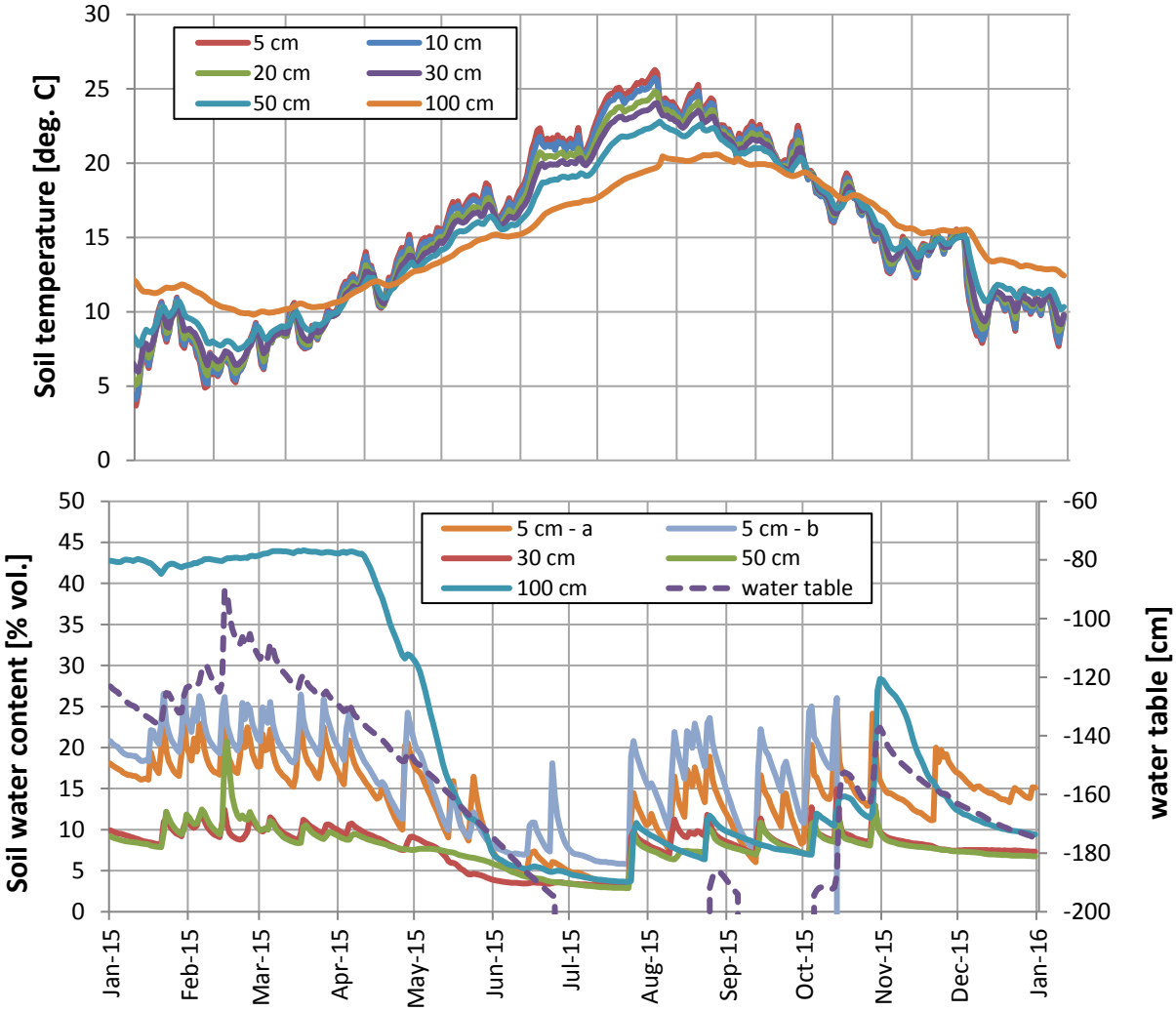

Fig. 59: Profiles of soil temperature (top) and soil water content plus water table (bottom) measured as daily averages.

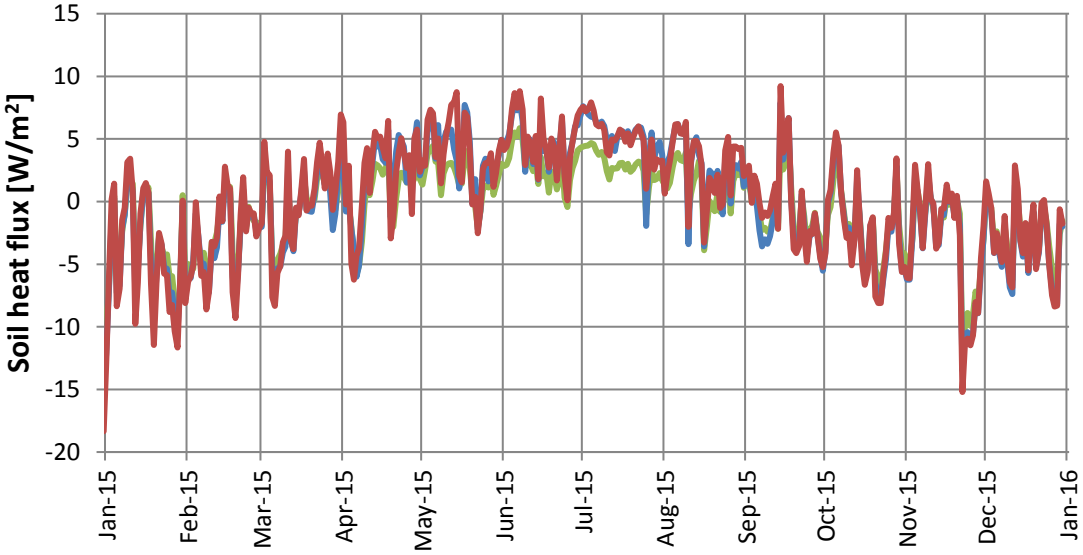

Fig. 60: Soil heat fluxes measured with three identical sensors located some meters apart.

5.4.3. Soil variables

The soil variables monitored in 2015 were the temperature at six different depths (5, 10, 20, 30, 50 and 100 cm), soil water content profile (2 replicates at 5 cm, 30, 50 and 100 cm), soil heat flux (3 replicates at 5 cm, a few meters apart) plus water table depth measured with a well requiring a minimum water level of 195 cm below ground. The daily averages of these measurements are illustrated in Fig. 59. During most part of July to September 2015, the water level was below 195 cm and thus not measured. The soil heat flux measured with three identical sensors located a few meters apart in the forest soil is shown in Fig. 60, using the convention that positive values indicate a heat flux into the soil, negative values out of the soil. The slight differences between the three sensors originate from the different light intercept by the canopy at the different locations and the soil inhomogeneity.

5.4.4. Eddy covariance Flux measurements

The daily averages of CO_2 and heat fluxes measured during 2015 are shown in Fig. 61 and Fig. 63, respectively. To obtain the eddy covariance flux data for the 30 minute measurement periods, the high frequency data from the LiCor 7200 infrared gas analyser for CO_2 and H_2O have been evaluated together with the anemometer data using the EdiRe software package from the University of Edinburgh.

The Carboeurope quality classification for the flux data points for 2015 is used also for San Rossore. A value of 0 indicates strong turbulence and good stationarity, giving reliable EC flux values. A QF = 1 indicates acceptable quality and flux data with QF = 2 are unreliable and thus should not be used in further calculations. For the measurements at San Rossore, the distribution of quality flags for all flux data are given in Table 9, which shows that 65 – 80 % of the data depending on the flux type are usable for further data evaluation and interpretation.

Table 9: Total number of flux data points and percentage of data points with quality flags according to the Carboeurope methodology (H: sensible heat, LE latent heat, FC CO_2 flux).

	H [%]	LE [%]	FC [%]
data points	17398	17370	17364
QF = 0	16	7	12
QF = 1	64	58	62
QF = 2	20	35	26

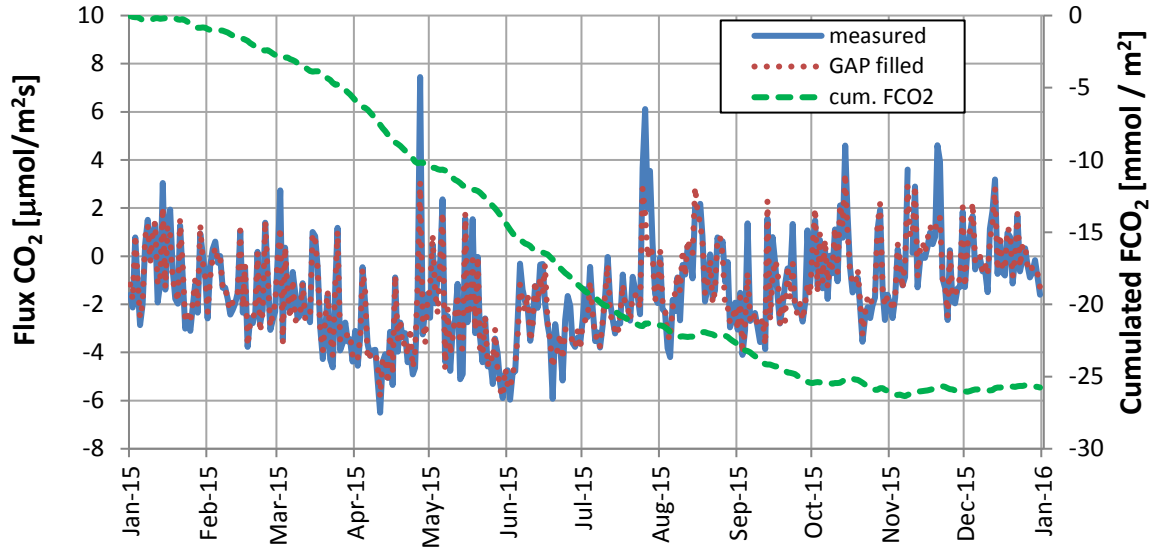

Fig. 61: Daily averages of measured (blue), gap filled (red) and cumulated (green) CO_2 fluxes.

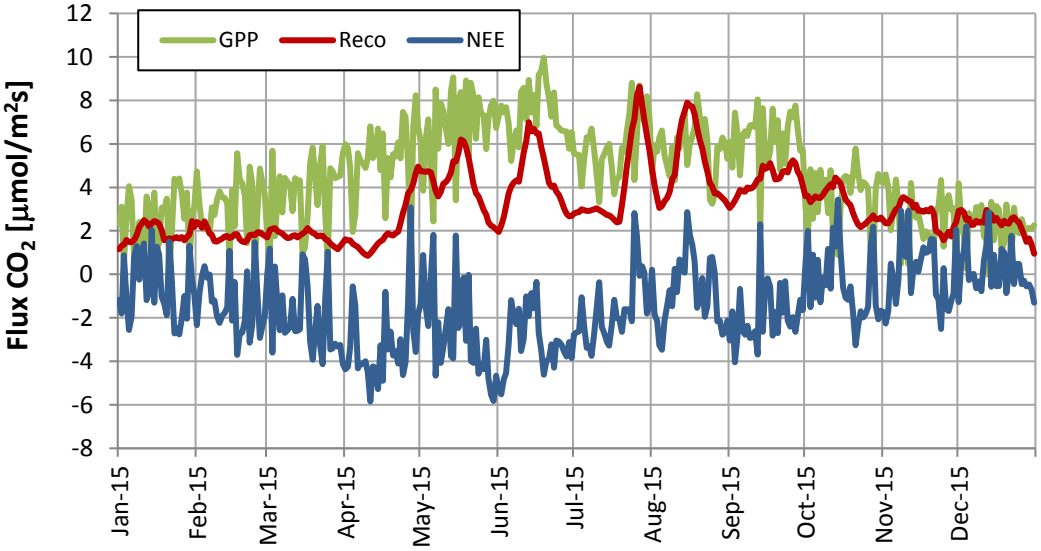

Fig. 62: Daily averages of NEE, GPP and Reco.

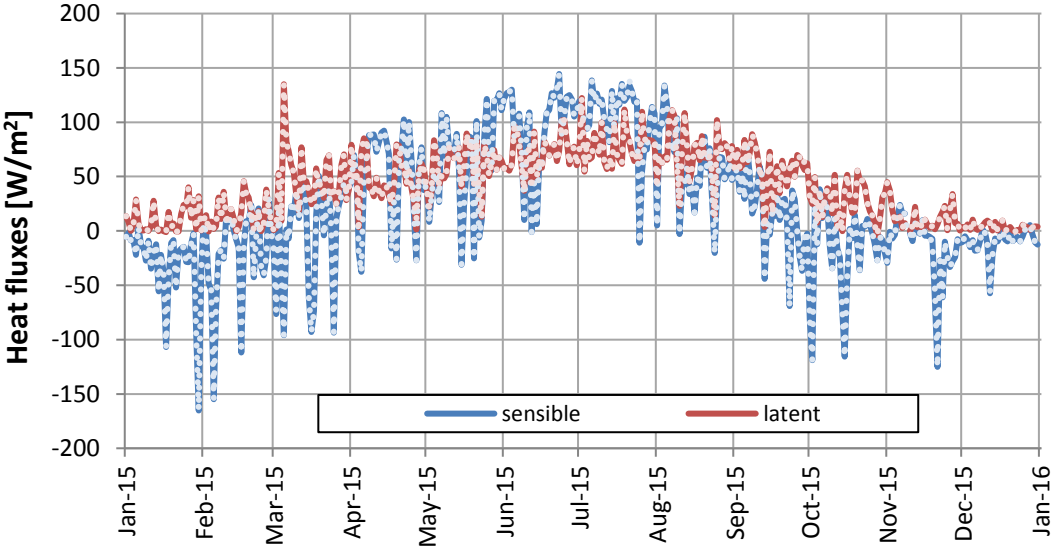

Fig. 63: Daily averages of latent (red) and sensible (blue) heat fluxes.

Gap filling of the dataset has been performed without filtering for friction velocities (u*) below a threshold (that would indicate how turbulent the wind is) using the 'Eddy covariance gap-filling & flux-partitioning tool' for missing and quality class 2 data online available at: www.bgc-jena.mpg.de/~MDIwork/eddyproc/. The cumulated sum of the gap filled 30 min CO_2 fluxes is shown in Fig. 61. The plot shows that in 2015 the Pinus pinea stand is a clear sink for CO_2 until October. Then ecosystem respiration and CO_2 uptake balance for the rest of the year. Using the flux partitioning module of the above mentioned online tool, the Net Ecosystem Exchange (NEE), i.e. the CO_2 flux measured, has been partitioned into Gross Primary Production (GPP) and Ecosystem Respiration (Reco) according to the equation: *NEE = Reco - GPP* and plotted as daily averages in Fig. 62. Calculating the budgets for 2015 (2014 in parenthesis), NEE sums up to -557 (-464) g C m^{-2} yr^{-1}, GPP to -1751 (-1942) g C m^{-2} yr^{-1} and Reco to 1194 (1478) g C m^{-2} yr^{-1}.

For San Rossore, comparing 2015 to 2014 it is very remarkable that NEE is significantly higher this year with a much lower rainfall during summer (246 mm) than last year (413 mm). This indicates that water availability from rainfall might not only be a limiting factor for the photosynthesis of the Pinus pinea trees, but even more for the ecosystem respiration.

At the ABC-IS forest station in Ispra (see Section 6), the budgets sum up in 2015 for NEE to -526 g C m^{-2} yr^{-1}, GPP to -2170 g C m^{-2} yr-1 and Reco to 1644 g C m^{-2} yr^{-1}. This indicates that carbon sequestration in the forest of San Rossore was slightly higher compared to the forest in Ispra during 2015.

5.4.5. Ozone measurements

Ozone concentrations have been measured above the canopy during an extended summer / autumn period from beginning of May all through the end of the year. Daily averages of the ozone concentration are plotted in Fig. 64. The maximum recorded hourly average of the O_3 concentration was 112 ppb (~220 µg/m^3) during the observation period. The information threshold for an hourly ozone concentration above 180 µg/m^3 (European Directive 2008/50/EC on ambient air quality and cleaner air for Europe) has been exceeded on 6 days for a total of 17 hours. The AOT40 value (Accumulated dose of Ozone over the Threshold of 40 ppb), an indicator used for crops exposure to ozone, summed up to 36800 ppb h during the observation period.

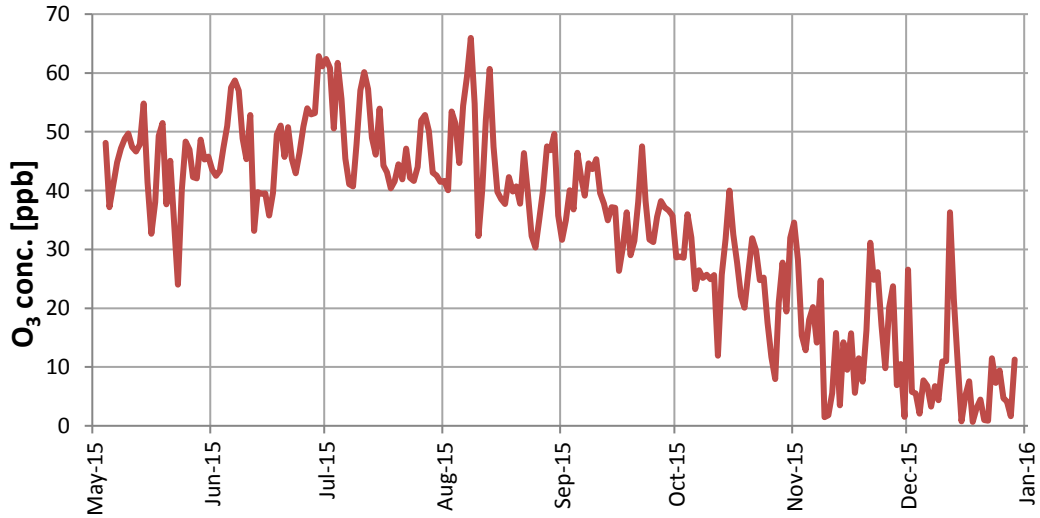

Fig. 64: Daily averages of the ozone concentration as measured at above the canopy.

Fig. 65: The 36 high self-standing tower at the ABC-IS Forest Flux Station in Ispra

6. Atmosphere – Biosphere flux monitoring at the forest flux tower of Ispra

6.1. Location and site description

The ABC-IS Forest Flux Station is part of the large ABC-IS infrastructure focussing on the measurement and monitoring of exchange processes of a forest ecosystem with the atmosphere, predominantly relying on the use of the eddy covariance technique for flux measurements. The measurement site (45°48'45.68"N, 8°38'2.09"E) is placed inside a small forest of approximately 10 ha that is part of the JRC Ispra premises. Situated in an almost flat area, this forest is unmanaged since the foundation of the JRC Ispra in the late 1950ies and therefore now characterized as a mixed, almost natural forest ecosystem. The tree species composition consists of ~80% Quercus robus, ~10% Alnus glutinosa, ~5% Popolus alba and ~3% Carpinus betulus, and the predominant soil type is Regosol.

The ABC-IS Forest Flux Station comprises a 36 m high self-standing tower (see Fig. 65) as a platform to hold instruments, an air-conditioned container for instrumentation and IT infrastructure plus the surrounding forest where above and below ground sensors are installed. A detailed project documentation can be found at Gruening et al., 2011. A report of the performance of the instruments at the site also in comparison with measurements from the EMEP station is given in Gruening et al., 2012.
Since 2013, the ABC-IS Forest Flux Station takes part in the European Fluxes Cluster and the measurement data have been submitted under the station name IT-Isp to the Fluxnet database at http://www.europe-fluxdata.eu.

6.2. Measurement program

The ABC-IS Forest Flux Station had been originally projected as a platform to perform long-term monitoring activities with the additional possibility to engage in short-term research projects, mainly in the frame of international collaborations.
It was originally planned that also the ABC-IS Forest Flux Station should become a class 2 Ecosystem Station within ICOS. For a brief description of ICOS and the obligatory parameters to be measured, please refer to the respective chapter in the description of the San Rossore Forest Flux Station on page 76.
2015 has been the last year of operation of this monitoring site as the priorities of work for the Air and Climate Unit have changed and consequently no resources will be available to continue.

6.3. Measurements in 2015

The main variables measured during the reported year are summarized in Table 10.

Table 10: ICOS variables measured during 2015 at the forest tower in Ispra

FLUXES	CO_2, latent heat, sensible heat, ozone
METEOROLOGY	3D wind speed, temperature, relative humidity, pressure, precipitation
RADIATION	short & long wave incoming & outgoing, direct, diffuse & reflected above canopy photosynthetic active radiation (PAR) incoming and ground reflected PAR below canopy
SOIL	temperature profile, water content profile, heat flux, water table height, respiration

In the same way as it is done at the San Rossore Forest Flux Station, fluxes of CO_2, H_2O, sensible heat and ozone were measured with eddy covariance technique and evaluated using the EdiRe software package from the University of Edinburgh (www.geos.ed.ac.uk/abs/research/micromet). The ancillary parameters (meteorology, radiation and soil) were obtained with respective sensors and the data quality checked for instrument malfunctioning, obvious outliers and consistency. In the following section the site specific instrumental descriptions are presented. Daily averages of the different parameters measured during the course of 2015 are presented further down.

6.4. Description of Instruments:

6.4.1. Infrastructural:

6.4.1.1 Sensor location

The instruments for the eddy covariance flux system, i.e. sonic anemometer and fast gas analysers, radiation and meteorological sensors plus gas inlets are mounted on the 36 m high self-standing tower. Soil parameters are measured in the vicinity on the tower on the forest ground approximately 35 m north-east.

6.4.1.2 Data acquisition

Eddy covariance flux data are acquired and stored with high frequency, i.e. 10 Hz, as chunks of 30 minutes on a local laptop connected to the sonic anemometer. Data from most other sensors are read every 10 s by a respective CR3000 data logger from Campbell Scientific (www.campbellsci.co.uk) which saves 30 minute averages of the acquired data. For eddy covariance flux data, the start time of every 30 minutes measurement period is saved as the reference time, whereas for all other data, the end of the 30 minutes measuring period is used. The time reference for all measurements is UTC.

6.4.2. Ecosystem fluxes:

6.4.2.1 Sonic Anemometer for 3D wind direction Gill HS-100

Sonic anemometers determine the three dimensional wind vectors at high frequency using the speed of sound. As the Gill HS-100 (www.gill.co.uk) is an instrument almost identical to the Gill HS-50 used at the San Rossore Forest Flux Station, please refer to the instrument description on page 74.

6.4.2.2 Fast infrared gas analyser for CO_2 & H_2O (IRGA) LI-7200 FM

As the IRGA is identical to the one operated at the San Rossore Forest Flux Station, please refer to page 75 for the instrument description.

6.4.2.3 Fast ozone sensor - Sextant FOS

The measurement principle of the Fast Ozone Sensor (FOS), manufactured by Sextant Technology Ltd. (www.s-t.co.nz), is based on chemiluminescence. In a measurement chamber, ambient air containing ozone passes above a 25 mm diameter disc coated with coumarin. The dye coumarin reacts with ozone under the emission of light. This emission is proportional to the ozone concentration in the air and the reaction and the air exchange in the reaction chamber is sufficiently fast to allow 10 Hz measurements of ozone concentrations.
The sensitivity of the coumarin discs unfortunately changes within hours. Therefore an independent measurement of the absolute value of the ozone concentration is mandatory and realized with a Thermo Scientific 49C Ozone Analyser sampling air at vicinity of the FOS. A linear calibration of the FOS is automatically done in data post-processing using the 30 minute mean values of the FOS signal and the 49C concentration plus zero as offset.
The lifetime of the coumarin-coated discs depends on the total ozone exposure and is limited to two to three weeks.

6.4.2.4 CO_2 and H_2O vertical profile system from ACU

The profile of CO_2 and H_2O within and above the canopy space is sampled with a manifold hosting 8 lines sampling air from different heights (0.5 1 2 4 8 16 29 37 m above ground). In order to avoid leaking of air into the sampling line, each line is equipped with a membrane pump that keeps the air pressure within the system slightly above ambient pressure.

The array of valves is controlled by two units:

- Data logger and control unit: Campbell CR3000
- Relay Controller: Campbell SDM-CD16AC AC/DC

Atmospheric mixing ratios of CO_2 and H_2O are monitored with a close-path InfraRed Gas Analyser (IRGA) LiCOR 7000. A measurement cycle per sampling line consists of 8 s flushing and 7 s of data acquisition.

Calibration is performed periodically using zero gas from a cylinder plus a dew point generator (RH CAL from EdgeTech), and a CO_2 standard from a cylinder.

6.4.3. Radiation instruments

6.4.3.1 Net radiometer Kipp & Zonen CNR1

See page 76 for instrument description

6.4.3.2 Photosynthetic active radiation Delta-T BF3

Refer to page 76 for instrument details.

6.4.3.3 Fraction of absorbed PAR – Apogee SQ110-L-10 sensor array

SQ110-L-10 quantum sensors from Apogee (www.apogeeinstruments.co.uk) are used to measure PAR originating from different directions. The Fraction of Absorbed Photosynthetic Active Radiation (FAPAR) can be calculated from the measurements of these four distinct PAR fluxes: above canopy incident (*PARi*) and reflected (*PARr*), below canopy transmitted (*PARgi*) and ground reflected (*PARgr*):

$$FAPAR = 1 - \frac{PAR_r + PAR_{gi} - PAR_{gr}}{PAR_i}$$

As a trade-off between complexity of the setup and the inhomogeneity of the forest canopy and changing incoming solar radiation conditions, the setup consists of one sensor each for PAR_i and PAR_r, mounted on the top of the flux tower. On the forest ground, 5 sensors are mounted on ~2 m high poles facing downwards for PAR_{gr} and 15 sensors on ~1.5 m high poles facing upwards for PAR_{gi} measurements. Data for all sensors are stored as 1 minute averages instead of 30 minutes to account for transients in incoming radiation.

6.4.4. Meteorological sensors

6.4.4.1 Weather transmitter WXT 510 from Vaisala

A WXT510 weather transmitter from Vaisala (www.vaisala.com) records simultaneously the six weather parameters temperature, pressure, relative humidity, precipitation and horizontal wind speed and direction.

The wind data measurements utilise three equally spaced ultrasonic transducers that determine the wind speed and direction from the time it takes for ultrasound to travel from one transducer to the two others. The precipitation is measured with a piezoelectric sensor that detects the impact of individual raindrops and thus infers the accumulated rainfall. For the pressure, temperature and humidity measurements, separate sensors employing high precision RC oscillators are used. Due to problematic relative humidity measurement results, relative humidity and temperature were not used in 2015.

6.4.4.2 Temperature and relative humidity HMP155 from Vaisala

To measure ambient temperature and relative humidity, a combined sensor HMP155 (www.vaisala.de) installed into a passive radiation shield was used.

6.4.5. Soil instruments

6.4.5.1 Soil heat flux sensors Hukseflux HFP01

A group of 2 thermal sensors HFP01 from Hukseflux (www.hukseflux.com) have been buried 10 centimetres underground in the undisturbed soil in the vicinity of the tower to obtain a good spatial averaging of the soil heat flux (see page 77 for description).

6.4.5.2 Soil water content vertical profile with TRIME-TDR from IMKO

Profile measurements of soil water content are performed using the TRIME-TDR (Time domain Reflectometry with Intelligent MicroElements) from IMKO (www.imko.de). Please refer to the instrument description for San Rossore on page 77 for details. At the ABC-IS forest flux station, the sensors are buried at depths of 10, 30, 50, 100 cm below ground to provide the soil humidity profile.

6.4.5.3 Soil temperature profile with Th3-v probe from UMS

For the measurement of soil temperatures at different depths a Th3-v probe from UMS (www.ums-muc.de) is used. This probe features a convenient set of 6 temperature probes in a profile system buried at 5, 10, 20, 30, 50 and 100 cm below ground.

6.4.5.4 Ground water level with Diver CS456 from Campbell

The ground water level is monitored with Diver from Campbell (www.campbellsci.co.uk). As the device is the same as the one used at San Rossore, please refer to page 79 for details. The maximum depth at the ABC-IS forest flux station is 2.6 m below ground.

6.4.6. Flux data processing

The evaluation of flux data is performed in the very same way as at the San Rossore Forest Flux Station. Therefore please refer to page 79 for a detailed description.

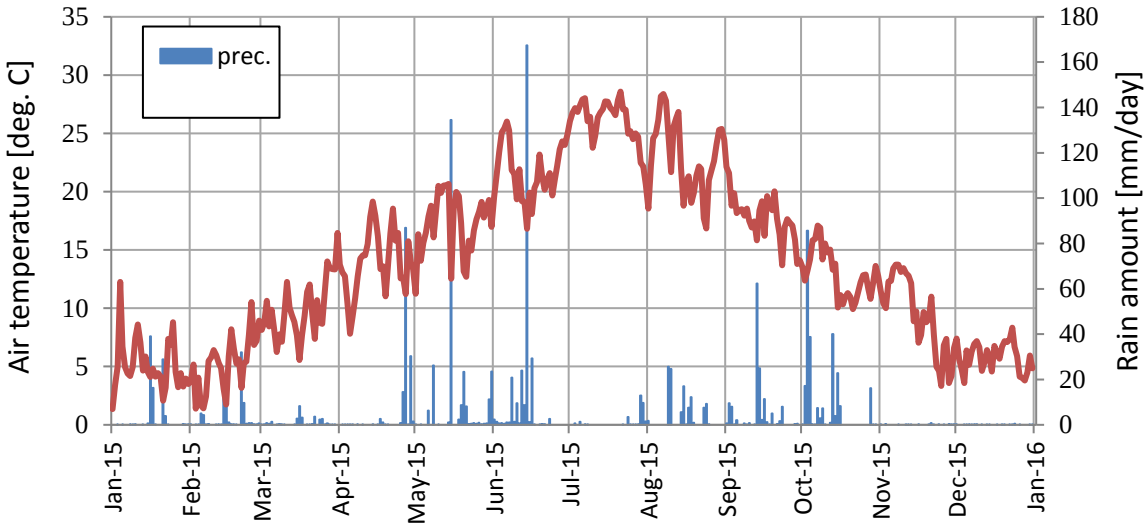

Fig. 66: Daily average of the air temperature (red) and daily sum of the precipitation (blue) measured at the tower top.

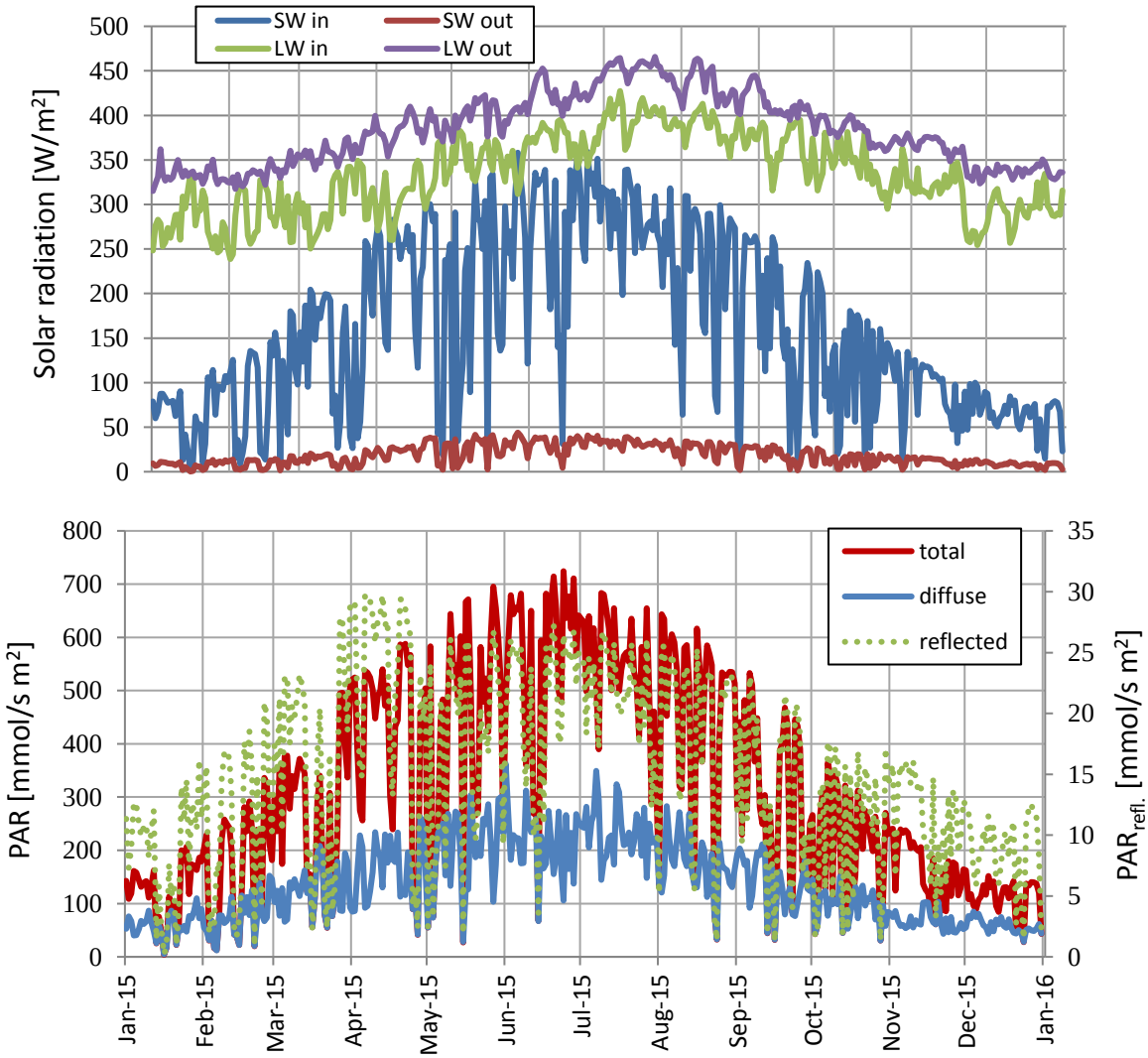

Fig. 67: Solar radiation parameters measured with the net radiometer (top) and the sensor for Photosynthetic Active Radiation (bottom).

6.5. Results of the year 2015

6.5.1. Meteorology

Daily averages of the air temperature and daily sums of the precipitation measured at the top of the ABC-IS Forest Flux Tower are shown in

Fig. 66. The annual mean temperature above the forest canopy at 37 m was 14.0 °C and the total amount of rainfall summed up to 1410 mm.

The wind measurements obtained with the 3D sonic anemometer indicate that north north-west is the predominant wind direction. Fig. 68 shows in red the frequency distribution of the wind directions for wind speeds > 0.5 m/s; the blue line indicates the average wind speeds per directional bin. Wind speeds with a value larger than 0.5 m/s occurred during ~80 % of the measurements intervals. Time periods with air coming from either east or west occur only during very few occasions and wind from the south is rather infrequent as well.

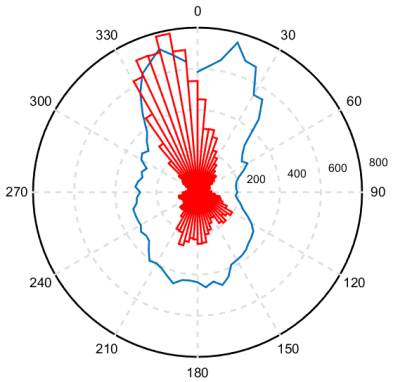

Fig. 68: Wind rose for 30 min. averages of wind measurements with wind speeds >0.5 m/s. Red: directions of the wind origin, blue: average wind speeds per direction interval in a.u.

6.5.2. Radiation

Different parameters regarding solar radiation are plotted in Fig. 67. On top, the daily averages of short & long wavelength incoming & outgoing radiation are plotted as measured with the CNR1 net radiometer above the forest canopy at 36 m. The surface albedo, i.e. the ratio between SWout and SWin (305 – 2800 nm) averages to approximately 0.12 for the summer period and 0.10 for the winter period of the measurement. On the bottom part of Fig. 67, the photosynthetic active radiation (PAR) part of the solar spectrum (approx. 400 – 700 nm) is shown as total & diffuse incoming (left axis) and reflected radiation (right axis). During the vegetative period, i.e. late spring, summer and early autumn, the surface albedo at this part of the solar spectrum is approximately 0.04. The albedo increases in winter up to 0.07 as the deciduous trees in the forest lose their leaves.

Measurements for the FAPAR were running throughout 2015. Averaging the 15 ground PAR sensors facing upwards, the 5 ground PAR sensors facing downwards and calculating FAPAR every minute during daytime according to

$$FAPAR = 1 - \frac{PAR_r + PAR_{gi} - PAR_{gr}}{PAR_i}$$

results in an FAPAR value of 0.92 (+/- 0.01) during the vegetative period when the leaves of the deciduous trees and thus the canopy is fully developed.

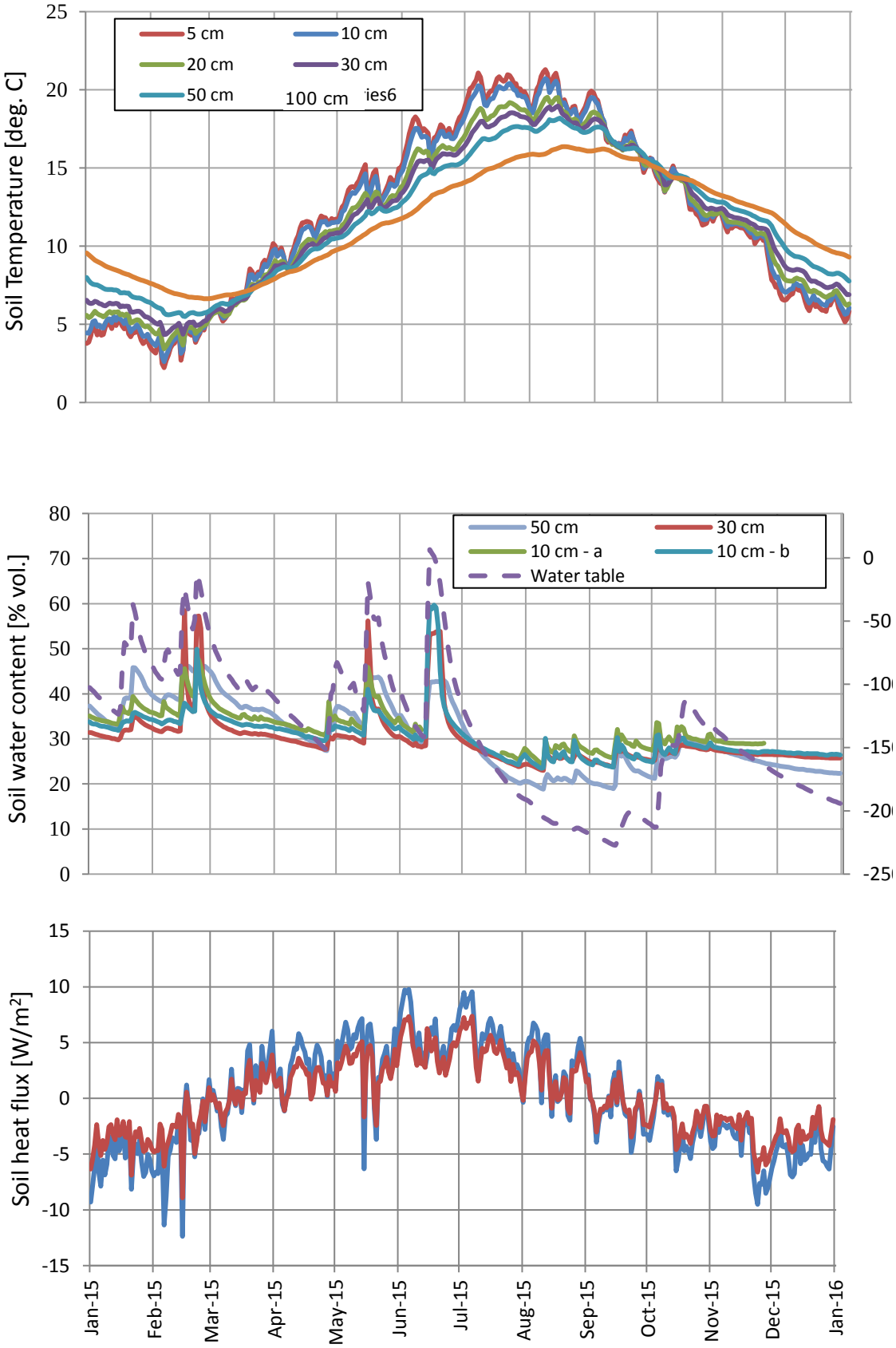

Fig. 69: Timeline of daily averages of soil parameters measured at the ABC-IS forest flux site from top to bottom: soil temperature profile, soil water content profile plus water table below surface and soil heat flux at two replicates (10 cm below surface).

6.5.3. Soil variables

The soil variables measured at the ABC-IS Forest Flux Station are shown in the three plots of Fig. 69. In the top one, daily temperature averages at 6 different depths are plotted. As expected, soil temperature decreases with measurement depth during summer and increases during winter. The tipping points when the temperature profile is reversed occurred in the middle of March and at the end of September.

The plot in the middle depicts the soil water content (SWC) at different depths (left axis) and the water table (right). Jumps in the daily averages of the SWC occur during precipitation events and thereafter the soil starts to dry again. The differences seen at the surface replicates at 10 cm give a glimpse on the heterogeneity of the soil and the forest environment. In the middle of June the measurement area was briefly flooded with a maximum water level of 6 cm above ground because of heavy rainfall.

In the bottom plot of Fig. 69, the soil heat flux measured at two locations is presented. Obviously during summer time the soil heats up due to solar irradiation and in in winter time it cools down. Again, the differences of the heat fluxes at the two sensor positions are due to different environmental situations at the two locations, i.e. different irradiance by the sunlight and to a lesser extend soil variation.

6.5.4. Eddy covariance fluxes

The timelines of daily averages of the different fluxes calculated from measured data using EdiRe, following the Carboeurope methodology (no correction for storage), are shown in *Fig. 70* and Fig. 71. Gap filling and flux partitioning of the dataset has been performed without u* filtering using the 'Eddy covariance gap-filling & flux-partitioning tool' for missing and quality class 2 data online available at: www.bgc-jena.mpg.de/bgi/index.php/Services/REddyProcWeb.

During the cold season when the deciduous trees in the Ispra forest are without leaves, the CO_2 flux (FC) of the forest is positive and ecosystem acts a source of CO_2 (see Fig. 71). During the growing season on the other hand, the flux is negative and the forest is a strong sink of CO_2 due to photosynthesis.

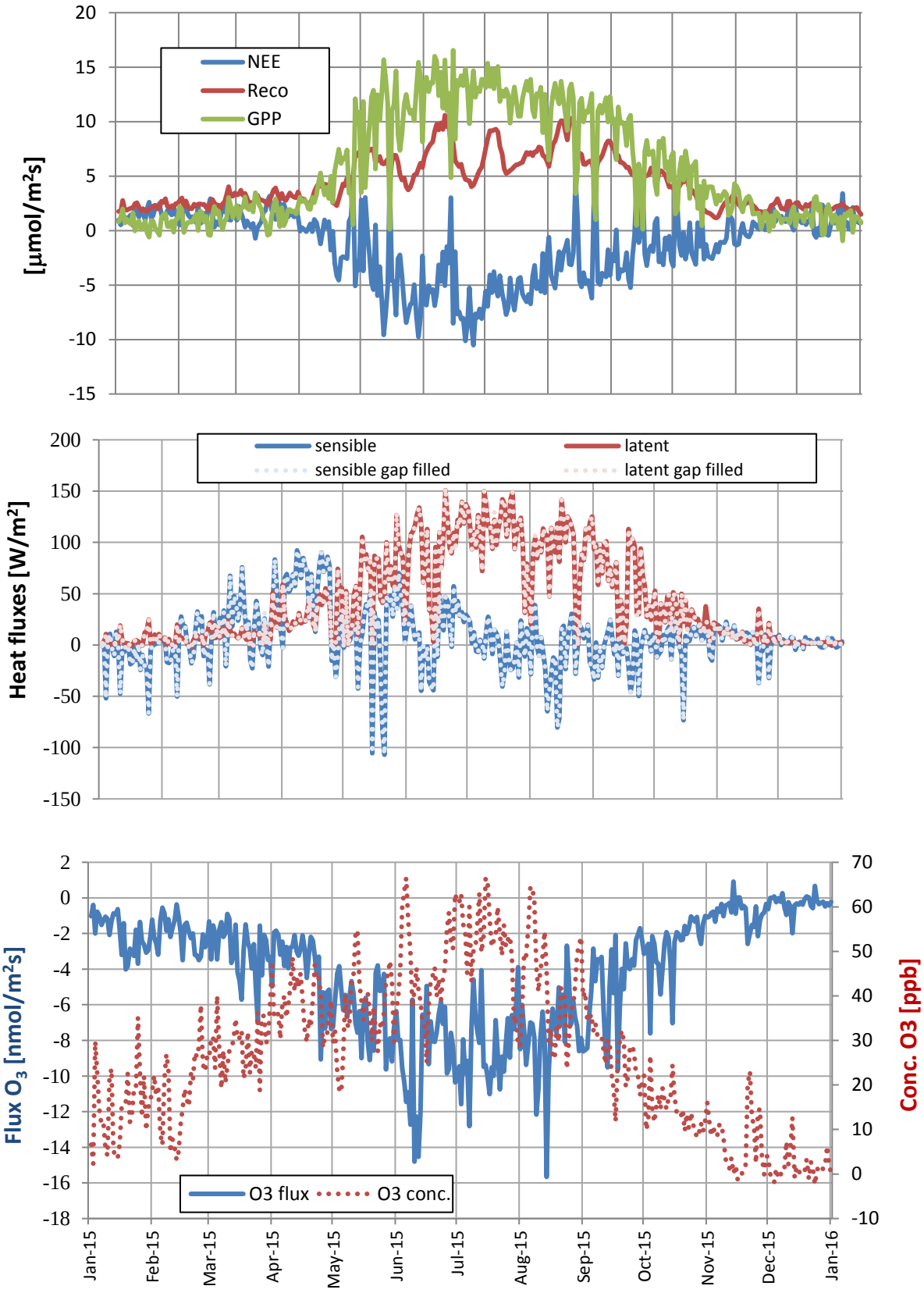

Fig. 70: Timelines of daily averages of fluxes calculated from data measured at the ABC-IS forest flux site, from top to bottom: CO_2 fluxes, i.e. NEE, GPP & Reco, sensible & latent heat flux plus ozone flux & concentration.

Partitioning CO_2 flux data as *NEE = Reco - GPP* results in the daily averages plotted in *Fig. 70*, top panel. Despite the increased ecosystem respiration (Reco) during summer compared to winter, the photosynthetic activity of the plants results in an even higher Gross Primary Production (GPP) and thus leads to net uptake of CO_2 by the forest. Calculating the budgets for 2015 and in parenthesis those for 2014, NEE sums up to -526 (-457) g C m^{-2} $year^{-1}$, GPP to -2170 (-1754) g C m^{-2} $year^{-1}$ and Reco to 1644 (1297) g C m^{-2} $year^{-1}$.

Fig. 70 middle panel shows the latent (red, LE) and sensible (blue, H) heat fluxes for 2015 as daily averages. The latent heat flux, i.e. water vapour flux, especially during the warm summer period, is much higher than the sensible heat flux. This is characteristic of rather humid ecosystems with high water availability also during warm periods as it is the case in Ispra.

O_3 concentration and flux (FO3) were measured continuously in 2015 (*Fig. 70* bottom panel) from the top of the flux tower. The information threshold for an hourly ozone concentration above 180 µg/m3 was exceeded on 18 days during the year. The AOT40 value (Accumulated dose of Ozone over the Threshold of 40 ppb summed up to 32000 ppb h during the observation period (similar to the value obtained at the EMEP-GAW station). The flux measurements indicate that the forest is a significant sink for ozone during the entire year. In 2015, the annual O_3 deposition flux was 6.4g m^{-2} $year^{-1}$ (lower limit). As both O_3 concentrations and the activity of the ecosystem increase in late spring, also ozone deposition into the ecosystem increases.

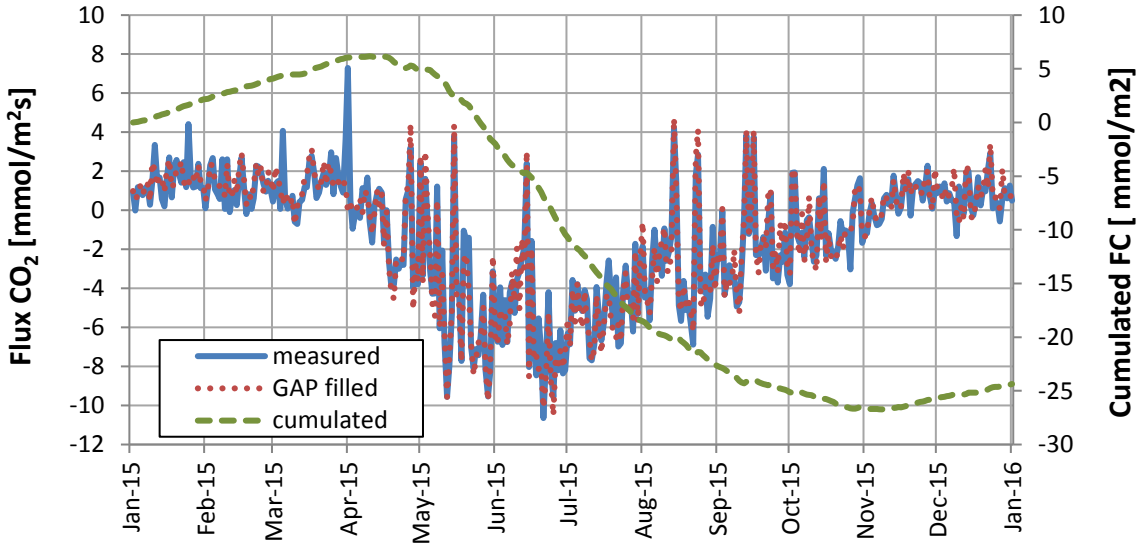

Fig. 71: Daily averages of measured (blue), gap filled (red) and cumulated (green) CO_2 fluxes.

The assessment of the applicability of the eddy covariance (EC) method to measure fluxes at any time is given by the stationarity and integral turbulence tests. They are combined in the Carboeurope methodology into a quality flag (QF) for every data point. A value of 0 indicates strong turbulence and good stationarity, giving reliable EC flux values. A QF = 1 indicates acceptable quality, and flux data with QF = 2 are unreliable and thus should not be used in further calculations. For the measurements at the ABC-IS station, the distribution of quality flags for all flux data are given in Table 11. The table shows that 60 – 67 % of the data depending on the flux type are usable for further data evaluation and interpretation.

Table 11: Total number of flux data points and percentage of data points with quality flags according to the Carboeurope methodology (H: sensible heat, LE latent heat, FC CO_2 flux, FO_3 ozone flux).

	H [%]	LE [%]	FC [%]	FO_3 [%]
data points	16208	15791	15786	15449
QF = 0	12	8	9	9
QF = 1	57	52	55	58
QF = 2	31	40	36	33

7. References

Adam, M., J. P. Putaud, S. Martins dos Santos, A. Dell'Acqua, and C. Gruening, Aerosol hygroscopicity at a regional background site (Ispra) in Northern Italy, Atmos. Chem. Phys., 12, 5703–5717, 2012

Anderson, T.L., and Ogren, J.A., Determining aerosol radiative properties using the TSI3563 integrating nephelometer, *Aerosol Sci. Technol.*, **29**, 57-69, 1998.

Arnott, W.P., Hamasha, K., Moosmüller, H., Sheridan, P.J., and Ogren, J.A., Towards aerosol light-absorption measurements with a 7-wavelength Aethalometer: Evaluation with a photoacoustic instrument and a 3 wavelength nephelometer, *Aerosol Sci. Technol.*, **39**, 17-29, 2005.

Barnaba, F., Putaud, J.P., Gruening, C., Dell'Acqua, A., Dos Santos, S., Co-located in-situ, total-column and height-resolved aerosol observations: Implications for ground-level PM estimation from remote sensing. *J. Geophys. Res.*, **115**, D10204, doi:10.1029/2009JD012451, 2010.

Bergamaschi P. and D. Brunner, Analysis of the sensitivity of atmospheric measurements at the JRC Ispra Atmosphere - Biosphere - Climate Integrated monitoring Station, Footprint analysis based on FLEXPART-COSMO model, JRC technical report, EUR 27131 EN, 2015.

Cavalli, F., Putaud, J.P., Toward a standardised thermal-optical protocol for measuring atmospheric organic and elemental carbon: the EUSAAR protocol, *Atmos. Meas. Tech.*, **3**, 79-89, 2010.

Cooke, W.F., Liousse, C., Cachier, H., and Feichter, J., Construction of a 1x1°fossil fuel emission data set for carbonaceous aerosol and implementation and radiative impact in the ECHAM4 model, *J Geophys. Res.*, **104**; 22,137-22, 1999.

Dell'Acqua, A., Putaud J.P., Gruening, C., Study of the JRC-Ispra EMEP site representativeness for short-lived atmospheric species measurements, *JRC report* EUR 24312 EN, 2010.

Dlugokencky, E.J., P.M. Lang, J.W. Mund, A.M. Crotwell, M.J. Crotwell, and K.W. Thoning (2016), Atmospheric Carbon Dioxide Dry Air Mole Fractions from the NOAA ESRL Carbon Cycle Cooperative Global Air Sampling Network, 1968-2015, Version: 2016-08-30, Path: ftp://aftp.cmdl.noaa.gov/data/trace_gases/co2/flask/surface/

EMEP manual for sampling and chemical analysis (1995). *EMEP/CCC-Report 1/95.* (*Revised 1996; 2001; 2002).* 1995.

European Directive 2008/50/EC. On ambient air quality and cleaner air for Europe. 2008.

Gruening C., Goded I., Jensen N.R., Cescatti A., Cieslik S., Project Document ABC-IS forest flux tower, ARES(2011)1288711, (2011)

Gruening C., Goded I., Cescatti A., D. Fachinetti, I. Fumagalli, M. Duerr, ABC-IS Forest Flux Station, Report on Instrumentation, Operational Testing and First Months of Measurements, EUR 25705 EN, (2012), JRC76928.

Hess, M., Koepke, P. Schult, I., Optical Properties of Aerosols and Clouds: The Software Package OPAC, *Bull. of Am. Meteorol. Soc.*, **79**; 831-844, 1998.

Jensen, N. R., Gruening, C., Adams, M., Cavalli, F., Cavalli, P., Grassi, F., Dell'Acqua, A., Martins Dos Santos, S., Roux, D., Putaud, J.-P. JRC Ispra EMEP – GAW regional station for atmospheric research, 2009 report, *EUR 24678 EN*, (2010), *JRC62602*.

Kiehl, J. T., Schneider, T. L., Rasch, P. J., Barth, M. C., Wong, J., Radiative forcing due to sulfate aerosols from simulations with the National Center for Atmospheric Research Community Climate Model, Version 3 (Paper 1999JD900495), *J. Geophys. Res.,* **105**; 1441-1458, 2000.

McMurry, P., Wang, X., Park, K., and Ehara, K. The relationship between mass and mobility for atmospheric particles: A new technique for measuring particle density, *Aerosol Sci. Tech*., **36**, 227–238, 2002.

Mira-Salama, D., Van Dingenen, R., Gruening, C., Putaud, J.-P, Cavalli, F., Cavalli, P., Erdmann, N., Dell'Acqua, A., Dos Santos, S., Hjorth, J., Raes, F., Jensen, N.R. Using Föhn conditions to characterize urban and regional sources of particles, *Atmospheric Research* **90**, 159–16, 2008.

Pépin L., Schmidt M., Ramonet M., Worthy D.E.J. and Ciais, P. Notes des Activités Instrumentales, A new gas chromatographic experiment to analyze greenhouse gases in flask samples and in ambient air in the region of Saclay, Institut Pierre-Simon Laplace (2001), http://www.ipsl.jussieu.fr.

Petzold, A., H., Schönlinner, M., Multi-angle absorption photometry - A new method for the measurement of aerosol light absorption and atmospheric black carbon, *Journal of Aerosol Science*, **35** (4), 421-441, 2004.

Putaud, J.-P., et al. (21 authors), 2004, A European aerosol phenomenology—2: chemical characteristics of particulate matter at kerbside, urban, rural and background sites in Europe. *Atmospheric Environment*, **38**, 2579-2595.

Putaud, J.-P., et al. (39 authors), 2010, A European aerosol phenomenology—3: Physical and chemical characteristics of particulate matter from 60 rural, urban, and kerbside sites across Europe. *Atmospheric Environment*, **44**, 1308-1320.

Putaud, J.P., F. Cavalli, S. Martins dos Santos, and A. Dell'Acqua, Long-term trends in aerosol optical characteristics in the Po Valley, Italy, Atmos. Chem. Phys., 14, 9129–9136, 2014.

Putaud J.P., Bergamaschi P., Bressi M, Cavalli F., Cescatti A., Daou D., Dell'Acqua A., Douglas K., Duerr M., Fumagalli I., Goded I., Grassi F., Gruening C., Hjorth J., Jensen N.R., Lagler F., Manca G., Martins Dos Santos S., Matteucci M., Passarella R., Pedroni V., Pokorska O., Roux D. JRC – Ispra Atmosphere – Biosphere – Climate Integrated monitoring Station. 2013 report, JRC report EUR 26995 EN, 2014.

Russell, L.M.: Aerosol organic-mass-to-organic carbon ratio measurements, *Environ. Sci. Technol.*, **37**, 2982-2987, 2003.

Schmid, O., et al., Spectral light absorption by ambient aerosols influenced by biomass burning in the Amazon Basin I: comparison and field calibration of absorption measurements techniques, *Atmos. Chem. Phys.*, **6**, 3443-3462, 2006.

Scheeren, H. A., P. Bergamaschi et al., An analysis of four years of CO_2, CH_4, N_2O and SF_6 observations and ^{222}Radon-based emission estimates from the monitoring station at Ispra (Italy), for submission to Atmos. Chem. Phys. Discuss., 2013.

Schembari, C., F. Cavalli, E. Cuccia, J. Hjorth, G. Calzolai., N. Pérez, J. Pey, P. Prati, F. Raes: Impact of a European directive on ship emissions on air quality in Mediterranean harbours, Atmospheric Environment (2012), doi: 10.1016/j.atmosenv.2012.06.047.

Schembari, C., M.C. Bove, E. Cuccia, F. Cavalli, J. Hjorth, D. Massabò, S. Nava, R. Udisti, P. Prati, Source apportionment of PM_{10} in the Western Mediterranean based on observations from a cruise ship. Atmospheric Environment 98, 510–518, 2014.

Stratmann, F., Wiedensohler, A. A new data inversion algorithm for DMPS-measurements. *J. Aerosol Sci.*, **27** (Suppl 1), 339-340, 1996.

Van Dingenen, R., et al. (28 authors), 2004, A European aerosol phenomenology –1: Physical characterization of particulate matter at kerbside, urban, rural and background sites in Europe, *Atmospheric Environment*, **38**, 2561-2577.

Velchev, K., Cavalli F., Hjorth J., Vignati E., Dentener F., Raes F., Ozone over Western Mediterranean Sea-results from two years of shipborne measurements., Atmospheric Chemistry and Physics, 11, 675-688, 2011.

Weingartner, E., Saathoff, H., Schnaiter, M., Streit, N., Bitnar, B., and Baltensperger, U., Absorption of light by soot particles: determination of the absorption coefficient by means of aethalometers, *J. Aerosol Sci.*, **34**, 1445-1463, 2003.

Weitkamp, C. (editor), LIDAR Range-Resolved Optical Remote Sensing of the Atmosphere, *Springer*, New York, 2005.

WHO, Health risks of ozone from long-range transboundary air pollution, 2008.

Worthy, D. E. F., I. Levin, N. B. A. Trivett, A. J. Kuhlmann, J. F. Hopper, and M. K. Ernst, Seven years of continuos methane observations at a remote boreal site in Ontario, Canada, J. Geophys. Res., 103 (D13), 15995-16007, 1998.

Zahorowski, W., S. D. Chambers, A. Henderson-Sellers, Ground based radon-222 observations and their application to atmospheric studies, J. Environm. Radioact., 76, 3-33, 2004.

Links

ACTRIS, *www.actris.eu*

ARPA Lombardia, *ita.arpalombardia.it/ITA/qaria/doc_RichiestaDati.asp*

Calipso, *www.nasa.gov/mission_pages/calipso/main*

Chemical Co-ordinating Centre of EMEP, *www.nilu.no/projects/ccc*

CLRTAP, *www.unece.org/env/lrtap/welcome.html*

EARLINET, *www.earlinet.org*

EMEP, *www.emep.int*

EPTR, European Pollutant Release & Transfer Register, prtr.ec.europa.eu/MapSearch.aspx

European Committee for Standardisation (CEN), *www.cen.eu/cen/pages/default.aspx*

EUSAAR, *www.eusaar.net*

Global Atmosphere Watch (GAW), *www.wmo.int/pages/prog/arep/gaw*

ICOS, www.icos-ri.eu

InGOS, www.ingos-infrastructure.eu

WDCA, *www.gaw-wdca.org*

World Meteorological Organization (WMO), *www.wmo.int/pages/index_en.html*.

List of figures

List of tables

Europe Direct is a service to help you find answers to your questions about the European Union.

Freephone number (*)**:**

00 800 6 7 8 9 10 11

(*) The information given is free, as are most calls (though some operators, phone boxes or hotels may charge you).

More information on the European Union is available on the internet (http://europa.eu).

HOW TO OBTAIN EU PUBLICATIONS

Free publications:

- one copy:
  via EU Bookshop (http://bookshop.europa.eu);
- more than one copy or posters/maps:
  from the European Union's representations (http://ec.europa.eu/represent_en.htm);
  from the delegations in non-EU countries (http://eeas.europa.eu/delegations/index_en.htm);
  by contacting the Europe Direct service (http://europa.eu/europedirect/index_en.htm) or
  calling 00 800 6 7 8 9 10 11 (freephone number from anywhere in the EU) (*).

  (*) The information given is free, as are most calls (though some operators, phone boxes or hotels may charge you).

Priced publications:

- via EU Bookshop (http://bookshop.europa.eu).

KJ-NA-28513-EN-N

JRC Mission

As the science and knowledge service of the European Commission, the Joint Research Centre's mission is to support EU policies with independent evidence throughout the whole policy cycle.

EU Science Hub
ec.europa.eu/jrc

@EU_ScienceHub

EU Science Hub - Joint Research Centre

Joint Research Centre

EU Science Hub

Publications Office

doi:10.2760/409157

ISBN 978-92-79-66612-4